Accepted Manuscript



MicroRNA-31 Reduces Inflammatory Signaling and Promotes Regeneration in Colon Epithelium, and Delivery of Mimics in Microspheres Reduces Colitis in Mice

Yuhua Tian, Jiuzhi Xu, Yuan Li, Ran Zhao, Sujuan Du, Cong Lv, Wei Wu, Ruiqi Liu, Xiaole Sheng, Yongli Song, Xueyun Bi, Guilin Li, Mengzhen Li, Xi Wu, Pengbo Lou, Huiwen You, Wei Cui, Jinyue Sun, Jianwei Shuai, Fazheng Ren, Bing Zhang, Mingzhou Guo, Xiaohua Hou, Kaichun Wu, Lixiang Xue, Hongquan Zhang, Maksim V. Plikus, Yingzi Cong, Christopher J. Lengner, Zhanju Liu, Zhengquan Yu

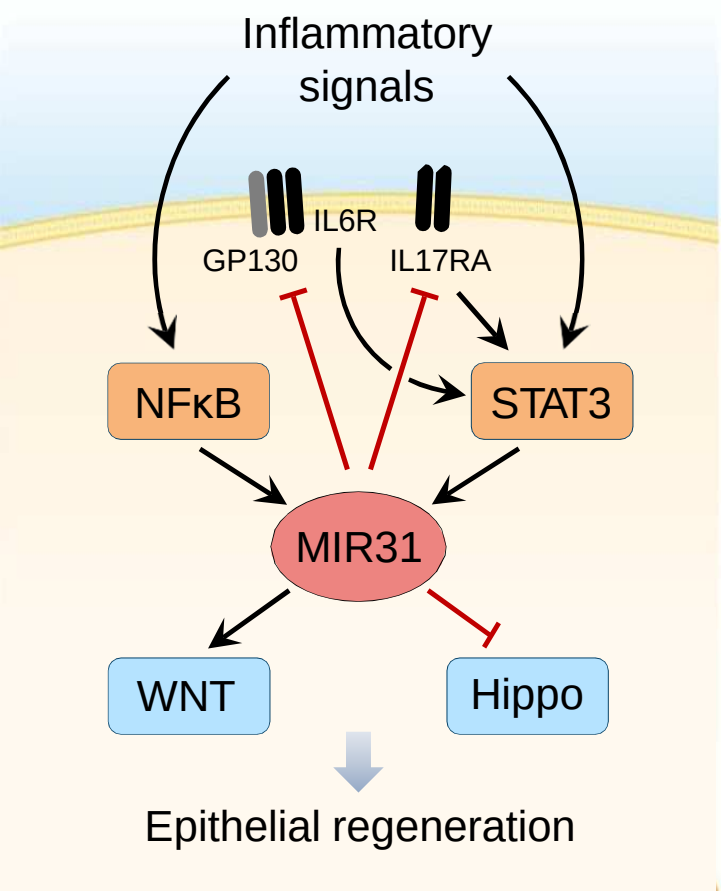
PII: S0016-5085(19)30396-8
DOI: https://doi.org/10.1053/j.gastro.2019.02.023
Reference: YGAST 62483

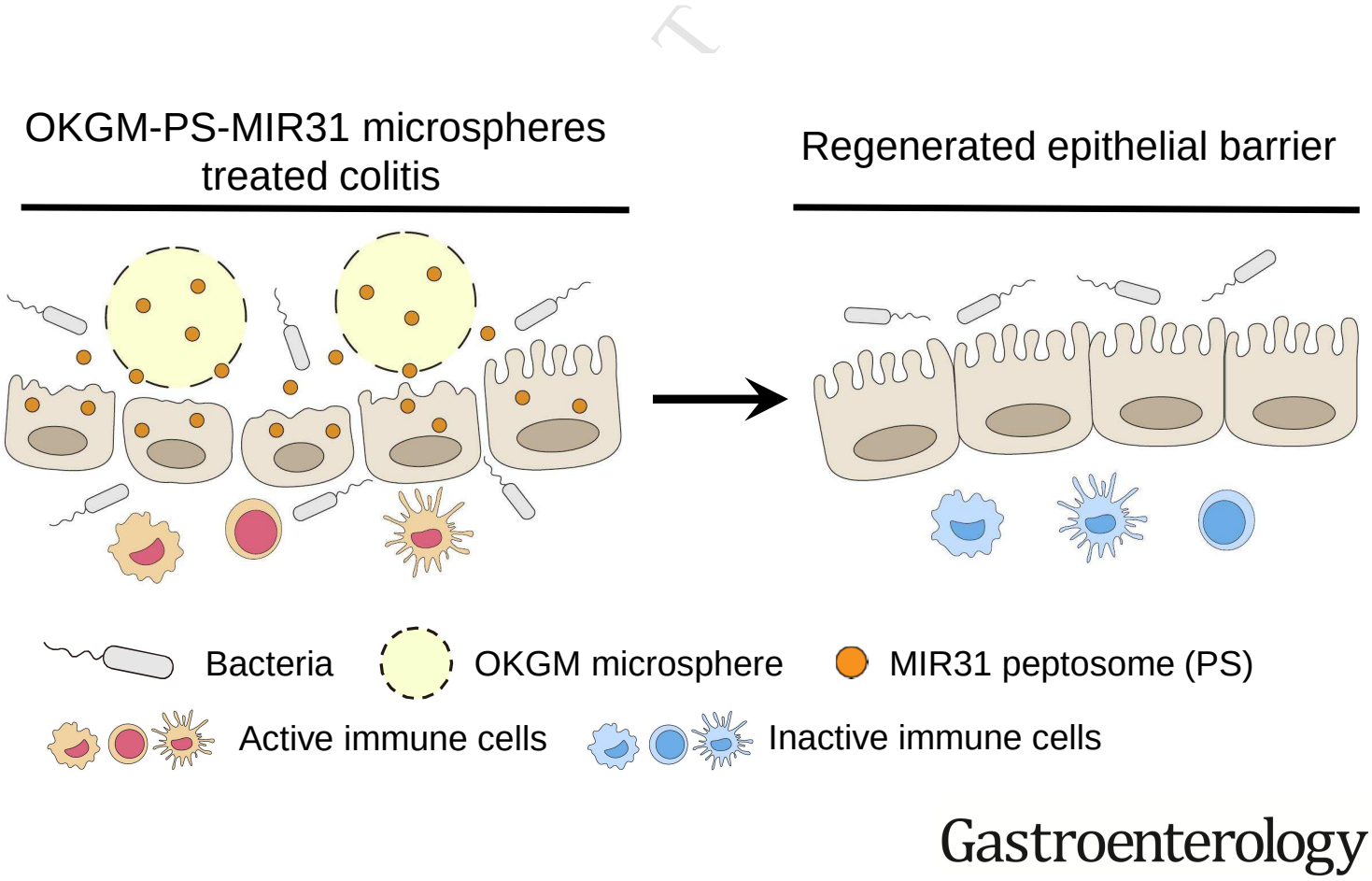
To appear in: *Gastroenterology*
Accepted Date: 13 February 2019

Please cite this article as: Tian Y, Xu J, Li Y, Zhao R, Du S, Lv C, Wu W, Liu R, Sheng X, Song Y, Bi X, Li G, Li M, Wu X, Lou P, You H, Cui W, Sun J, Shuai J, Ren F, Zhang B, Guo M, Hou X, Wu K, Xue L, Zhang H, Plikus MV, Cong Y, Lengner CJ, Liu Z, Yu Z, MicroRNA-31 Reduces Inflammatory Signaling and Promotes Regeneration in Colon Epithelium, and Delivery of Mimics in Microspheres Reduces Colitis in Mice, *Gastroenterology* (2019), doi: https://doi.org/10.1053/j.gastro.2019.02.023.

This is a PDF file of an unedited manuscript that has been accepted for publication. As a service to our customers we are providing this early version of the manuscript. The manuscript will undergo copyediting, typesetting, and review of the resulting proof before it is published in its final form. Please note that during the production process errors may be discovered which could affect the content, and all legal disclaimers that apply to the journal pertain.

ACCEPTED MANUSCRIPT





Gastroenterology

ACCEPTED MANUSCRIPT

MicroRNA-31 Reduces Inflammatory Signaling and Promotes Regeneration in Colon Epithelium, and Delivery of Mimics in Microspheres Reduces Colitis in Mice

Short title: Role of microRNA-31 in IBD

Yuhua Tian,[1#] **Jiuzhi Xu,**[1#] **Yuan Li,**[2#] Ran Zhao,[1] Sujuan Du,[1] Cong Lv,[1] Wei Wu,[3] Ruiqi Liu,[1] Xiaole Sheng,[1] Yongli Song,[1] Xueyun Bi,[1] Guilin Li,[1] Mengzhen Li,[1] Xi Wu,[1] Pengbo Lou, [1] Huiwen You,[4] Wei Cui,[1,5] Jinyue Sun,[6] Jianwei Shuai,[7] Fazheng Ren,[2] Bing Zhang,[8] Mingzhou Guo[9], Xiaohua Hou,[10] Kaichun Wu,[11] Lixiang Xue,[12] Hongquan Zhang,[13] Maksim V. Plikus,[14] Yingzi Cong,[15] Christopher J. Lengner,[16] Zhanju Liu,[3]* and Zhengquan Yu[1$]*

[1]State Key Laboratories for Agrobiotechnology and Beijing Advanced Innovation Center for Food Nutrition and Human Health and, College of Biological Sciences, China Agricultural University, Beijing, China; [2]Beijing Advanced Innovation Center for Food Nutrition and Human Health and, College of Food Sciences and nutritional engineering, China Agricultural University, Beijing, China; [3]Department of Gastroenterology, The Shanghai Tenth People's Hospital, Tongji University, Shanghai, China; [4]School of Pharmaceutical Sciences, Capital Medical University, Beijing, China; [5]Institute of Reproductive and Developmental Biology, Faculty of Medicine, Imperial College London, UK; [6]Institute of Agro-Food Science and Technology, Shandong Academy of Agricultural Sciences, Jinan, China; [7]Department of Physics and State Key Laboratory of Cellular Stress Biology, Innovation Center for Cell Signaling Network, Xiamen University, Xiamen, China; [8]College of Veterinary Medicine, China Agricultural University,

Beijing, China; [9]Division of Gastroenterology, Union Hospital，Tongji Medical College, Huazhong University of Technology and Science, Wuhan, China 430022; [10]Department of Gastroenterology and Hepatology, Chinese PLA General Hospital, Beijing, China; [11]Department of Gastroenterology, Xijing Hospital, The Fourth Military Medical University, Xi'an, China; [12]Medical Research Center. Department of Radiation Oncology, Peking University Third Hospital, Beijing, China; [13]Laboratory of Molecular Cell Biology and Tumor Biology, Department of Anatomy, Histology and Embryology, Beijing 100191, China.[14]Department of Developmental and Cell Biology, Sue and Bill Gross Stem Cell Research center, Center for Complex Biological Systems, University of California, Irvine, Irvine, CA, USA; [15]Department of Microbiology and Immunology, University of Texas Medical Branch, Galveston, TX; [16]Department of Biomedical Sciences, School of Veterinary Medicine, and Institute for Regenerative Medicine, University of Pennsylvania, Philadelphia, PA, USA

[#]Authors share the co-first authorship.

Funding

This work was funded by grants from the National Natural Science Foundation of China (81772984, 81572614, 81630017, 81740117); Beijing Nature Foundation Grant (5162018); the Major Project for Cultivation Technology (2016ZX08008001，2014ZX08008001); Basic Research Program

(2015QC0104, 2015TC041, 2016SY001, 2016QC086); SKLB Open Grant (2018SKLAB6-12).

Abbreviations used in this paper: IBD, inflammatory bowel disease; UC, ulcerative colitis; CD, Crohn's disease; DSS, dextran sulfate sodium. ChIP, chromatin immunoprecipitation; PS, peptosome; KO, Knockout; cKO, conditional knockout; OKGM, oxidized konjac glucomannan; α-La, α-lactalbumin; STAT3, signal transduction and activator of transcription 3; IECs, intestinal epithelial cells; RNAi, RNA interference; 3'UTR, 3' untranslated region; BrdU, bromodeoxyuridine; TNBS, 2,4,6-trinitrobenzene sulfonic acid; Mal, maleimide; CRP, C-reaction protein; ESR, erythrocyte sedimentation rate; UCEIS, ulcerative colitis endoscopic index of severity; CDAI, Corhn's disease activity index; SES-CD, simple endoscopic score for Crohn's disease values.

[$]Lead contact

***Co-corresponding authors:**

Address requests for reprints to: Zhengquan Yu, PhD

State Key Laboratories for Agrobiotechnology and Beijing Advanced Innovation Center for Food Nutrition and Human Health and, College of Biological Sciences, China Agricultural University, Yuanmingyuan West Rd. 2, Haidian District, Beijing, 100193, China, E-mail: zyu@cau.edu.cn;

Tel. 86-10-62734420; Fax: 86-10-62733904;

Zhanju Liu, MD, PhD,

Department of Gastroenterology, The Shanghai Tenth People's Hospital, Tongji University, Shanghai 200072, China; e-mail: liuzhanju88@126.com; fax: +86-21-66303983.

Conflicts of interests

The authors disclose no conflicts.

Transcript Profiling: GSE123556

Writing Assistance: NO

Author Contributions: ZY and YL designed project; YT, JX, YL, RZ, XB, SD, CL, XS, RL, WW, ZL, ML, XW, HY, GL, PL, BZ, YS performed research; WC, JS, JS, FR, KW, LX, HZ, MP, YC, XH, MG, HY, ZL, ZY analyzed data; YT, CL, ZY wrote manuscript.

Acknowledgements: The authors thank the members from the laboratory animal center in China Agricultural University for their assistance of animal care.

ACCEPTED MANUSCRIPT

Abstract

Background & Aims: Levels of microRNA 31 (MIR31) are increased in intestinal tissues from patients with inflammatory bowel diseases and colitis-associated neoplasias. We investigated the effects of this microRNA on intestinal inflammation by studying mice with colitis.

Methods: We obtained colon biopsy samples from 82 patients with ulcerative colitis (UC), 79 patients with Crohn's disease (CD), and 34 healthy individuals (controls) at Shanghai Tenth People's Hospital. MIR31- knockout mice and mice with conditional disruption of *Mir31* specifically in the intestinal epithelium (MIR31 conditional knockouts) were given dextran sulfate sodium (DSS) or 2,4,6-trinitrobenzene sulfonic acid (TNBS) to induce colitis. We performed chromatin immunoprecipitation (ChIP) and luciferase assays to study proteins that regulate expression of MIR31, including STAT3 and p65, in LOVO colorectal cancer cells and organoids derived from mouse colon cells. Partially hydrolyzed alpha-lactalbumin (alpha-La) was used to generate peptosome nanoparticles, and MIR31 mimics were loaded onto their surface using electrostatic adsorption. Peptosome–MIR31 mimic particles were encapsulated into oxidized konjac glucomannan (OKGM) microspheres, which were administered by enema into the large intestines of mice with DSS-induced colitis. Intestinal tissues were collected and analyzed by histology and immunohistochemistry.

Results: Levels of MIR31 were increased in inflamed mucosa from patients with CD or UC, and from mice with colitis, compared with controls. STAT3 and NF-□B activated transcription of MIR31 in colorectal cancer cells and organoids in response to TNF and IL6. MIR31-knockout and conditional-knockout mice developed more severe colitis in response to DSS and TNBS, with increased immune responses, compared to control mice. MIR31 bound to 3' untranslated regions of *Il17ra* and *Il7r* mRNAs (which encode receptors for the inflammatory cytokine IL17) and *Il16st* mRNA (which encodes GP130, a cytokine signaling protein). These mRNAs and proteins were greater in MIR31-knockout mice with colitis, compared with control mice; MIR31 and MIR31 mimics inhibited their expression. MIR31 also promoted epithelial regeneration by regulating the WNT and Hippo signaling pathways. OKGM peptosome–MIR31 mimic microspheres localized to colonic epithelial cells in mice with colitis; they reduced the inflammatory response, increased body weight and colon length, and promoted epithelial cell proliferation.

Conclusions: MIR31, increased in colon tissues from patients with CD or UC, reduces the inflammatory response in colon epithelium of mice by preventing expression of inflammatory cytokine receptors (Il7R and Il17RA) and signaling proteins (IL6ST). MIR31 also regulates the WNT and Hippo signaling pathways to promote epithelial regeneration following injury. OKGM peptosome–MIR31 microspheres localize to the colon epithelium of mice to reduce features of colitis.

KEY WORDS: IBD, nanoparticle deliver system, post-transcriptional processing, gene regulation

ACCEPTED MANUSCRIPT

Introduction

Inflammatory bowel disease (IBD), including ulcerative colitis (UC) and Crohn's disease (CD), encompasses chronic inflammatory diseases characterized by the submucosal accumulation of inflammatory cells and damage to the epithelial layer.[1] During inflammatory reaction, immune cells involving both innate and adaptive immunity secrete proinflammatory cytokines to promote mucosal immunity, consequently removing pathogen-infected cells.[2] Increasing evidence indicates that epithelial cells play a central role in regulating the immune response in the intestines. In response to inflammatory signals, intestinal epithelial cells (IECs) are exposed to many proinflammatory cytokines secreted by immune and stromal cells, and respond to these signals through numerous cell surface receptors including IL17RA, GP130, and IL7R.[2] IECs themselves also produce a variety of cytokines to modulate intestinal mucosal immunity. For example, when IL6 binds to its coreceptor GP130 to activate the STAT3 signaling pathway in IECs, it results in the production of proinflammatory cytokines.[3] In addition, epithelial IL17RA has been implicated in controlling autoimmune inflammation.[4] Thus, the cytokines secreted by both epithelial cells and immune cells are involved in a cellular cross-talk that promotes the activation of mucosal immunity. In addition to modulation of the immune system, epithelial cells play a fundamental and intrinsic role against IBD, i.e. restoration and maintenance of barrier function. Multiple signaling pathways, including the WNT, Notch, and Hippo pathways, have been identified to promote epithelial regeneration.[5-7] While some cytokines appear to concomitantly promote both

mucosal immunity and epithelial regeneration,[8] it is clear that the immunomodulatory and regenerative functions of the epithelium can be controlled by distinct signals,[9, 10] However, it is still not fully understood how the signals are coordinated in controlling the immune response and epithelial regeneration. Therefore, elucidating the precise molecular mechanisms coordinating inflammation and epithelial regeneration is fundamental for understanding IBD, and will provide avenues for therapeutic development.

Increasing evidence indicates that many miRNAs are altered in IBD, and play important roles in regulating the pathogenesis of IBD through the direct suppression of different functional targets.[11, 12] Among them, MIR31 is increased in IBD,[13, 14] and further up-regulated during the progression of inflammation-associated intestinal neoplasia.[15] Recently, we identified MIR31 as an important modulator of intestinal stem cells, promoting epithelial regeneration in response to DNA damaging injury by activating dormant stem cells that survive high-dose radiation exposure.[16] Furthermore, *in vitro* evidence indicates that MIR31 directly targets IL25 to regulate Th1/Th17 cell-mediated mucosal inflammation in colitis,[17] suggesting a critical role of MIR31 in inflammation. Therefore, we aimed to determine how MIR31 coordinates epithelial regeneration and the immune response *in vivo* in mouse models of IBD.

Our results showed that MIR31 was upregulated in IBD tissues, directly via the NF-κB and STAT3 signaling pathways. In turn, MIR31 attenuated the inflammatory response by directly targeting *Il17ra*, *Il7r* and *Il116st* (encoding Gp130) within the colonic epithelium, while concomitantly promoting epithelial

cell proliferation by regulating both WNT and Hippo signaling pathways. Moreover, we developed an MIR31-based microsphere delivery system that can suppress the inflammatory response and promote epithelial regeneration in experimental colitis, suggesting a viable therapeutic approach for the treatment of IBD.

ACCEPTED MANUSCRIPT

MATERIALS AND METHODS

Note: The full Materials and Methods section is included in the supplementary documents.

Subjects

All patients with IBD were recruited from the Department of Gastroenterology, Shanghai Tenth People's Hospital of Tongji University (Shanghai, China) from January 2017 to November 2018. The diagnosis of IBD was based on conventional clinical, radiological and endoscopic features and was finally confirmed by histological examination of intestinal biopsies. Inflamed ileal and/or colonic tissues were collected from 79 patients with CD and 82 patients with UC who underwent endoscopy. Biopsies were collected from sites of active inflammation adjacent to ulcerations or normal mucosa according to the experimental requirement. Macroscopically and microscopically unaffected ileal and/or colonic mucosa samples were also collected from 34 healthy controls. Clinical characteristics of patients with IBD and controls are shown in supplementary Table 1. This study was approved by the Institutional Review Board for Clinical Research of the Shanghai Tenth People's Hospital of Tongji University and the methods were carried out in accordance with the approved guidelines. Informed consent was obtained from all subjects.

Mouse Strains

The *MIR31*$^{-/-}$ and MIR31 floxed mice have been previously described[16, 18]. *Villin-Cre* mice were purchased from National Resource Center of Model Mice

(stock number: T000142). Axin2-LacZ mice were obtained from the Yi Zeng laboratory (Shanghai Institute of Biochemistry and Cell Biology). All mouse experiment procedures and protocols were evaluated and authorized by the Regulations of Beijing Laboratory Animal Management and were strictly in accordance with the guidelines of the Institutional Animal Care and Use Committee of China Agricultural University (approval number: SKLAB-2011-04-03).

Statistical Analysis

Most statistical analyses were performed in at least triplicate, and the means obtained were used for independent t-tests. Means and standard deviations from at least three independent experiments are presented in all graphs. Asterisks denote statistical significance (*P < .05; **P < .01; ***P < .001). Statistical analysis was performed using one-way analysis of variances (ANOVA) for Figure 1*A*. Pearson's correlation analysis was performed for Figure 1*C* and *D*.

ACCEPTED MANUSCRIPT

Results

MIR31 is increased in inflamed mucosa of IBD and regulated by the STAT3 and NF-κB signaling pathways

To determine the role of MIR31 in the pathogenesis of IBD, we examined MIR31 expression in human samples from active UC and CD patients, as well as disease in remission. We found that MIR31 was dramatically upregulated in the inflamed mucosa of active UC and CD patients, and reduced to the levels similar to unaffected controls in patients in remission (**Figure 1*A***). Compared to unaffected mucosa, MIR31 was significantly upregulated in the inflamed mucosa from the same patients (**Figure 1*B***). *In situ* hybridization also showed that MIR31 expression was elevated in inflamed mucosa from both CD (n=10) and UC (n= 10) patients relative to unaffected controls (**Supplementary Figure 1*A***). The levels of MIR31 expression in inflamed intestinal mucosa were positively correlated to the values of CRP (C-reaction protein), ESR (erythrocyte sedimentation rate), Mayo score, and UCEIS (ulcerative colitis endoscopic index of severity) in UC patients, and the values of CRP, ESR, CDAI (Crohn's disease activity index), and SES-CD (simple endoscopic score for Crohn's disease) in CD patients, respectively (**Figure 1*C* and *D***). We next employed dextran sulfate sodium (DSS) in drinking water to induce experimental colitis in mice. We observed a dramatic upregulation of MIR31 in inflamed colon following DSS treatment (**Figure 1*E* and *F***). Two days after DSS withdrawal following a 5-day pulse, MIR31 expression rapidly decreased, returning to the pretreatment baseline (**Figure 1*E***). We found that MIR31 expressed predominantly in colonic

epithelial cells; however DSS-induced MIR31 expression was also observed in leukocytes and stromal cells (**Supplementary Figure 1*B***). We previously identified one STAT3 and two NF-κB binding sites in the promoter of MIR31 (**Supplementary Figure 1*C***).[16, 18] Thus, we investigated whether the induction of MIR31 was due to the activation of these signaling pathways. In response to DSS treatment, both STAT3 and NF-κB pathways were activated in the colon (**Supplementary Figure 1*D***). To test whether the STAT3 and NF-κB activities induce MIR31 expression, we treated LOVO colorectal cancer cells with IL6 and TNF to stimulate STAT3 and NF-κB signaling, respectively. We found that TNF induced MIR31 expression concomitant with NF-κB pathway activation (**Supplementary Figure 1*E***). Similarly, MIR31 expression was induced in response to IL6 treatment concomitant with STAT3 pathway activation (**Supplementary Figure 1*F***). Conversely, knockdown of STAT3 with siRNA suppressed MIR31 expression (**Supplementary Figure 1*G***). To eliminate the possibility that these effects were influenced by the malignant LOVO cells, we also verified that MIR31 was induced in primary mouse colon organoids in response to TNF and IL6 (**Supplementary Figure 1*H***). Luciferase reporter assays revealed that mutation of p-STAT3 or p65 (the transcriptional effector of NF-κB signaling) binding sites blocked the reporter activity of MIR31 (**Supplementary Figure 1*I***), and chromatin immunoprecipitation (ChIP) further proved that p-STAT3 and p65 interact with their binding sites in the MIR31 promoter (**Supplementary Figure 1*J***). Taken together, these findings indicate that the STAT3 and NF-κB signaling pathways directly mediate the induction of

MIR31 in IBD.

Loss of MIR31 exacerbates the inflammatory response and delays epithelial regeneration

Next, we examined the effect of MIR31 loss on the colon utilizing both MIR31 germline knockout (KO) and *Villin-Cre*-driven colonic epithelial conditional KO (cKO) mice (**Supplementary Figure 2*A***). We have previously shown that these mice have no apparent gross phenotypes.[16] The colon length was not significantly altered in MIR31 KO and cKO mice as compared to the controls (**Supplementary Figure 2*B***). No significant difference was found in cell proliferation in crypts, apoptosis at the tip, or the number of Goblet cells between WT and KO mice (**Supplementary Figure 2*C-I***).

To further assess the role of MIR31 in colitis, we induced colitis in both WT and MIR31 KO mice by administering DSS in drinking water. DSS was administered for 5 days, followed by 3 days of recovery. After 4 days of DSS treatment, *MIR31*$^{-/-}$ mice exhibited considerably more weight loss than WT mice and showed no weight recovery upon termination of the treatment (**Figure 2*A***). This was accompanied by a lower survival rate (**Figure 2*B***), shorter colon length (**Figure 2*C* and *D***), larger spleens (**Figure 2*C* and *D***), and higher clinical disease scores (**Figure 2*E***) compared with controls. A time-course analysis showed a severe inflammatory response upon DSS treatment and an impaired regenerative response after DSS removal in *MIR31*$^{-/-}$ mice (**Figure 2*F***). A reduction in proliferative epithelial cells was found in *MIR31*$^{-/-}$ mice (**Figure 2*G***), which was further confirmed by BrdU (Bromodeoxyuridine) incorporation assay

(**Supplementary Figure 3*A* and *C***). In contrast, the number of apoptotic cells was markedly increased in the colonic epithelium of *MIR31*$^{-/-}$ mice (**Supplementary Figure 3*B* and *D***). There was also a decrease in the number of Goblet cells in *MIR31*$^{-/-}$ colonic epithelium upon DSS treatment (**Supplementary Figure 3*E***). Furthermore, permeability assays revealed reduced barrier function in the colonic epithelium of *MIR31*$^{-/-}$ mice following 3 days of DSS treatment (**Supplementary Figure 3*F***). Similar consequences of MIR31 deletion were also found in another model of 2,4,6-trinitrobenzene sulfonic acid (TNBS) induced colitis in mice (**Supplementary Figure 4*A*-*G***). In contrast, MIR31 overexpression inhibited colitis in TNBS-induced murine colitis (**Supplementary Figure 5*A*-*F***). Furthermore, MIR31 deletion also resulted in exacerbated inflammatory response in TNBS-induced chronic colitis in mice (**Supplementary Figure 6*A*-*E***). Taken together, our results demonstrate that MIR31 plays a key role in suppressing the inflammatory response and promoting epithelial regeneration in colitis.

We next characterized the enhanced immune response in *MIR31*$^{-/-}$ mice after DSS treatment. We found increased numbers of leukocytes and macrophages (**Figure 3*A* and *B***), increased levels of proinflammatory cytokines and inflammasome components, and decreased levels of the inflammatory suppressor IL10 in *MIR31*$^{-/-}$ mice upon DSS treatment (**Figure 3*C*-*G***). Consistently, the proinflammatory NF-κB and STAT3 signaling pathways were overactivated in *MIR31*$^{-/-}$ mice (**Figure 3*H* and *I***). Our findings demonstrate that loss of MIR31 results in a hyperactive immune reaction to DSS treatment.

To test whether the phenotypes observed upon MIR31 loss were of

epithelial origin, we examined the phenotypes of *Villin-Cre;MIR31*$^{fl/fl}$ (cKO) mice upon DSS treatment. Similar to the *MIR31*$^{-/-}$ mice, cKO mice exhibited enhanced immune response and delayed regeneration in response to DSS treatment (**Supplementary Figure 7*A-F* and Supplementary Figure 8*A-D***), implying an epithelial cell-autonomous role of MIR31.

MIR31 directly suppresses the expression of *Il6st* (encoding GP130), *Il7r* and *Il17ra* within colonic epithelium.

To understand how MIR31 suppresses the immune response in the colonic epithelium, we analyzed MIR31 binding sites in 3' untranslated regions (3'UTRs) of transcripts encoding proteins involved in the intestinal immune response using TargetScan algorithms. Genes containing MIR31 binding sites include *Il6st* (encoding GP130), *Il7r* and *Il17ra* (**Supplementary Figure 9*A***). The RNA and protein levels of *Il6st*, *Il7r* and *Il17ra* were significantly increased in the colon of *MIR31*$^{-/-}$ mice after DSS treatment (**Figure 4*A* and *B***). The numbers of GP130^{+}, IL7R^{+} and IL17RA^{+} cells were significantly increased in *MIR31*$^{-/-}$ colon following 5 days of DSS treatment (**Figure 4*C-F***). Additionally, *in vitro* analysis revealed that MIR31 mimics inhibited the expression of *Il6st*, *Il7r* and *Il17ra*, while MIR31 inhibitors promoted their upregulation (**Figure 4*G***), suggesting that these putative target genes are regulated by MIR31 in a cell autonomous manner. 3'UTR-Luciferase reporter assays revealed that MIR31 mimics significantly suppressed wild type *Il6st*, *Il7r* and *Il17ra* 3'UTR activity but had no significant influence on the reporters in which the MIR31 binding site was mutated (**Figure**

4*H* and Supplementary Figure 9*B*). Expression of *Il6st*, *Il7r* and *Il17ra* declined over the course of DSS treatment (**Figure 4*I* and *J***), inversely correlating to the MIR31 level. The upregulation of these MIR31 target genes was further validated in cKO colon (**Figure 4*K* and *L***). The reduction in GP130 was also found in human UC tissue (**Figure 4*M***). Together, our findings demonstrate that transcripts of *Il6st*, *Il7r* and *Il17ra* are direct targets of MIR31, and that their regulation may account for the effect of MIR31 in repression of the immune reaction in intestinal mucosa.

MIR31 promotes epithelial regeneration by directly regulating WNT and Hippo signaling

To investigate the molecular mechanisms of MIR31 regulation of immune reaction and epithelial regeneration, we compared colonic epithelial cells transcriptomes between WT (n=3) and *MIR31*$^{-/-}$ (n=3) mice. We defined the differentially expressed genes (DEGs) as those with $P < .05$ and fold change > 1.5. This approach yielded 178 downregulated genes and 285 upregulated genes in *MIR31*$^{-/-}$ mouse (**Supplementary Figure 10*A***). The enriched KEGG pathways included Complement and coagulation, Sphingolipid metabolism, TGFβ and WNT signaling pathways (**Supplementary Figure 10*B***). Of them, activity of the canonical WNT pathway is a major driving force for epithelial regeneration after injury[19]. We recently demonstrated that MIR31 promotes the proliferative expansion of small intestinal stem cells by activating WNT signaling[16]. We thus examined the effect of MIR31 on WNT activity in DSS-induced colitis. We utilized

Axin2-LacZ reporter mice as a proxy for activity of the canonical WNT pathway and observed that reporter activity was activated throughout the colonic epithelium in WT mice before or after 5-day DSS treatment, while its activity was markedly reduced in the *MIR31*$^{-/-}$ colon (**Figure 5*A* and Supplementary Figure 11*A***). Consistently, the expression levels of *Ctnnb1* (encoding β-catenin) and the WNT target genes, *Ccnd1* (encoding *cyclin D1)* and *Axin2*, were significantly reduced in the colon of *MIR31*$^{-/-}$ mice both at the RNA and protein levels after DSS treatment (**Figure 5*B* and Supplementary Figure 11*B***). Additionally, the RNA and/or protein expression levels of *Ccnd1* and *Axin2* were significantly downregulated in LOVO cells upon MIR31 inhibition (**Supplementary Figure 11*C***), while the expression of these genes was markedly increased in MIR31-overexpressing cells (**Supplementary Figure 11*D***), suggesting a direct effect of MIR31 on WNT activity. Wnt antagonists *Axin1*, *Gsk3β* and *Dkk1* have been identified as MIR31 targets in intestinal stem cells (**Supplementary Figure 9*A***)[16]. In agreement, the levels of these Wnt antagonists were upregulated in the colon of *MIR31*$^{-/-}$ mice after 5 days of DSS treatment (**Figure 5*C* and Supplementary Figure 11*E***). In contrast, a reduction in DKK1 and AXIN1 was observed in human UC samples (**Supplementary Figure 11*F***). *In vitro* assays also showed that the expression of these putative target genes was upregulated upon treatment with MIR31 inhibitors (**Figure 5*D***), and downregulated in response to MIR31 mimics (**Supplementary Figure 11*G***). 3'UTR-luciferase reporter assays revealed that MIR31 mimics significantly suppressed WT *Axin1*, *Gsk3b* and *Dkk1* 3'UTR activity but had no significant influence on the reporters in which the

MIR31 binding site was mutated (**Figure 5*E* and Supplementary Figure 9*B***). Thus, our findings indicate that MIR31 activates WNT signaling pathway by directly suppressing Wnt antagonists *Axin1*, *Gsk3b* and *Dkk1* in DSS-induced colitis, consequently promoting epithelial regeneration.

The Hippo signaling pathway is essential for tissue regeneration in the colon after DSS-mediated injury[6]. We found that the Yap::pYap ratio was reduced in the colon of *MIR31*$^{-/-}$ mice before DSS treatment (**Supplementary Figure 12*A***), becoming more pronounced after 5 days of DSS treatment (**Figure 5*F***), suggesting an activation of the Hippo signaling pathway in *MIR31*$^{-/-}$ mice. Consistently, the number of Yap^{+} cells within colonic epithelium was significantly reduced after DSS treatment (**Figure 5*G* and Supplementary Figure 12*B***). Furthermore, we found that MIR31 mimics increased the Yap::pYap ratio in LOVO cells (**Supplementary Figure 12*C***), whereas MIR31 inhibition decreased it (**Figure 5*H***), suggesting a direct effect of MIR31 on Hippo activity. *Ctgf*, *Cyr61* and *Ankrd1* are well-characterized Yap target genes,[20] and their expression was decreased after 5 days of DSS treatment in the *MIR31*$^{-/-}$ mice (**Supplementary Figure 12*D***). *In vitro,* MIR31 inhibitors significantly suppressed these Yap target genes, while MIR31 mimics promoted them (**Supplementary Figure 12*E* and *F***). Taken together, both *in vivo* and *in vitro* findings demonstrate that MIR31 represses the Hippo signaling pathway during DSS-induced colitis.

To understand how MIR31 regulates Hippo signaling, we analyzed MIR31 binding sites in the 3'UTRs of transcripts encoding inhibitors of Hippo pathway using TargetScan algorithms. We found that the 3'UTR in transcripts of *Lats2,*

Dlg1 and *Dlg5* included MIR31 binding sites (**Supplementary Figure 9*A***), and the RNA and protein levels of *Lats2, Dlg1* and *Dlg5* were up-regulated in the colon of *MIR31*$^{-/-}$ mice after DSS treatment (**Figure 5*I***), as well as in LOVO cells treated with MIR31 inhibitors (**Supplementary Figure 12*G***). Conversely, MIR31 mimics suppressed their expression (**Supplementary Figure 12*G***). The numbers of Dlg1^{+} and Lats2^{+} cells were increased in MIR31 cKO colonic epithelium following 5 days of DSS treatment (**Figure 5*J***). 3'UTR-luciferase reporter assays revealed that MIR31 mimics significantly repressed WT *Lats2, Dlg1* and *Dlg5* 3'UTR activity, but had no significant influence on the reporters in which the MIR31 binding site was mutated (**Figure 5*K* and Supplementary Figure 9*B***). These findings indicate that *Lats2, Dlg1* and *Dlg5* transcripts are direct targets of MIR31, accounting for the effect of MIR31 suppressing Hippo signaling pathway. Collectively, our data demonstrate that MIR31 promotes epithelial regeneration by regulating WNT and Hippo signaling pathways during DSS-induced colitis. Furthermore, the alteration of MIR31 mediated-WNT and -Hippo signaling pathways was further confirmed in TNBS-induced murine colitis (**Supplementary Figure 13*A*-*F***).

MIR31-based OKGM-PS microsphere delivery is sufficient to alleviate DSS-induced inflammation

microRNA-based nanodelivery systems have garnered significant interest as therapeutic strategies for a variety of diseases, including IBD.[21] To determine the feasibility of targeting MIR31 with nanoparticles in colitis, we designed a

protein-based, encapsulating microsphere as a MIR31 mimics delivery system (**Figure 6*A***). In this system, α-lactalbumin (α-La) is partially hydrolyzed at Glu and Asp sites to produce amphiphilic peptides, which can self-assemble into approximately 20 nm peptosomes (PSs)[22] with numerous negatively charged carboxyl groups (**Figure 6*B* and *C***). To attach MIR31 mimics via electrostatic adsorption, we utilized maleimide (Mal) to reverse the zeta potential on the surface of PSs (**Figure 6*C***). The size (diameter) and zeta potential of PS+Mal were stable over time (**Figure 6*D-F***). MIR31 mimics were then loaded onto α-La PSs using Mal (**Figure 6*G***). The MIR31 mimic-loaded PS (PS-MIR31) nanoparticles exhibited low cytotoxicity (**Figure 6*H***) and were capable of delivering MIR31 into cells (**Figure 6*I***). To avoid rapid degradation of the peptide-based nanoparticles in the gut, we encapsulated them inside microspheres formed by cross-linking the carboxyl-abundant TEMPO-oxidized konjac glucomannan (OKGM) with Fe^{3+} ions (OKGM-PS-MIR31) (**Figure 6*J***). The size of OKGM-PS-MIR31 microspheres ranged from 10 to 50 μm (**Figure 6*J***). The OKGM-PS-MIR31 microspheres were then administered by enema to examine their therapeutic effect *in vivo*. We found that OKGM-PS-MIR31 can release PS-MIR31 into colonic epithelial cells (**Figure 6*K***), leading to an increase in MIR31 levels (**Figure 6*K***), while OKGM-PS exhibited no toxicity (**Supplementary Figure 14**).

We ultimately tested whether the OKGM-PS-MIR31 microspheres could rescue the phenotypes of *MIR31*$^{-/-}$ mice in the process of DSS-induced colitis. We fed the *MIR31*$^{-/-}$ mice drinking water with 3.5% DSS, and concomitantly

administered OKGM-PS-MIR31 microspheres to the large bowel. Compared to treatment with OKGM-PS negative controls, treatment with OKGM-PS-MIR31 microspheres resulted in a slower loss of body weight and abrogated colon shortening (**Supplementary Figure 15*A*-*C***). The OKGM-PS-MIR31 microsphere-treated *MIR31*$^{-/-}$ mice also exhibited reduced inflammation and increased epithelial cell proliferation (**Supplementary Figure 15*D* and *E***). These findings indicate that the OKGM-PS-MIR31 microspheres can significantly rescue DSS colitis-associated phenotypes in *MIR31*$^{-/-}$ mice. We next sought to test the preventative effect of OKGM-PS-MIR31 microspheres against DSS-induced colitis in WT mice. Strikingly, OKGM-PS-MIR31 microspheres alleviated inflammation and the impairment of colonic epithelial integrity, as indicated by an increased body weight, reduced immune response, longer colon length, and increased epithelial cell proliferation (**Figure 7*A*-*G***). Consistent with our previous findings, WNT and Hippo signaling pathways were altered in the colon of OKGM-PS-MIR31-treated mice (**Figure 7*G* and Supplementary Figure 16*A* and *B***), while MIR31 target genes were reduced (**Figure 7*H* and Supplementary Figure 16*C***). To test its therapeutic efficacy of this system, we first established acute colitis in mice and then treated with OKGM-PS-MIR31 microspheres. The recovery of body weight and colon length were significantly enhanced in OKGM-PS-MIR31-treated mice (**Supplementary Figure 17*A*-*D***), concomitant with an organized colonic histology, a reduced inflammatory response and increased epithelial cell proliferation (**Supplementary Figure 17*E*-*G***), as well as Hippo signaling pathway suppression and downregulation of MIR31 target gene

expression (**Supplementary Figure 17*H* and *I***). These phenotypes were consistent with the recovery from colitis caused by MIR31 *in vivo* overexpression (**Supplementary Figure 18*A-F***), reflecting a high efficiency of OKGM-PS-MIR31 microsphere in delivering MIR31 mimics. These findings indicated that OKGM-PS-MIR31 microspheres are effective in treating active colitis in mice. Taken together, our findings suggest that OKGM-PS-MIR31 microspheres might be a potent therapeutic approach for treating IBD.

Discussion

Here, we demonstrated that MIR31 expression was highly induced in IBD and in experimental murine colitis through activation of NF-κB and STAT3 signaling. In turn, inflammatory signal-induced MIR31 expression suppressed the immune response of epithelial cells by inhibiting multiple receptors including GP130, IL17RA and IL7R, and concomitantly promoted the regenerative capacity of epithelial cells by regulating WNT and Hippo signaling pathways (**Supplementary Figure 19**).

Epithelial cells are known to enhance mucosal immunity by producing proinflammatory cytokines in the inflammatory reaction.[2] Multiple receptors such as GP130, IL17RA and IL7R have been localized to the colonic/intestinal epithelium[3, 23, 24] and found to respond to signals from immune cells. Among them, IL7/IL7RA and IL6/GP130 can activate STAT3 signaling,[3, 25] which is critical for immune function in the epithelium.[26] The interaction between epithelia

and immune cells is necessary to rapidly promote mucosal immunity. However, an exacerbated immune response can lead to epithelial barrier dysfunction.[10] Our findings indicate that MIR31 suppresses the immune response in the epithelium through a negative-feedback loop.

Conversely, MIR31 also promotes epithelial regeneration through the WNT and Hippo signaling pathways.[5-7] Consistent with our findings, previous studies have demonstrated that knockdown of the Wnt antagonist *Dkk1* (a target of MIR31) promotes recovery from intestinal inflammation during acute colitis.[7] Taken together, our findings identified MIR31 as a critical regulator in suppressing immune response and promoting epithelial regeneration in the inflamed epithelium characteristic of IBD.

Given our findings, MIR31 is an attractive candidate for therapeutic strategies for IBD. We therefore developed an MIR31-based nanosystem capable of alleviating DSS-induced colitis in mice. To the best of our knowledge, this represents the first miRNA-based nanosystem for IBD treatment. RNA interference (RNAi)-based nanosystems for treating IBD are increasingly emerging. Among them, TNF is often selected as a RNAi target[27-29]. Although TNF plays an important role in promoting the immune response, the knockdown of TNF is not sufficient to suppress the inflammatory reaction due to the redundant effects of other proinflammatory cytokines. In comparison, the MIR31-based nanosystem can concomitantly target at least nine genes including *Il6st* (encoding GP130), *Il7r*, *Il17ra*, *Axin1*, *Gsk3b*, *Dkk1*, *Lats2, Dlg1* and *Dlg5*, making it a more powerful strategy for alleviating inflammation in IBD. To deliver

MIR31 efficaciously, we developed a system consisting of OKGM-microsphere containing α-La PSs to release MIR31 mimics, which was characterized by safe, effective, degradable and capable of slow release. The α-La peptide has been previously described as a safe drug carrier for breast cancer treatment.[22] In our study, MIR31 mimic-loaded PS nanoparticles were protected by larger OKGM microspheres to avoid rapid degradation of PSs and MIR31. The OKGM-PS-MIR31 microspheres were found more stable than liposome- and polysaccharide-based nanoparticles, which are easily degraded by enzymes in the gut.[30, 31] Compared with synthetic polymer-based nanocarriers[32], OKGM-PS-MIR31 microspheres have no stimulatory effects on the immune system and exhibit low toxicity. Therefore, OKGM-PS-MIR31 microspheres represent a safe and effective system with high potential for treating IBD.

ACCEPTED MANUSCRIPT

References:

1. Kim DH, Cheon JH. Pathogenesis of Inflammatory Bowel Disease and Recent Advances in Biologic Therapies. Immune Netw 2017;17:25-40.
2. Neurath MF. Cytokines in inflammatory bowel disease. Nat Rev Immunol 2014;14:329-42.
3. Ernst M, Thiem S, Nguyen PM, et al. Epithelial gp130/Stat3 functions: an intestinal signaling node in health and disease. Semin Immunol 2014;26:29-37.
4. Kumar P, Monin L, Castillo P, et al. Intestinal Interleukin-17 Receptor Signaling Mediates Reciprocal Control of the Gut Microbiota and Autoimmune Inflammation. Immunity 2016;44:659-671.
5. Kuhnert F, Davis CR, Wang HT, et al. Essential requirement for Wnt signaling in proliferation of adult small intestine and colon revealed by adenoviral expression of Dickkopf-1. Proc Natl Acad Sci U S A 2004;101:266-71.
6. Deng F, Peng L, Li Z, et al. YAP triggers the Wnt/beta-catenin signalling pathway and promotes enterocyte self-renewal, regeneration and tumorigenesis after DSS-induced injury. Cell Death Dis 2018;9:153.
7. Koch S, Nava P, Addis C, et al. The Wnt antagonist Dkk1 regulates intestinal epithelial homeostasis and wound repair. Gastroenterology 2011;141:259-68, 268 e1-8.
8. Kuhn KA, Manieri NA, Liu TC, et al. IL-6 stimulates intestinal epithelial proliferation and repair after injury. PLoS One 2014;9:e114195.
9. Okamoto R, Watanabe M. Role of epithelial cells in the pathogenesis and treatment of inflammatory bowel disease. J Gastroenterol 2016;51:11-21.
10. Martini E, Krug SM, Siegmund B, et al. Mend Your Fences: The Epithelial Barrier and its Relationship With Mucosal Immunity in Inflammatory Bowel Disease. Cell Mol Gastroenterol Hepatol 2017;4:33-46.
11. Wu F, Zikusoka M, Trindade A, et al. MicroRNAs are differentially expressed in ulcerative colitis and alter expression of macrophage inflammatory peptide-2 alpha. Gastroenterology 2008;135:1624-1635 e24.
12. Tili E, Michaille JJ, Piurowski V, et al. MicroRNAs in intestinal barrier function, inflammatory bowel disease and related cancers-their effects and therapeutic potentials. Curr Opin Pharmacol 2017;37:142-150.
13. Schaefer JS, Attumi T, Opekun AR, et al. MicroRNA signatures differentiate Crohn's disease from ulcerative colitis. BMC Immunol 2015;16:5.
14. **Beres NJ**, **Kiss Z**, Sztupinszki Z, et al. Altered mucosal expression of microRNAs in pediatric patients with inflammatory bowel disease. Dig Liver Dis 2017;49:378-387.
15. Olaru AV, Selaru FM, Mori Y, et al. Dynamic changes in the expression of MicroRNA-31 during inflammatory bowel disease-associated neoplastic transformation. Inflamm Bowel Dis 2011;17:221-31.

16. **Tian Y**, **Ma X**, **Lv C**, et al. Stress responsive miR-31 is a major modulator of mouse intestinal stem cells during regeneration and tumorigenesis. Elife 2017;6.
17. Shi T, Xie Y, Fu Y, et al. The signaling axis of microRNA-31/interleukin-25 regulates Th1/Th17-mediated inflammation response in colitis. Mucosal Immunol 2017;10:983-995.
18. **Lv C**, **Li F**, **Li X**, **Tian Y**, et al. MiR-31 promotes mammary stem cell expansion and breast tumorigenesis by suppressing Wnt signaling antagonists. Nat Commun 2017;8:1036.
19. Clevers H, Loh KM, Nusse R. Stem cell signaling. An integral program for tissue renewal and regeneration: Wnt signaling and stem cell control. Science 2014;346:1248012.
20. Yu FX, Zhao B, Panupinthu N, et al. Regulation of the Hippo-YAP pathway by G-protein-coupled receptor signaling. Cell 2012;150:780-91.
21. Chen WX, Ren LH, Shi RH. Implication of miRNAs for inflammatory bowel disease treatment: Systematic review. World J Gastrointest Pathophysiol 2014;5:63-70.
22. Li Y, Li W, Bao W, et al. Bioinspired peptosomes with programmed stimuli-responses for sequential drug release and high-performance anticancer therapy. Nanoscale 2017;9:9317-9324.
23. Zhang Z, Zheng M, Bindas J, et al. Critical role of IL-17 receptor signaling in acute TNBS-induced colitis. Inflamm Bowel Dis 2006;12:382-8.
24. Shalapour S, Deiser K, Kuhl AA, et al. Interleukin-7 links T lymphocyte and intestinal epithelial cell homeostasis. PLoS One 2012;7:e31939.
25. Palmer MJ, Mahajan VS, Trajman LC, et al. Interleukin-7 receptor signaling network: an integrated systems perspective. Cell Mol Immunol 2008;5:79-89.
26. Han J, Theiss AL. Stat3: friend or foe in colitis and colitis-associated cancer? Inflamm Bowel Dis 2014;20:2405-11.
27. **Zhang Y**, **Cristofaro P**, **Silbermann R**, et al. Engineering mucosal RNA interference in vivo. Mol Ther 2006;14:336-42.
28. Laroui H, Theiss AL, Yan Y, et al. Functional TNFalpha gene silencing mediated by polyethyleneimine/TNFalpha siRNA nanocomplexes in inflamed colon. Biomaterials 2011;32:1218-28.
29. Kriegel C, Amiji MM. Dual TNF-alpha/Cyclin D1 Gene Silencing With an Oral Polymeric Microparticle System as a Novel Strategy for the Treatment of Inflammatory Bowel Disease. Clin Transl Gastroenterol 2011;2:e2.
30. Xue HY, Guo P, Wen WC, et al. Lipid-Based Nanocarriers for RNA Delivery. Curr Pharm Des 2015;21:3140-7.
31. Chourasia MK, Jain SK. Polysaccharides for colon targeted drug delivery. Drug Deliv 2004;11:129-48.
32. Frede A, Neuhaus B, Klopfleisch R, et al. Colonic gene silencing using siRNA-loaded calcium phosphate/PLGA nanoparticles ameliorates intestinal inflammation in vivo. J Control Release 2016;222:86-96.

ACCEPTED MANUSCRIPT

Author names in bold designate shared co-first authorship

ACCEPTED MANUSCRIPT

Figure Legends

Figure 1 MIR31 expression is upregulated in human IBD and mouse colitis. (*A*) MIR31 expression was significantly increased in inflamed mucosa of IBD patients. Total RNA was isolated from intestinal biopsies of healthy controls (HC, n = 34), inflamed mucosa of patients with active UC (A-UC, n = 45) or active CD (A-CD, n = 41), and intestinal mucosa of UC patients with remission (R-UC, n = 37) or CD patients with remission (R-CD, n = 38). MIR31 expression was analyzed by qRT-PCR and normalized to U6. ***$P < .001$. Statistical analysis was performed using one-way analysis of variances (ANOVA). (*B*) Expression of MIR31 in inflamed and unaffected mucosa from the same IBD patients. Total RNA was extracted from freshly obtained inflamed and unaffected mucosal biopsies from 15 CD and 18 UC patients, and analyzed for MIR31 expression by qRT-PCR. Statistical analysis was performed using paired t-test. ***$P < .001$. (C) Pearson's correlation analysis was performed between the relative levels of MIR31 expression of intestinal mucosa and CRP (C-reaction protein), ESR (erythrocyte sedimentation rate), Mayo score, and UCEIS (ulcerative colitis endoscopic index of severity) from 52 UC patients (Spearman's rank correlation coefficient, R = .5513, $P < .0001$ for CRP; R = .5060, $P < .0001$ for ESR; R = .4824, $P < .0001$ for Mayo score; R = .5982, $P < .0001$ for UCEIS). (D) Pearson's correlation analysis was performed between the relative levels of MIR31 expression of intestinal mucosa and CRP, ESR, CDAI (Corhn's disease activity index), SES-CD (simple endoscopic score for Crohn's disease values) from 69 CD patients (Spearman's rank correlation coefficient, R = .6514, $P < .0001$ for

CRP; R = .6620, *P* < .0001 for ESR; R = .6507, *P* < .0001 for CDAI; R = .5614, *P* < .0001 for SES-CD). (*E*) qRT-PCR for MIR31 in colonic epithelium at indicated time points after DSS treatment. n = 4 at each time points. Statistical analysis was performed using paired t-test. ***P* < .01; ****P* < .001. (*F*) *In situ* hybridization for *MIR31* in colons with or without a 5-day DSS treatment. *MIR31*$^{-/-}$ colon was used as a negative control. Scale bar: 50 μm. The dashed boxes indicated the high magnification images in the bottom panel.

Figure 2. Exacerbated immune response and impaired epithelial regeneration in *MIR31*$^{-/-}$ mice following DSS treatment. (*A*) Quantification of weight loss in WT and *MIR31*$^{-/-}$ littermates after DSS treatment. n = 11 biological replicates for each genotype. **P* < .05; ***P* < .01. (*B*) Survival curve of WT and *MIR31*$^{-/-}$ mice after DSS treatment. n = 25 biological replicates for both WT and *MIR31*$^{-/-}$ mice. ****P* < .001. (*C*) Representative gross images of colon and spleen from WT and *MIR31*$^{-/-}$ littermates following 5 days of DSS treatment. WT, n = 9; *MIR31*$^{-/-}$ mice, n = 9. (*D*) Quantification of colon length and spleen weight in Panel C. ***P* < .01. (*E*) Quantification of the clinical scores in WT and *MIR31*$^{-/-}$ mice after DSS treatment. WT, n = 7; *MIR31*$^{-/-}$, n = 7. **P* < .05; ****P* < .001. (*F*) Histological images of colonic tissue from WT and *MIR31*$^{-/-}$ mice at the indicated time points after DSS treatment. WT, n ≥ 6 at each timepoint; *MIR31*$^{-/-}$, n ≥ 6 at each timepoint. Scale bar: 50 μm. (*G*) Double immunofluorescence for Ki67 and β-catenin in colon from WT and *MIR31*$^{-/-}$ littermates at indicated time points following DSS treatment. WT, n ≥ 6 at each time point; *MIR31*$^{-/-}$ mice, n ≥ 6 at

each time point. Scale bar: 50 μm. Statistical analysis was performed using independent *t*-test for panels A, B, D, E.

Figure 3. Mucosal immunity is hyper-reactive in *MIR31*$^{-/-}$ mice following DSS treatment. (*A* and *B*) Immunofluorescence for CD45 (*A*) and F4/80 (*B*) in the colon from control and *MIR31*$^{-/-}$ mice following 5 days of DSS treatment. n = 4. Scale bar: 50 μm. (*C*) qRT-PCR analysis for *Il6*, *Tgfb*, *Il10*, *Il12*, *Tnfa*, *Ifng*, *Il23a*, *Il17a*, *Il22*, *Il25*, *Tslp*, *Defb1* and *Camp* in the colon from WT and *MIR31*$^{-/-}$ mice following 5 days of DSS treatment. **P* < .05; ***P* < .01. n = 5 biological replicates. (*D*) Immunohistochemistry for IFNγ in the colon from WT and *MIR31*$^{-/-}$ mice following 5 days of DSS treatment. n = 3. Scale bar: 50 μm. (*E*) qRT-PCR analysis for *Nlpr3*, *Caspase 1*, *Il1b* and *Il18* in WT and *MIR31*$^{-/-}$ colon following 5 days of DSS treatment. ****P* < .001. n = 5. (*F*) Western blotting for Nlrp3, Caspase 1, Pro-caspase 1 and IL1β in the colon WT and *MIR31*$^{-/-}$ mice after 5 days of DSS treatment. β-actin was used as a loading control. n = 3. (*G*) Immunohistochemistry for IL1β in the colon from WT and *MIR31*$^{-/-}$ mice following 5 days of DSS treatment. n = 3. Scale bar: 50 μm. (*H* and *I*) Immunohistochemistry (*H*) and western blotting (*I*) for p65 and p-STAT3 in the colon from WT and *MIR31*$^{-/-}$ mice following 5 days of DSS treatment. Scale bar: 50 μm. β-actin was used as a loading control, which is identical to panel F. n = 3. Statistical analysis was performed using independent *t*-test for panels C and E.

Figure 4. MIR31 directly targets *Il6st*, *Il7r* and *Il17ra* to suppress immune

response. (*A*) qRT-PCR analysis for *Il6st*, *Il7r* and *Il17ra* in the colon of WT and *MIR31*$^{-/-}$ mice after 2 and 5 days of DSS treatment. **P* < .05; ****P* < .001. n = 5. (*B*) Western blotting for Gp130, IL7R and IL17RA in the colon of WT and *MIR31*$^{-/-}$ mice after 5 days of DSS treatment. β-Tubulin was used as a loading control. n = 3. (*C-E*) Immunostaining for Gp130 (*C*), IL7R (*D*) and IL17RA (*E*) in the colon of WT and *MIR31*$^{-/-}$ mice following 5 days of DSS treatment. Scale bar: 50 μm. n = 3. (*F*) Quantification of Gp130^{+}, IL7R^{+} and IL17RA^{+} cells in panels C-E. n = 3. **P* < .05; ****P* < .001. (*G*) qRT-PCR analysis for *Il6st*, *Il7r* and *Il17ra* in LOVO colorectal cancer cells upon treatment of MIR31 mimics (left panel) and inhibitor (right panel). n = 3 technical replicates. **P* < .05; ***P* < .01; ****P* < .001. (*H*) Ratio of luciferase activity of MIR31 mimics versus scrambled RNA in WT and mutant 3'UTR constructs for *Il6st*, *Il7r* and *Il17ra* genes based on 3 independent experiments. **P* < .05; ***P* < .01; ****P* < .001. n = 3 technical replicates. (*I*) qRT-PCR analysis for *Il6st*, *Il7r* and *Il17ra* in WT colon on days 0, 2 and 5 after DSS treatment. n = 3 for each time point. (*J*) Western blotting for Gp130 and IL17RA in WT colon at indicated time points after DSS treatment. GAPDH was used as a loading control. n = 3. (*K*) qRT-PCR analysis for *Il6st*, *Il7r* and *Il17ra* in *Vil-Cre* and cKO colon 5 days after DSS treatment. ***P* < .01; ****P* < .001. n = 4. (*L*) Immunohistochemistry for Gp130 in the colon of *Vil-Cre* and cKO mice after 5 days of DSS treatment. n = 3. Scale bar: 50 μm. (*M*) Immunohistochemistry for Gp130 in normal human colon (n = 4) and human UC samples (n = 5). Scale bar: 100 μm. Statistical analysis was performed using independent *t*-test for panels A, F, G, H and K.

Figure 5. MIR31 regulates WNT and Hippo signaling pathways upon DSS treatment. (*A*) WNT activity was evaluated by *Axin2-LacZ* reporter activity in the colon of WT and *MIR31*$^{-/-}$ mice following 5 days of DSS treatment. Blue, LacZ signals. n = 3 biological replicates. Scale bar: 50 μm. (*B*) qRT-PCR analysis for *Ctnnb1, Ccnd1*, and *Axin2* (left panel), as well as Western blotting for Cyclin D1 and β-catenin (right panel) in the colon of WT and *MIR31*$^{-/-}$ mice following 5 days of DSS treatment. **P* < .05; ****P* < .001. β-Tubulin was used as a loading control. n = 5 biological replicates. (*C*) qRT-PCR analysis for *Dkk1*, *Gsk3b* and *Axin1* (left), as well as Western blotting for Dkk1, Gsk3β and Axin1 (right) in WT and *MIR31*$^{-/-}$ colon following 5-day DSS treatment. n = 3 biological replicates. ***P* < .01; ****P* < .001. β-Tubulin was used as a loading control, which is identical to panel B. (*D*) qRT-PCR analysis for *Dkk1*, *Gsk3b* and *Axin1* in LOVO cells in response to MIR31 inhibitor. **P* < .05; ***P* < .01; ****P* < .001. n = 3 technical replicates. (*E*) Ratio of luciferase activity of *MIR31* mimics versus scramble RNA in WT and mutant 3'UTR constructs for *Dkk1*, *Gsk3b* and *Axin1* genes based on 3 independent experiments. ***P* < .01; ****P* < .001. (*F*) Western blotting for p-Yap and Yap in the colon from WT and *MIR31*$^{-/-}$ littermates following 5 days of DSS treatment. n = 3 biological replicates. β-Tubulin was used as a loading control. Quantification of Yap/p-Yap ratio is shown in right panel. ****P* < .001. (*G*) Immunofluorescence for Yap in WT and *MIR31*$^{-/-}$ colon following 5-day DSS treatment. Scale bar: 50 μm. Quantification of Yap^{+} cells per crypt is shown in right panel. ****P* < .001. n = 3 biological replicates. (*H*) Western blotting for p-Yap

and Yap in LOVO cells in response to MIR31 inhibitors. n = 3 technical replicates. β-Tubulin was used as a loading control. Quantification of Yap/p-Yap ratio is shown in right panel. ***P < .001. (*I*) qRT-PCR analysis for *Lats2*, *Dlg1* and *Dlg5*, and western blotting for 14-3-3, Lats1/2 and Dlg1 in the colon of WT and *MIR31*$^{-/-}$ mice following 5 days of DSS treatment. **P < .01. β-Tubulin was used as a loading control, which is identical to panel 4B. n = 3 biological replicates. (*J*) Immunohistochemistry for Dlg1 and Lats1/2 in the colon of *Vil-Cre* and cKO mice following 5-day DSS treatment. n = 3 biological replicates. Scale bar: 50 μm. (*K*) Ratio of luciferase activity of *MIR31* mimics versus scramble RNA in wild type and mutant 3'UTR constructs for *Lats2*, *Dlg1* and *Dlg5* genes based on 3 independent experiments. n = 3 technical replicates. ***P < .001. Statistical analysis was performed using independent *t*-test for panels B-I, and K.

Figure 6. Characterization of MIR31-based microsphere delivery system consisting of peptosome (PS)-in-oxidized konjac glucomannan (OKGM) microsphere. (*A*) Design and synthesis strategy of the OKGM-PS delivery system: PSs were self-assembled by partially hydrolyzed α-Lactalbumin (α-La), then MIR31 mimics were absorbed to the surface of maleimide (Mal)-modified PSs via electrostatic attraction. PS-MIR31 particles were subsequently encapsulated by OKGM microspheres to form the MIR31-based PS-in-OKGM microsphere delivery system (OKGM-PS-MIR31). (*B*) Transmission electron microscopy (TEM) images of PSs formed from partially hydrolyzed α-La. n = 5 technical replicates. Scale bar, 100 nm. (*C*) Zeta potential of hydrolyzed α-La PS

before and after modification with Mal (PS-Mal), in which Mal was linked to the PSs. n = 4 technical replicates. (*D*) Size distribution of PS-Mal micelles by intensity. n = 4 technical replicates. (*E*) Dynamic change in the diameter of PS-Mal micelles over time at room temperature. n = 4 technical replicates. (*F*) Dynamic change in the zeta potential of PS-Mal micelles over time, at room temperature. n = 4 technical replicates. (*G*) Efficiency of MIR31 mimics loading to PS-Mal micelles. The ratio represents MIR31 mimic::PS by weight. Bands: MIR31 mimics. The percentage at the bottom represents the amount of MIR31 mimic adsorbed to the surface of PS-Mal micelles relative to the original amount of MIR31 mimics (Control). n = 3 technical replicates. (*H*) CCK-8 analysis of the viability of LOVO cells treated with PS micelle (Micelle), PS-MIR31 micelle (Micelle/MIR31 mimics) and Curcumin (Cur) at indicated concentrations after 24 hours of incubation. Cur was used as a positive control for cytotoxicity. n = 3 technical replicates. (*I*) Confocal microscopy images showing the internalization of the MIR31 mimics (labeled by FAM) by LOVO cells delivered without (left) or with (right) PSs (labeled by Cy3) 6 hours after treatment. n = 4 technical replicates. Scale bar: 10 μM. (*J*) Microscopy images of OKGM microspheres encapsulating PSs (labeled by Cy3). Left, DIC image; middle, Cy3 fluorescence image; right, merged image. Arrow point to OKGM-PS microsphere; arrowhead points to OKGM microsphere without PSs. n = 4 technical replicates. Scale bar: 20 μm. (*K*) Fluorescence microscopy images showing the intake of PSs (Cy3) and MIR31 mimics (FAM) or negative control (NC) for MIR31 mimics (FAM) by epithelial cells in the colon. The mice were treated with MIR31-loaded PSs in

OKGM microspheres (OKGM-PS-MIR31) or scramble RNA-loaded PSs in OKGM microspheres (OKGM-PS-NC) by enema for 4 hours. n = 4 technical replicates. Scale bar: 25 μm. qRT-PCR analysis for MIR31 in the colon of mice treated with OKGM-PS-NC and OKGM-PS-MIR31 microspheres. *P < .05. Statistical analysis was performed using independent *t*-test for panel K.

Figure 7. OKGM-PS-MIR31 microsphere sufficiently alleviate DSS-induced colitis. (*A*) Quantification of weight loss in WT mice following 5 days of DSS treatment, coupled with OKGM, OKGM-PS-NC and OKGM-PS-MIR31 treatment. n = 6 biological replicates for each treatment. **P < .01; ***P < .001. (*B*) Representative gross images of the colon of mice treated with OKGM-PS, OKGM-PS-NC and OKGM-PS-MIR31 following 5 days of DSS treatment. n = 6 biological replicates for each treatment. (*C*) Quantification of colon length under the different conditions in panel B. **P < .01. (*D*) H&E staining in the colon from WT mice following 5 days of DSS treatment, and treated with OKGM-PS, OKGM-PS-NC and OKGM-PS-MIR31 microsphere. Scale bar: 50 μm. (*E*) Quantification of the clinical scores in WT mice following 5 days of DSS treatment, coupled with OKGM-PS, OKGM-PS-NC and OKGM-PS-MIR31 treatment. n = 6 for each treatment. ***P < .001. (*F*) Quantification of $Ki67^+$ cells in panel G. n = 6 for each treatment. ***P < .001. (*G*) Double immunofluorescence for Ki67 and β-catenin, Yap and β-catenin, and immunohistochemistry for p-STAT3 and p65 in the colon from WT mice following 5 days of DSS treatment, and treatment with OKGM-PS, OKGM-PS-NC and OKGM-PS-MIR31 microspheres. Scale bar: 50 μm. (*H*)

Western blotting for MIR31 targets IL7R, Gp130, IL17RA, Dkk1, Gsk3β, Axin1, Lats1/2 and Dlg1 in the colon of WT mice following 5 days of DSS treatment, and treatment with OKGM-PS, OKGM-PS-NC and OKGM-PS-MIR31 microsphere. β-Tubulin was used as a loading control. Statistical analysis was performed using independent *t*-test for panels A, C, E, and F.

ACCEPTED MANUSCRIPT

Figure 1

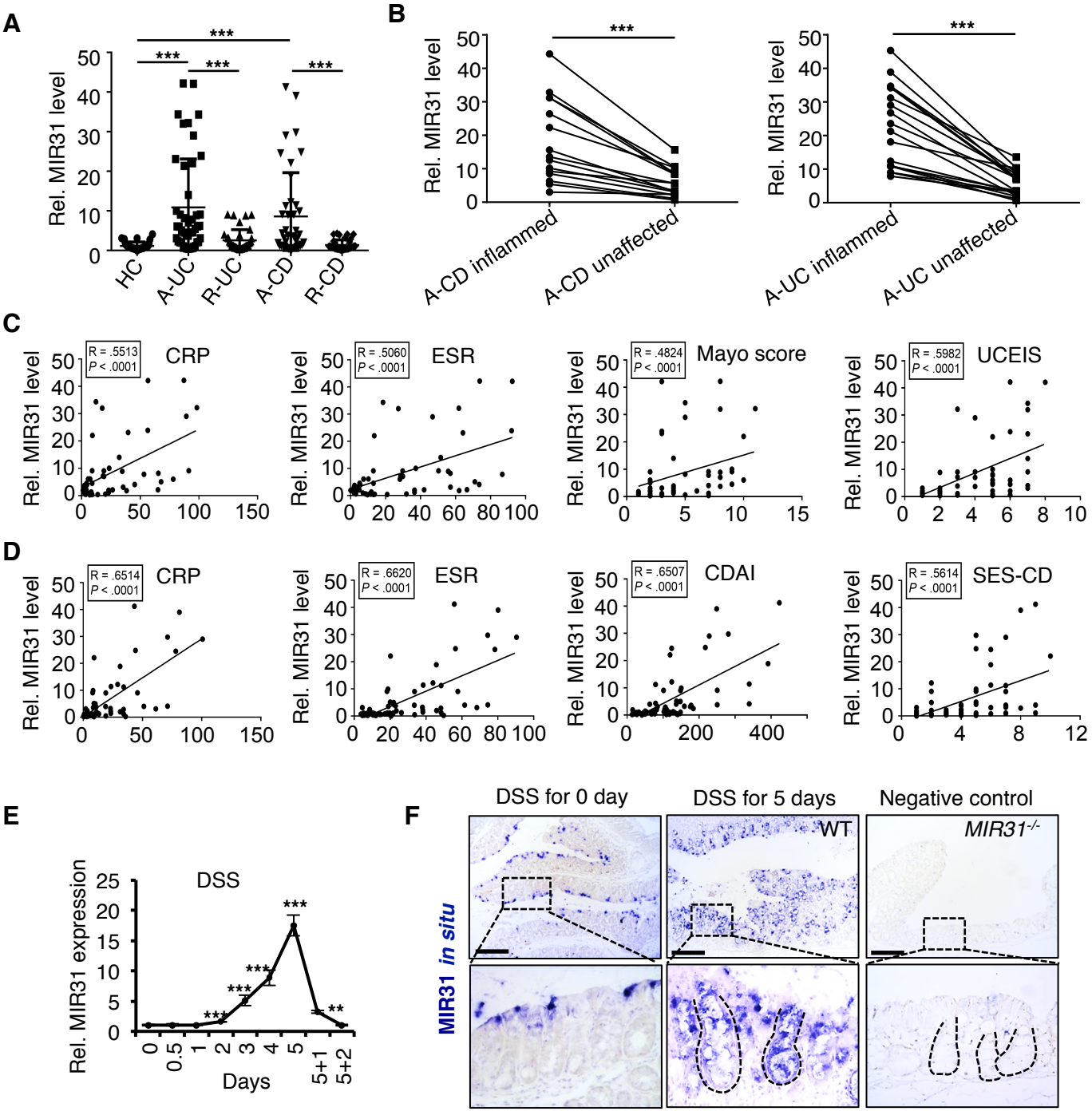

A
Rel. MIR31 level
HC
A-UC
R-UC
A-CD
R-CD
B
Rel. MIR31 level
A-CD inflammed
A-CD unaffected
A-UC inflammed
A-UC unaffected
C
CRP
ESR
Mayo score
UCEIS
R = .5513
R = .5060
R = .4824
R = .5982
P < .0001
D
CRP
ESR
CDAI
SES-CD
R = .6514
R = .6620
R = .6507
R = .5614
E
DSS
Rel. MIR31 expression
Days
F
DSS for 0 day
DSS for 5 days
Negative control
WT
MIR31-/-
MIR31 in situ

Figure 2

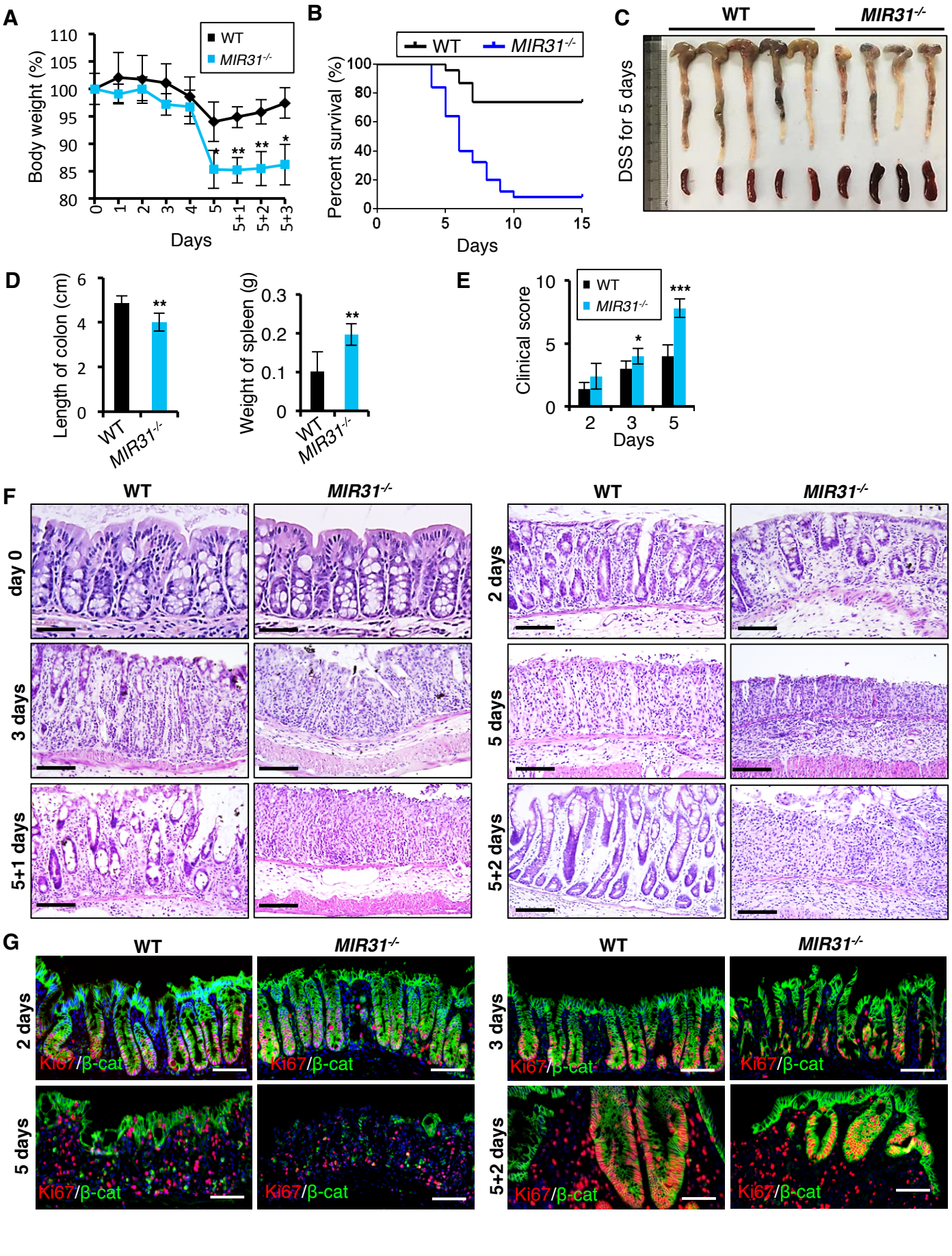

A
Body weight (%)
WT
MIR31-/-
Days
B
Percent survival (%)
WT
MIR31-/-
Days
C
WT
MIR31-/-
DSS for 5 days
D
Length of colon (cm)
Weight of spleen (g)
WT
MIR31-/-
E
Clinical score
WT
MIR31-/-
Days
F
WT
MIR31-/-
day 0
2 days
3 days
5 days
5+1 days
5+2 days
G
WT
MIR31-/-
2 days
3 days
5 days
5+2 days
Ki67/β-cat

Figure 3

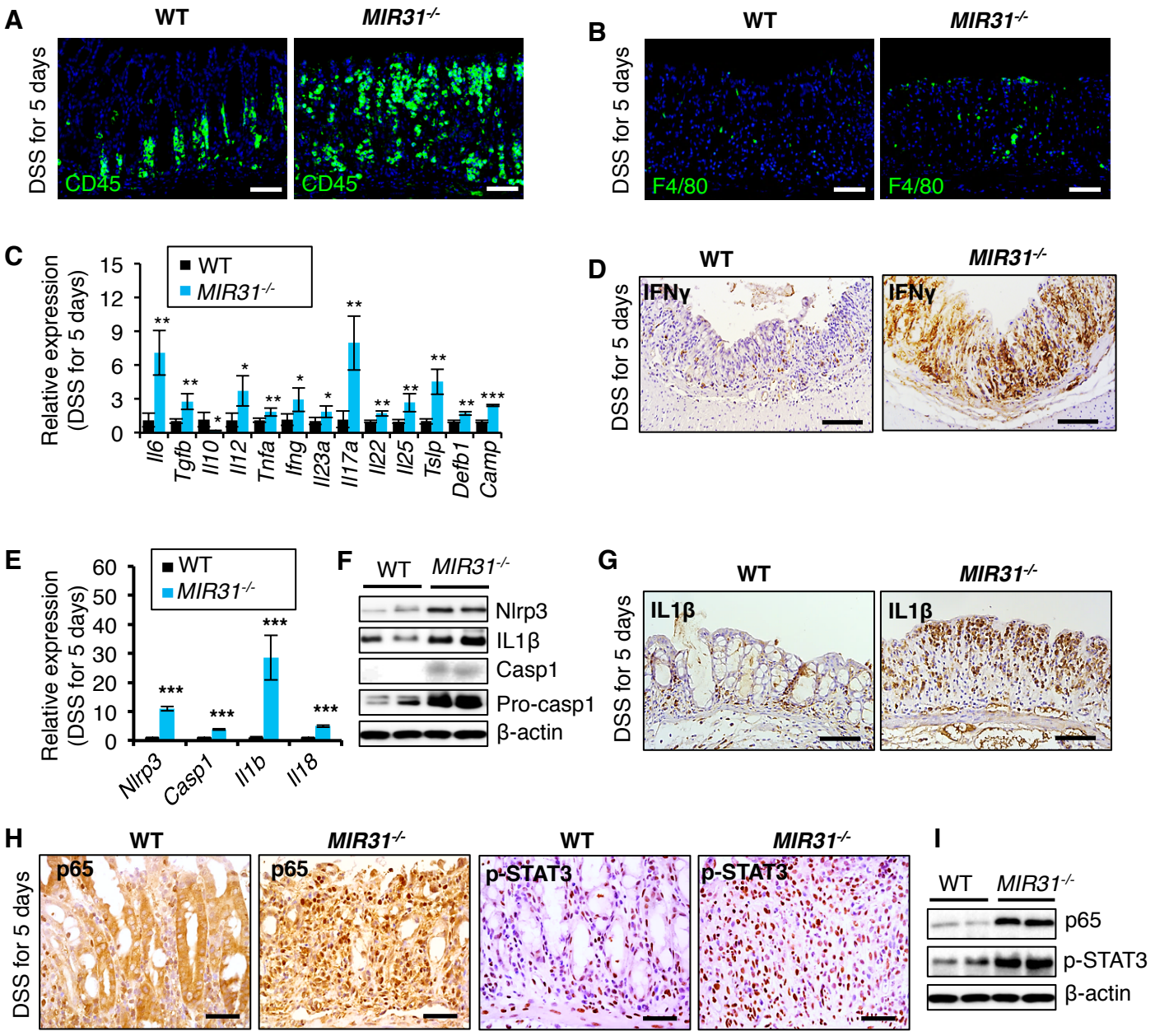

A
WT
MIR31-/-
DSS for 5 days
CD45
CD45
B
WT
MIR31-/-
DSS for 5 days
F4/80
F4/80
C
WT
MIR31-/-
Relative expression (DSS for 5 days)
15
12
9
6
3
0
Il6
Tgfb
Il10
Il12
Tnfa
Ifng
Il23a
Il17a
Il22
Il25
Tslp
Defb1
Camp
D
WT
MIR31-/-
DSS for 5 days
IFNγ
IFNγ
E
WT
MIR31-/-
Relative expression (DSS for 5 days)
60
50
40
30
20
10
0
Nlrp3
Casp1
Il1b
Il18
F
WT
MIR31-/-
Nlrp3
IL1β
Casp1
Pro-casp1
β-actin
G
WT
MIR31-/-
DSS for 5 days
IL1β
IL1β
H
WT
MIR31-/-
WT
MIR31-/-
DSS for 5 days
p65
p65
p-STAT3
p-STAT3
I
WT
MIR31-/-
p65
p-STAT3
β-actin

Figure 4

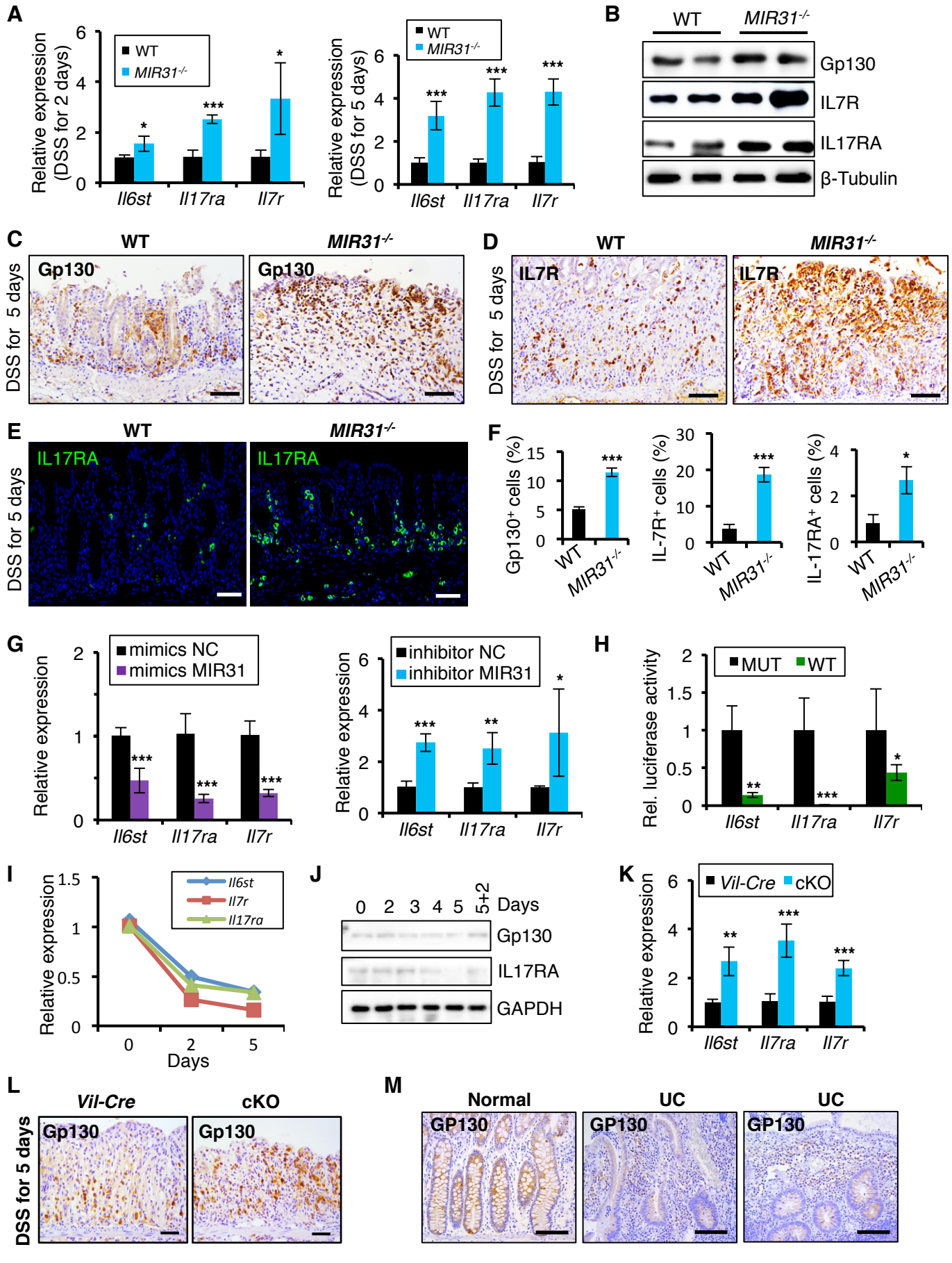

A
Relative expression (DSS for 2 days)
WT
MIR31-/-
Il6st
Il17ra
Il7r
Relative expression (DSS for 5 days)
B
WT
MIR31-/-
Gp130
IL7R
IL17RA
β-Tubulin
C
WT
MIR31-/-
DSS for 5 days
Gp130
D
IL7R
E
IL17RA
F
Gp130+ cells (%)
IL-7R+ cells (%)
IL-17RA+ cells (%)
G
mimics NC
mimics MIR31
inhibitor NC
inhibitor MIR31
H
MUT
WT
Rel. luciferase activity
I
Days
J
0 2 3 4 5 5+2 Days
GAPDH
K
Vil-Cre
cKO
L
Normal
UC
GP130

Figure 5

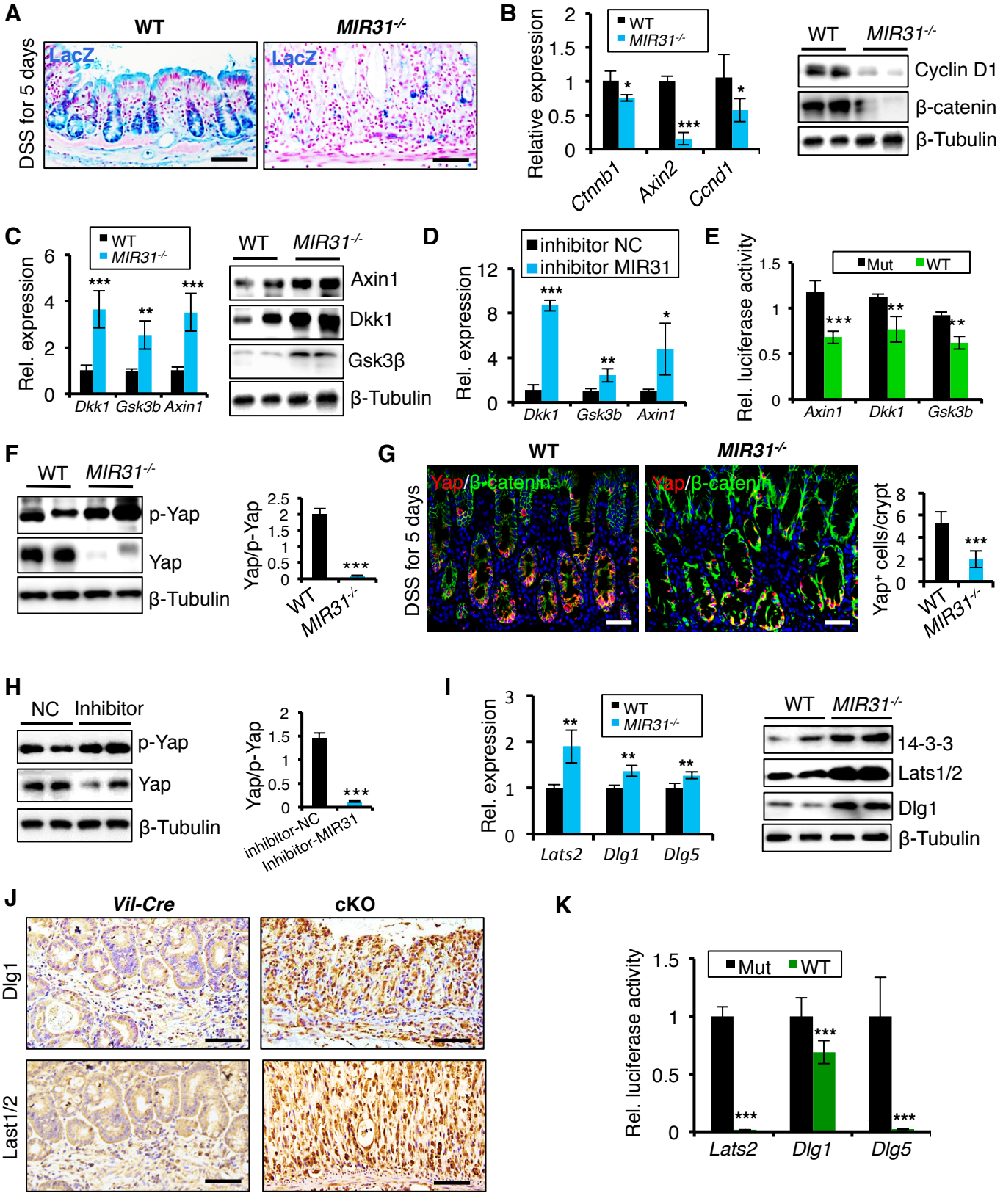

A
WT
MIR31-/-
DSS for 5 days
LacZ
LacZ
B
Relative expression
WT
MIR31-/-
Ctnnb1
Axin2
Ccnd1
WT
MIR31-/-
Cyclin D1
β-catenin
β-Tubulin
C
Rel. expression
WT
MIR31-/-
Dkk1
Gsk3b
Axin1
WT
MIR31-/-
Axin1
Dkk1
Gsk3β
β-Tubulin
D
Rel. expression
inhibitor NC
inhibitor MIR31
Dkk1
Gsk3b
Axin1
E
Rel. luciferase activity
Mut
WT
Axin1
Dkk1
Gsk3b
F
WT
MIR31-/-
p-Yap
Yap
β-Tubulin
Yap/p-Yap
WT
MIR31-/-
G
WT
MIR31-/-
DSS for 5 days
Yap/β-catenin
Yap/β-catenin
Yap+ cells/crypt
WT
MIR31-/-
H
NC
Inhibitor
p-Yap
Yap
β-Tubulin
Yap/p-Yap
inhibitor-NC
Inhibitor-MIR31
I
Rel. expression
WT
MIR31-/-
Lats2
Dlg1
Dlg5
WT
MIR31-/-
14-3-3
Lats1/2
Dlg1
β-Tubulin
J
Vil-Cre
cKO
Dlg1
Last1/2
K
Rel. luciferase activity
Mut
WT
Lats2
Dlg1
Dlg5

Figure 6

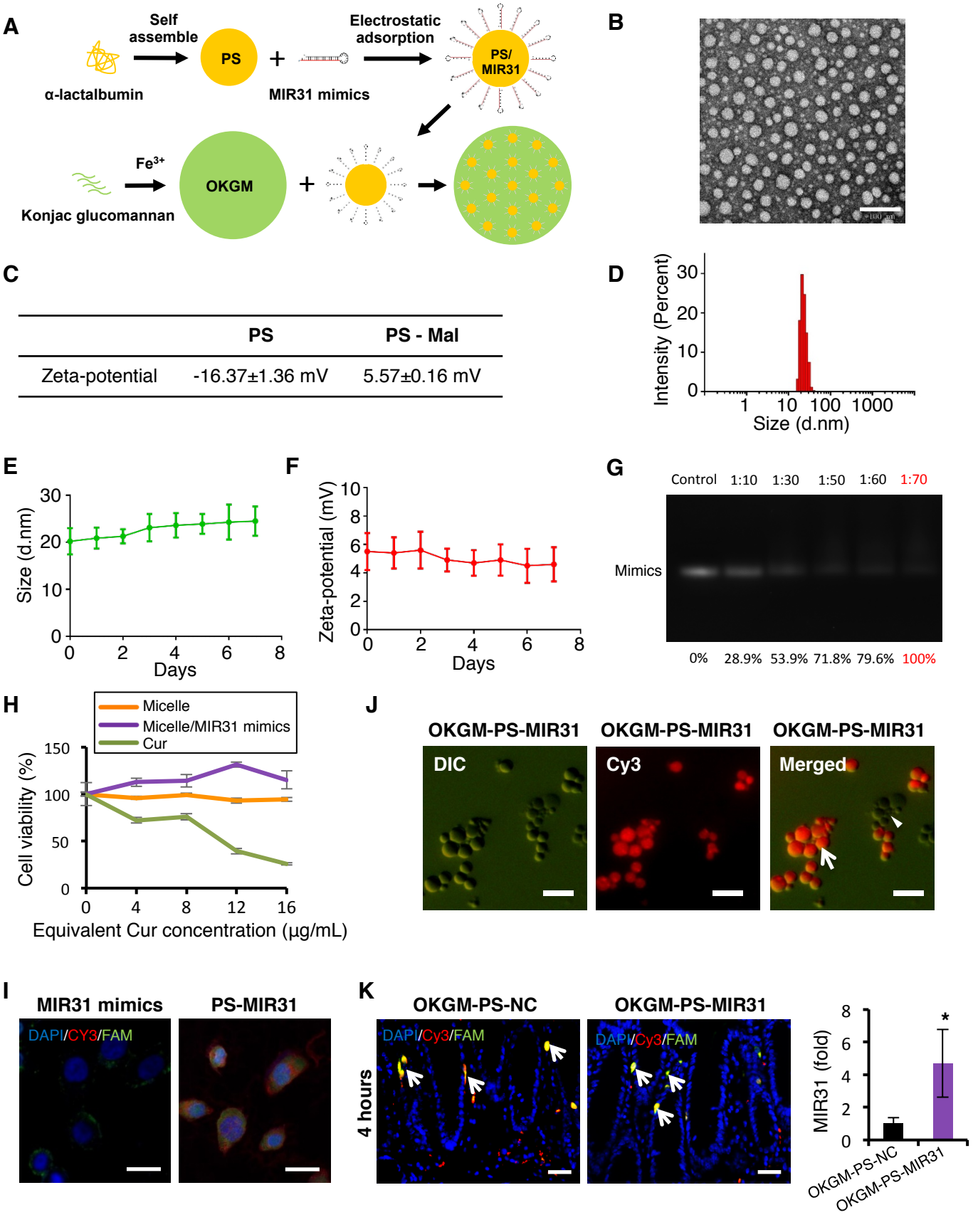
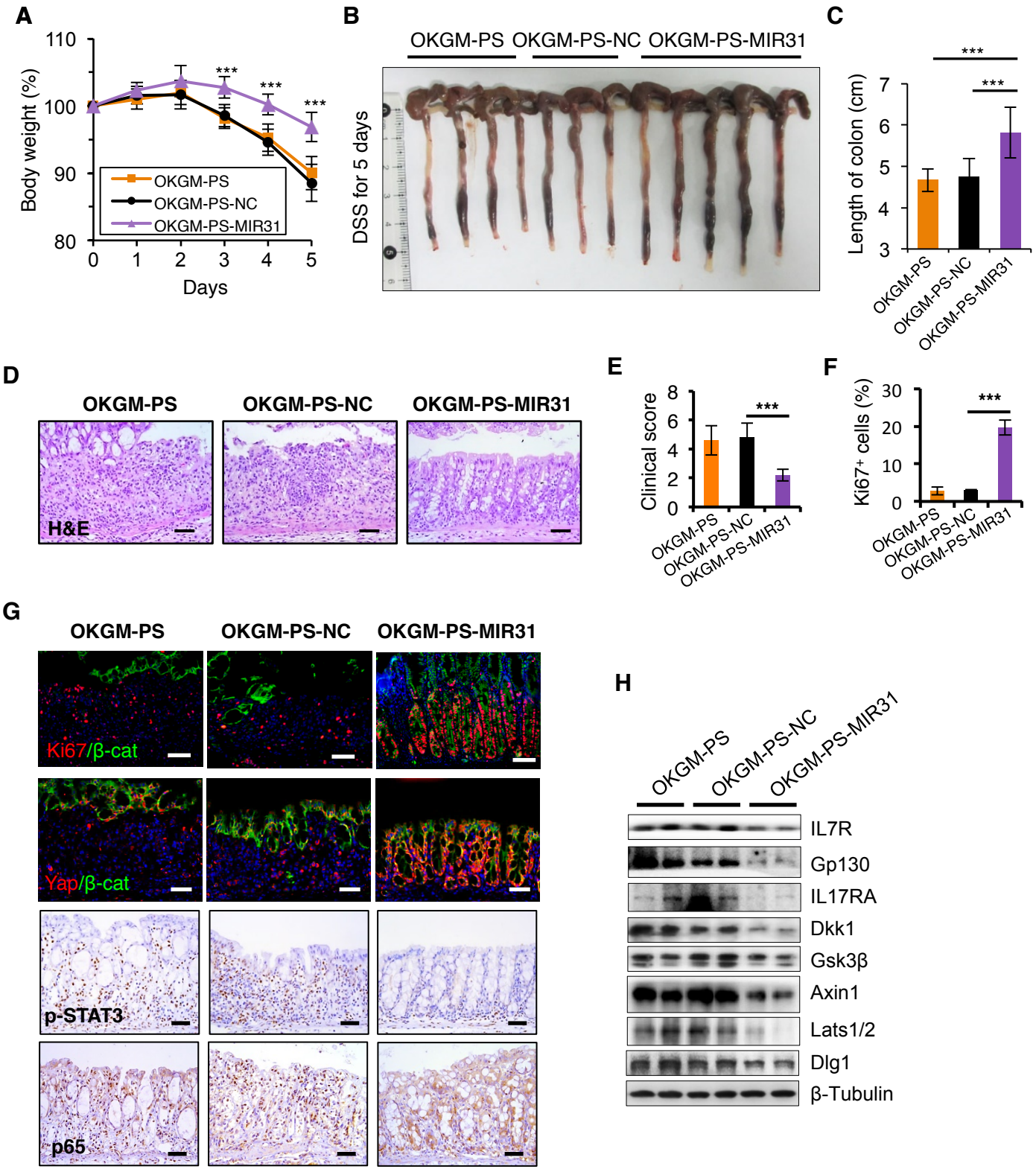

A
Self assemble
PS
Electrostatic adsorption
PS/ MIR31
α-lactalbumin
MIR31 mimics
Fe3+
OKGM
Konjac glucomannan
B
C
PS
PS - Mal
Zeta-potential
-16.37±1.36 mV
5.57±0.16 mV
D
Intensity (Percent)
Size (d.nm)
E
Size (d.nm)
Days
F
Zeta-potential (mV)
Days
G
Control
1:10
1:30
1:50
1:60
1:70
Mimics
0%
28.9%
53.9%
71.8%
79.6%
100%
H
Micelle
Micelle/MIR31 mimics
Cur
Cell viability (%)
Equivalent Cur concentration (μg/mL)
J
OKGM-PS-MIR31
DIC
Cy3
Merged
I
MIR31 mimics
PS-MIR31
DAPI/CY3/FAM
K
OKGM-PS-NC
OKGM-PS-MIR31
4 hours
DAPI/Cy3/FAM
MIR31 (fold)
OKGM-PS-NC
OKGM-PS-MIR31

Figure 7


A
Body weight (%)
110
100
90
80
0 1 2 3 4 5
Days
***
***
***
OKGM-PS
OKGM-PS-NC
OKGM-PS-MIR31
B
OKGM-PS OKGM-PS-NC OKGM-PS-MIR31
DSS for 5 days
C
Length of colon (cm)
7
6
5
4
3
***
***
OKGM-PS
OKGM-PS-NC
OKGM-PS-MIR31
D
OKGM-PS
OKGM-PS-NC
OKGM-PS-MIR31
H&E
E
Clinical score
8
6
4
2
0
***
OKGM-PS
OKGM-PS-NC
OKGM-PS-MIR31
F
Ki67+ cells (%)
30
20
10
0
***
OKGM-PS
OKGM-PS-NC
OKGM-PS-MIR31
G
OKGM-PS
OKGM-PS-NC
OKGM-PS-MIR31
Ki67/β-cat
Yap/β-cat
p-STAT3
p65
H
OKGM-PS
OKGM-PS-NC
OKGM-PS-MIR31
IL7R
Gp130
IL17RA
Dkk1
Gsk3β
Axin1
Lats1/2
Dlg1
β-Tubulin

ACCEPTED MANUSCRIPT

Supplementary information

This document includes Supplementary figures, Supplementary Figure Legends, Supplementary Tables and Supplementary Materials and Methods.

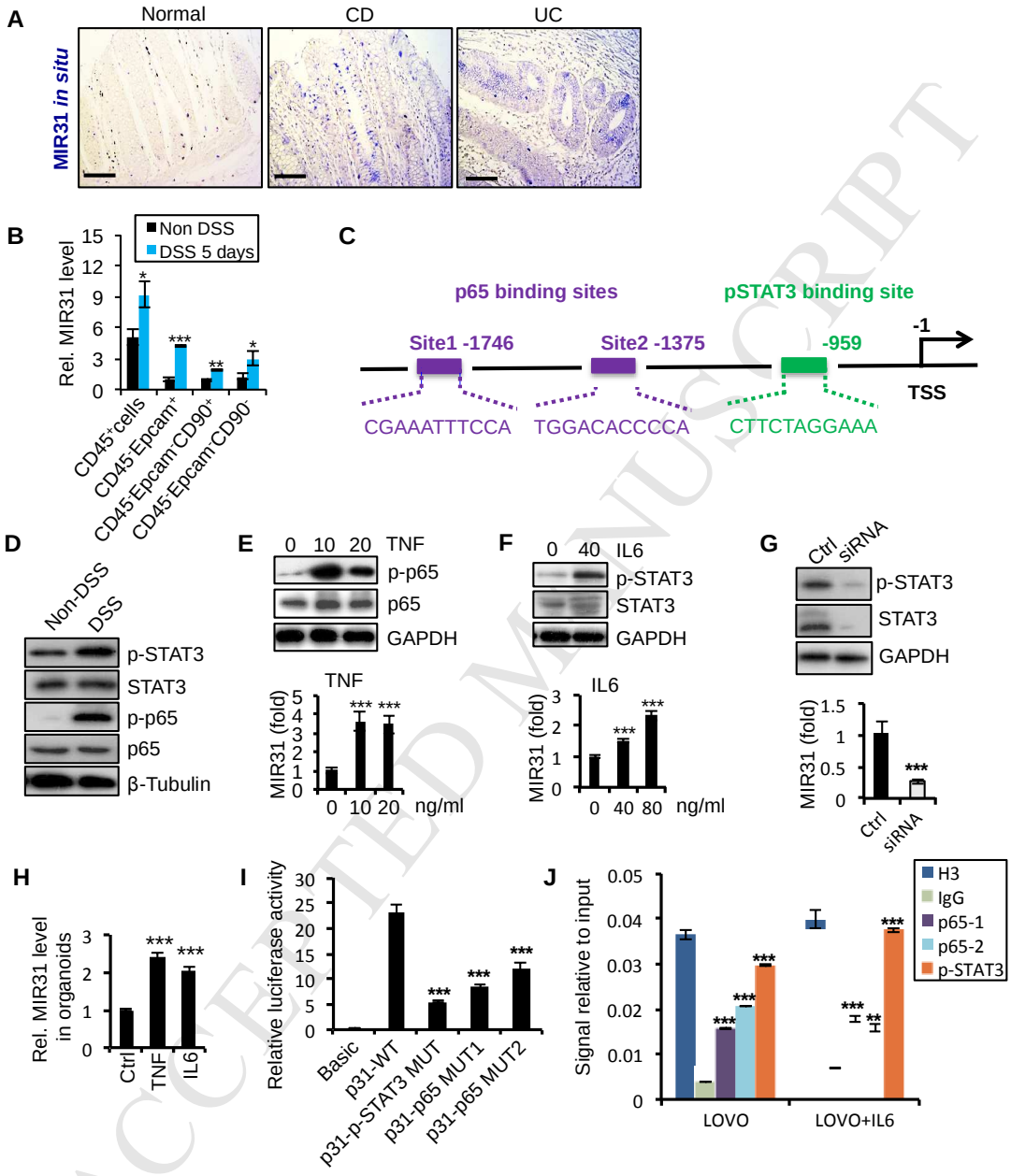
MicroRNA-31 Reduces Inflammatory Signaling and Promotes Regeneration in Colon Epithelium, and Delivery of Mimics in Microspheres Reduces Colitis in Mice

Short title: Role of microRNA-31 in IBD

Yuhua Tian,[1#] **Jiuzhi Xu,**[1#] **Yuan Li,**[2#] Ran Zhao,[1] Sujuan Du,[1] Cong Lv,[1] Wei Wu,[3] Ruiqi Liu,[1] Xiaole Sheng,[1] Yongli Song,[1] Xueyun Bi,[1] Guilin Li,[1] Mengzhen Li,[1] Xi Wu,[1] Pengbo Lou, [1] Huiwen You,[4] Wei Cui,[1,5] Jinyue Sun,[6] Jianwei Shuai,[7] Fazheng Ren,[2] Bing Zhang,[8] Mingzhou Guo[9], Xiaohua Hou,[10] Kaichun Wu,[11] Lixiang Xue,[12] Hongquan Zhang,[13] Maksim V. Plikus,[14] Yingzi Cong,[15] Christopher J. Lengner,[16] Zhanju Liu,[3]* and Zhengquan Yu[1$]*

ACCEPTED MANUSCRIPT

Supplementary Figure 1

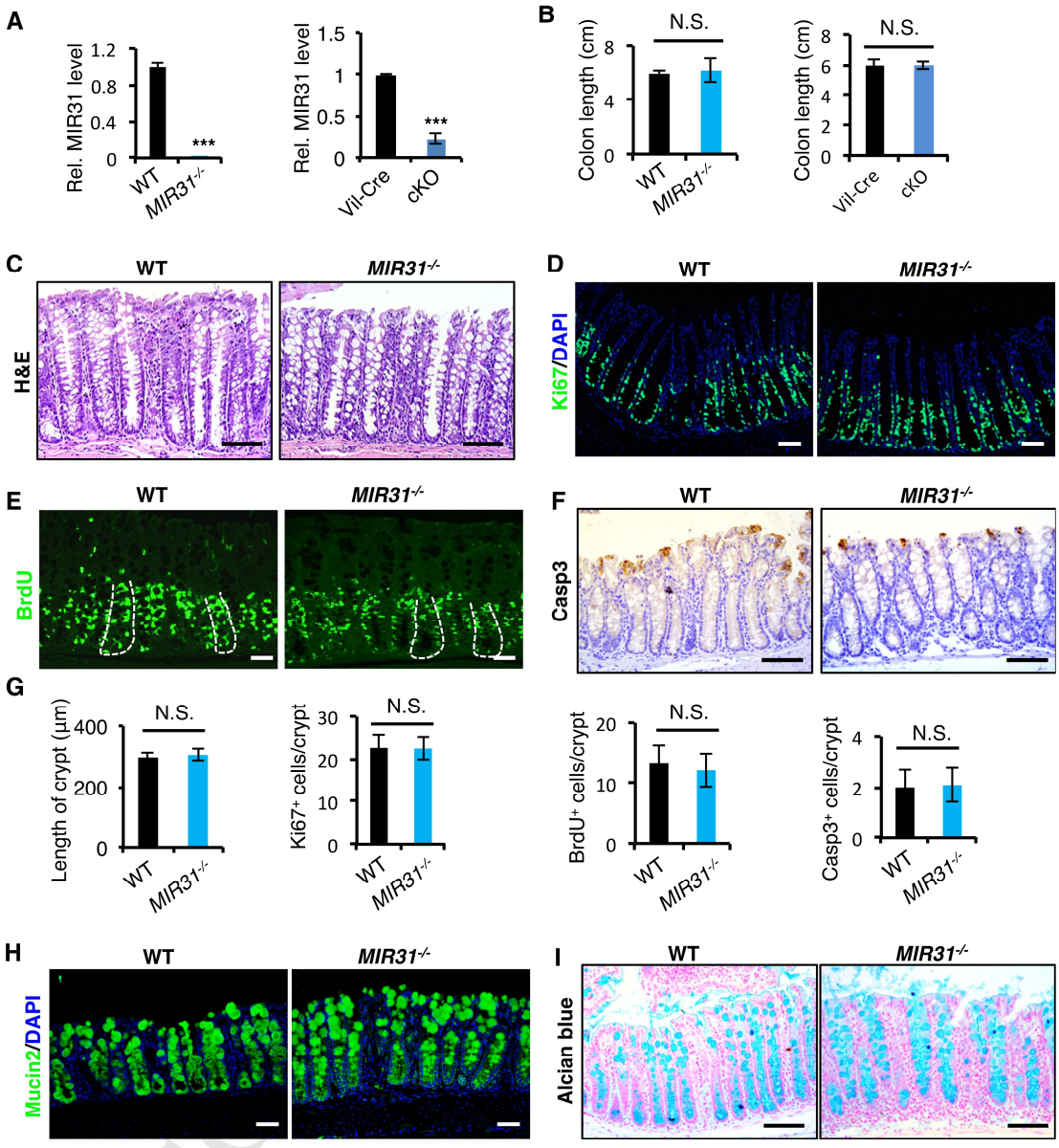


Supplementary Figure 1. MIR31 is directly up-regulated by the NF-κB and STAT3 signaling pathways. (*A*) *In situ* hybridization for MIR31 in colonic biopsies from healthy controls (n = 5), inflamed mucosa from active CD (n = 10) and UC (n = 10). Scale bar: 50 µm. (*B*) qRT-PCR analysis for MIR31 in $CD45^+$, $CD45^-Epcam^+$, $CD45^-Epcam^-CD90^+$ and $CD45^-Epcam^-CD90^-$ cells isolated from colon without DSS treatment or following 5 days of DSS treatment. n = 3 technical replicates. **P* < .05; ***P* < .001; ****P* < .001. (*C*) The schematic diagram

shows two potential p65 binding sites and one p-STAT3 binding site in the MIR31 promoter. (*D*) Western blotting for STAT3, p-STAT3, p65 and p-p65 in the colon without DSS treatment or following 5 days of DSS treatment. β-Tubulin was used as a loading control. n = 3 technical replicates. (*E)* Western blotting for p65 and p-p65 (upper panel) and qRT-PCR for MIR31 (lower panel) in LOVO cells treated with 10 and 20 ng/mL TNF. ***P < .001. GAPDH was used as a loading control. n = 3 technical replicates. (*F*) Western blotting for STAT3 and p-STAT3 (Upper panel) and qRT-PCR for MIR31 (Lower panel) in LOVO cells in response to IL6 with concentrations of 40 and/or 80 ng/mL. GAPDH was used as a loading control. n = 3 technical replicates. (*G*) Western blotting for STAT3 and p-STAT3 (upper panel) and qRT-PCR for MIR31 (lower panel) in LOVO cells treated with STAT3 siRNA. GAPDH was used as a loading control. ***P < .001. (*H*) qRT-PCR for MIR31 in cultured organoids treated with 80 ng/mL IL6 and 20 ng/mL TNF. ***P < .001. n = 3. (*I*) Luciferase activity in lysates of LOVO cells transfected with luciferase reporter plasmids of pGL3-basic empty vector (basic), wild type MIR31 promoter or mutant promoter with mutation of p-STAT3 or p65 binding sites. ***P < .001. n = 3. (*J*) Chromatin immunoprecipitation assay was carried out on LOVO cells using antibodies against p-STAT3, p65 and Histone 3. The antibody against Histone 3 was used as a positive control. The enrichment of p-STAT3 and p65 binding to MIR31 promoter was quantified using qPCR. **P < .01; ***P < .001. n = 3 technical replicates. Statistical analysis was performed using independent *t*-test for panels B, and E-J.

ACCEPTED MANUSCRIPT

Supplementary Figure 2

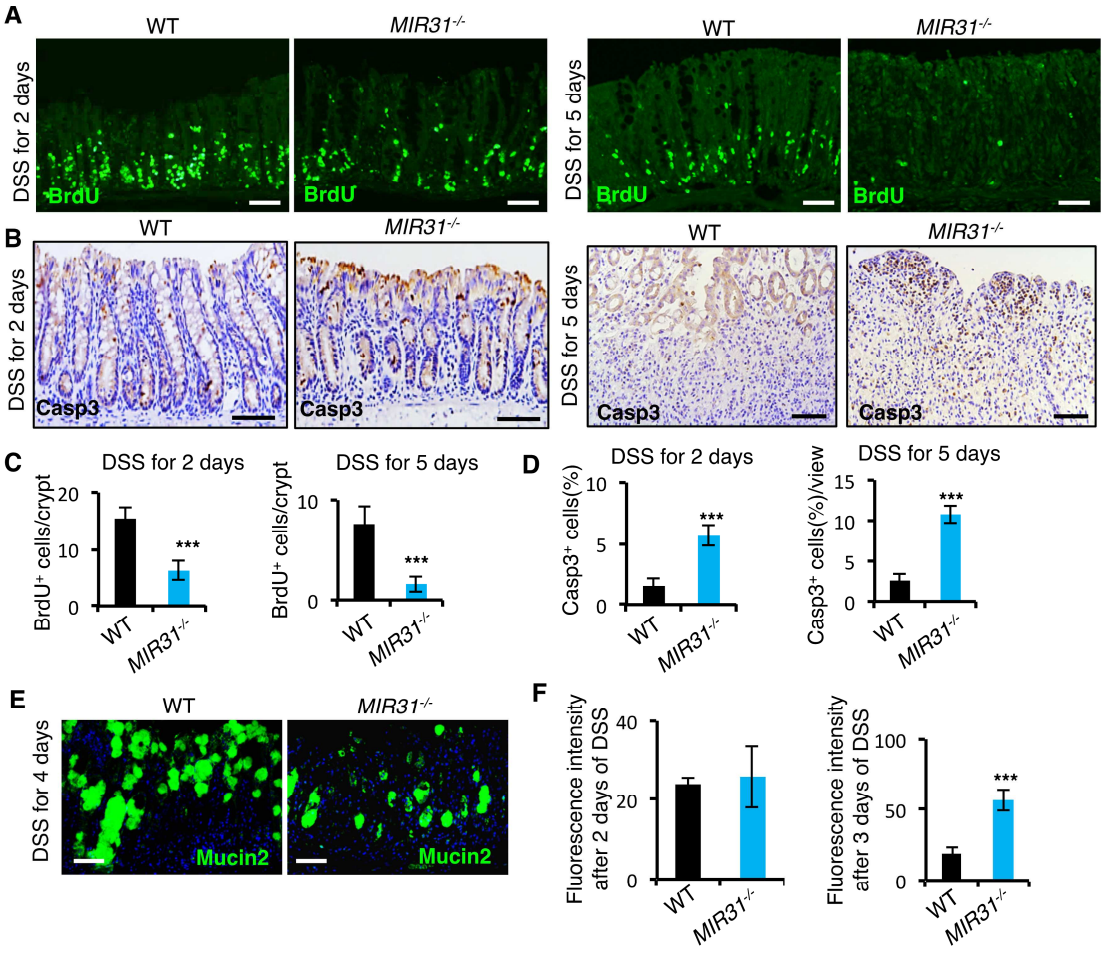


Supplementary Figure 2. No apparent gross phenotypes in *MIR31*$^{-/-}$ mice. (*A*) qRT-PCR analysis for MIR31 in the colon from *MIR31*$^{-/-}$ and *Villin-Cre*;*MIR31*$^{fl/fl}$ (cKO) mice. n = 3 biological replicates. ***P < .001. (*B*) Quantification of colon length from *MIR31*$^{-/-}$ and *Villin-Cre*;*MIR31*$^{fl/fl}$ (cKO) mice. N.S. indicated no significant difference. n = 3. (*C*) H&E staining in colons from WT and *MIR31*$^{-/-}$ mice. n = 3. Scale bar: 50 μm. (*D*) Immunofluorescence for Ki67 in the colon from WT and *MIR31*$^{-/-}$ mice. n = 3. Scale bar: 50 μm. (*E*) Immunofluorescence for BrdU in the colon from WT and *MIR31*$^{-/-}$ mice after 90 min of BrdU pulse. n = 3. (*F*) Immunohistochemistry for cleaved caspase 3 (Casp3) in the colon from WT and *MIR31*$^{-/-}$ mice. n = 3. Scale bar: 50 μm. (*G*)

Quantification of crypt length, $Ki67^+$ cells per crypt, $BrdU^+$ cells per crypt and $Casp3^+$ cells per crypt in panels C-F. N.S. indicated no significant difference. (*H*) Immunofluorescence for Mucin2 in the colon from WT and *MIR31*$^{-/-}$ mice. n = 3. Scale bar: 50 μm. (*I*) Alcian blue staining in the colon from WT and *MIR31*$^{-/-}$ mice. n = 3. Scale bar: 50 μm. Statistical analysis was performed using independent *t*-test for panels A, B, and G.

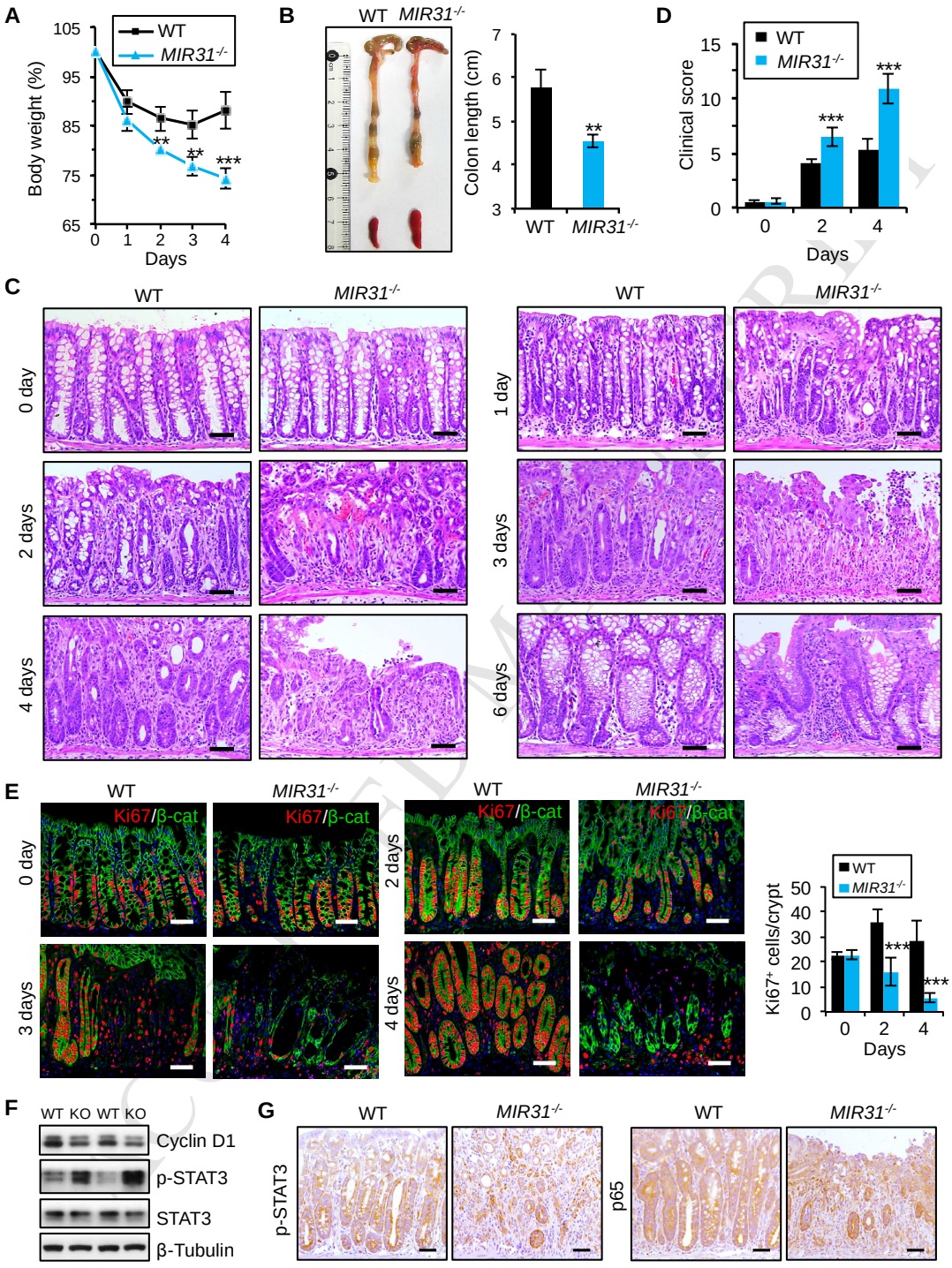
ACCEPTED MANUSCRIPT

Supplementary Figure 3



Supplementary Figure 3. MIR31 deficiency leads to reduced cell proliferation, increased cell apoptosis and impaired epithelial integrity. (*A*) Immunofluorescence for BrdU in the colon from WT and *MIR31*$^{-/-}$ mice following 2 and 5 days of DSS treatment. 90 min of BrdU pulse was performed before sacrifice the mice. n = 3. Scale bar: 50 μm. (*B*) Immunohistochemistry for cleaved caspase 3 (Casp3) in the colon from WT and *MIR31*$^{-/-}$ mice following 2 and 5 days of DSS treatment. n = 3. Scale bar: 50 μm. (*C*) Quantification of BrdU^{+} cells per crypt in panel A. ***P < .001. (*D*) Quantification of Casp3^{+} cells per crypt in panel B. ***P < .001. (*E*) Immunofluorescence of Mucin2 in colons from WT and *MIR31*$^{-/-}$ mice following 4 days of DSS treatment. n = 3. Scale bar: 50 μm. (*F*) Intestinal permeability assay of WT and *MIR31*$^{-/-}$ littermates following 2 or 3 days of DSS treatment. n = 3. ***P < .001. Statistical analysis was performed using independent *t*-test for panels C, D, and F.

Supplementary Figure 4

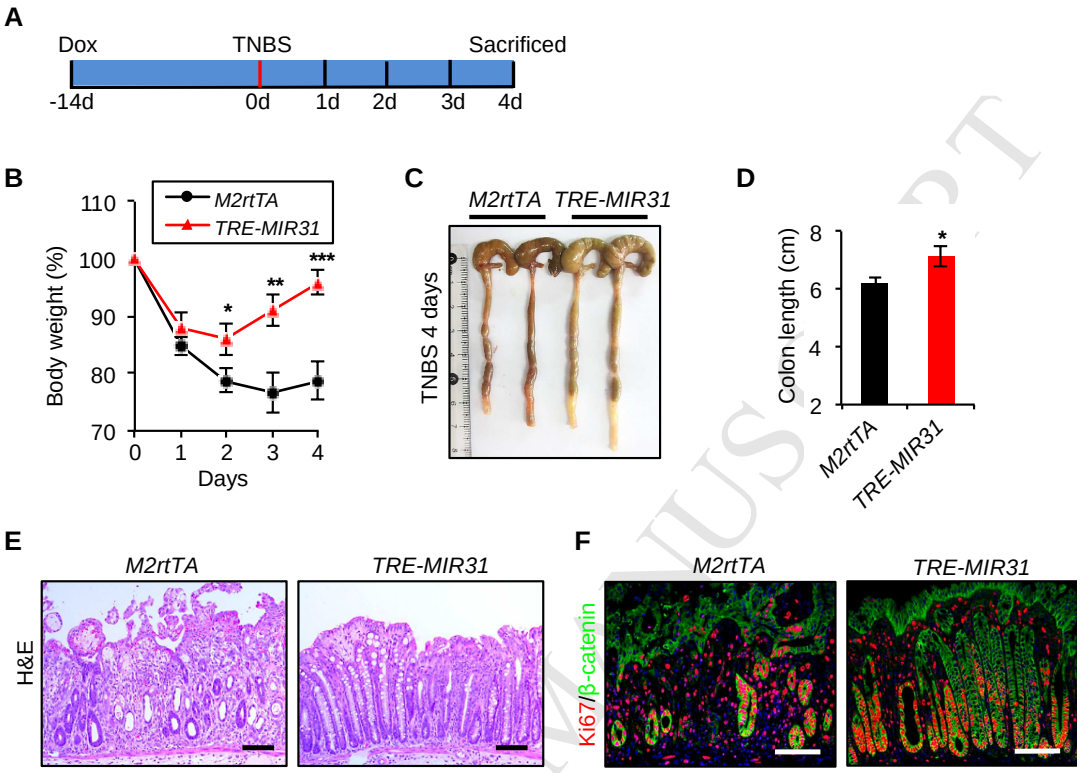


Supplementary Figure 4. MIR31 deletion resulted in exacerbated immune response and impaired epithelial regeneration in a model of TNBS-induced colitis. (*A*) Quantification of weight loss in WT and *MIR31*$^{-/-}$ littermates after TNBS treatment. n = 7 biological replicates for both WT and *MIR31*$^{-/-}$ littermates.

**P < .01; ***P < .001. (*B*) Gross images of colon and spleen from WT and *MIR31*$^{-/-}$ littermates after 4 days of TNBS treatment, and quantification on the length of colon. WT, n = 7; *MIR31*$^{-/-}$, n = 7. **P < .01. (*C*) Histological images of colon from WT and *MIR31*$^{-/-}$ mice at indicated time points after TNBS treatment. Day 4: WT, n = 7, *MIR31*$^{-/-}$, n = 7; Day 0-3, 6: WT, n = 3, *MIR31*$^{-/-}$, n = 3. Scale bar: 50 μm. (D) Quantification of clinical score after TNBS treatment. ***P < .001. (*E*) Double immunofluorescence for Ki67 and β-catenin in the colon from WT and *MIR31*$^{-/-}$ littermates at indicated time points after TNBS treatment. Scale bar: 50 μm. (*F*) Western blotting for Cyclin D1, p-STAT3 and STAT3 in WT and *MIR31*$^{-/-}$ colon 4 days after TNBS treatment. β-Tubulin was used as a loading control, which is identical to Supplementary 12D. n = 3. (*G*) Immunohistochemistry for p-STAT3 and p65 in the colon from WT and *MIR31*$^{-/-}$ littermates. Scale bar: 50 μm. Statistical analysis was performed using independent *t*-test for panels A-C.

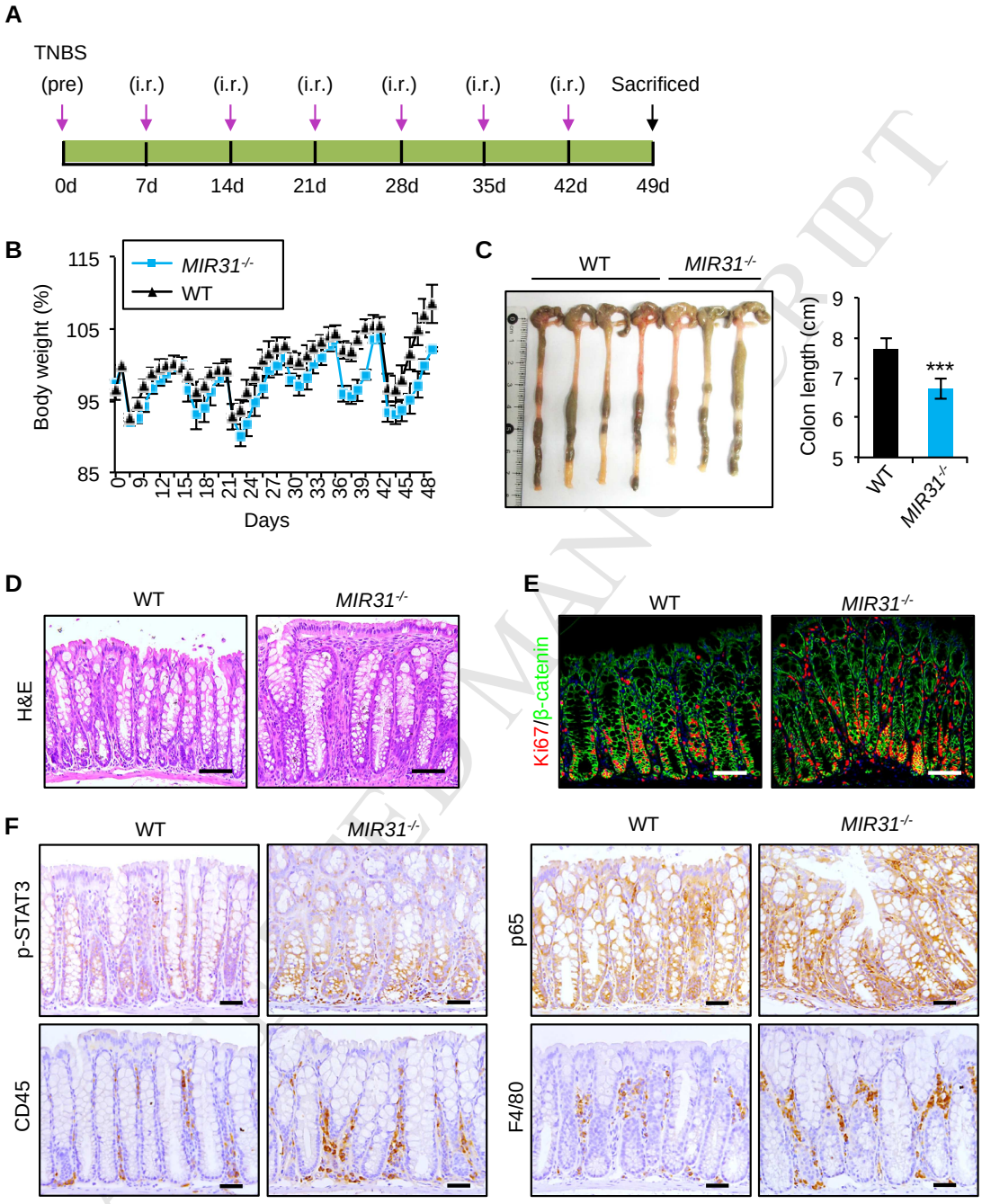
ACCEPTED MANUSCRIPT

Supplementary Figure 5



Supplementary Figure 5. MIR31 overexpression attenuates the immune response and promoted epithelial regeneration. (*A*) Strategy for TNBS-induced colitis in MIR31 overexpressing mice. (*B*) Quantification of weight loss in *M2rtTA* (n = 4) and *TRE-MIR31* (n = 4, *M2rtTA*;*TRE-MIR31*) littermates after TNBS treatment. (*C*) Gross images of colon from *M2rtTA* (n = 4) and *TRE-MIR31* (n = 4) littermates after 4 days of TNBS treatment. (*D*) Quantification of colon length in panel C. **P* < .05. (*E*) Histology of colon from *M2rtTA* and *TRE-MIR31* littermates after 4 days of TNBS treatment. n = 4. Scale bar: 100 μm. (*F*) Double immunofluorescence for Ki67 and β-catenin in colon from *M2rtTA* and *TRE-MIR31* littermates after 4 days of TNBS treatment. Scale bar: 100 μm. n = 3. Statistical analysis was performed using independent *t*-test for panels B, and D.

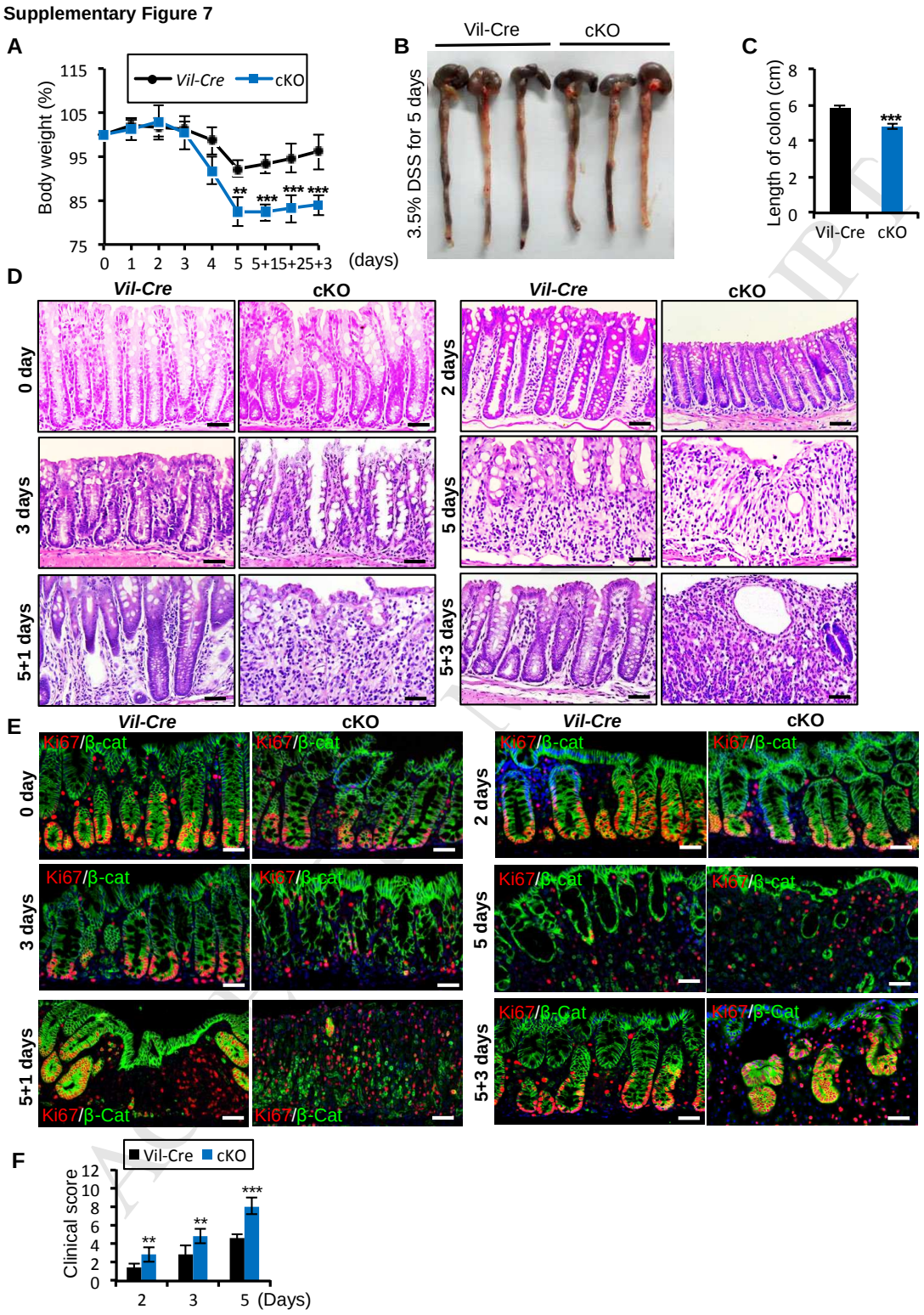
Supplementary Figure 6



Supplementary Figure 6. MIR31 deletion results in exacerbated immune response in TNBS-induced chronic colitis. (*A*) Strategy for generating TNBS-induced chronic colitis. Pre, before treatment; i.r., intrarectal delivery. (*B*) Quantification of body weight in WT (n = 7) and *MIR31*$^{-/-}$ (n = 5) littermates during colitis development. (*C*) Gross images of the colon from WT and *MIR31*$^{-/-}$ littermates after chronic colitis induction. Quantification of colon length in the

colon from WT and *MIR31*$^{-/-}$ littermates. ***P < .001. (*D*) Histological images in the colon from WT and *MIR31*$^{-/-}$ littermates after chronic colitis induction. Scale bar: 100 μm. (*E*) Double immunofluorescence for Ki67 and β-catenin in the colon from WT and *MIR31*$^{-/-}$ littermates after chronic colitis induction. Scale bar: 100 μm. (*F*) Immunohistochemistry for p-STAT3, p65, CD45 and F4/80 in the colon from WT and *MIR31*$^{-/-}$ littermates after chronic colitis induction. Scale bar: 50 μm. Statistical analysis was performed using independent *t*-test for panels C.

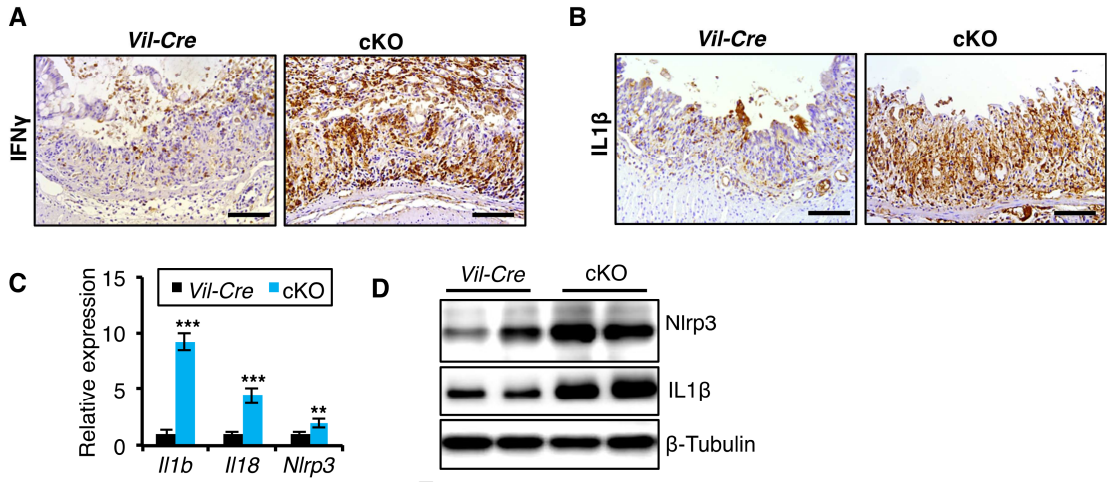
ACCEPTED MANUSCRIPT



Supplementary Figure 7. Exacerbated immune response and impaired epithelial regeneration in cKO mice following DSS treatment. (*A*)

Quantification of weight loss in *Vil-Cre* and cKO littermates after DSS treatment. n = 7 biological replicates for both *Vil-Cre* and cKO littermates. ***P* < .01; ****P* < .001. (*B*) Gross images of colon from *Vil-Cre* and cKO littermates following 5 days of DSS treatment. n=7 biological replicates. (*C*) Quantification on length of colon in Panel B. ****P* < .001. (*D*) Histological images of *Vil-Cre* and cKO colon at indicated time points after DSS treatment. n = 5 biological replicates. Scale bar: 50 μm. (*E*) Double immunofluorescence for Ki67 and β-catenin in *Vil-Cre* and cKO colon at indicated time points following DSS treatment. Scale bar: 50 μm. n = 5 biological replicates. (*F*) Quantification of clinical score in *Vil-Cre* and cKO mice after DSS treatment. n = 7 biological replicates. ***P* < .01; ****P* < .001. Statistical analysis was performed using independent *t*-test for panels A, C, and F.

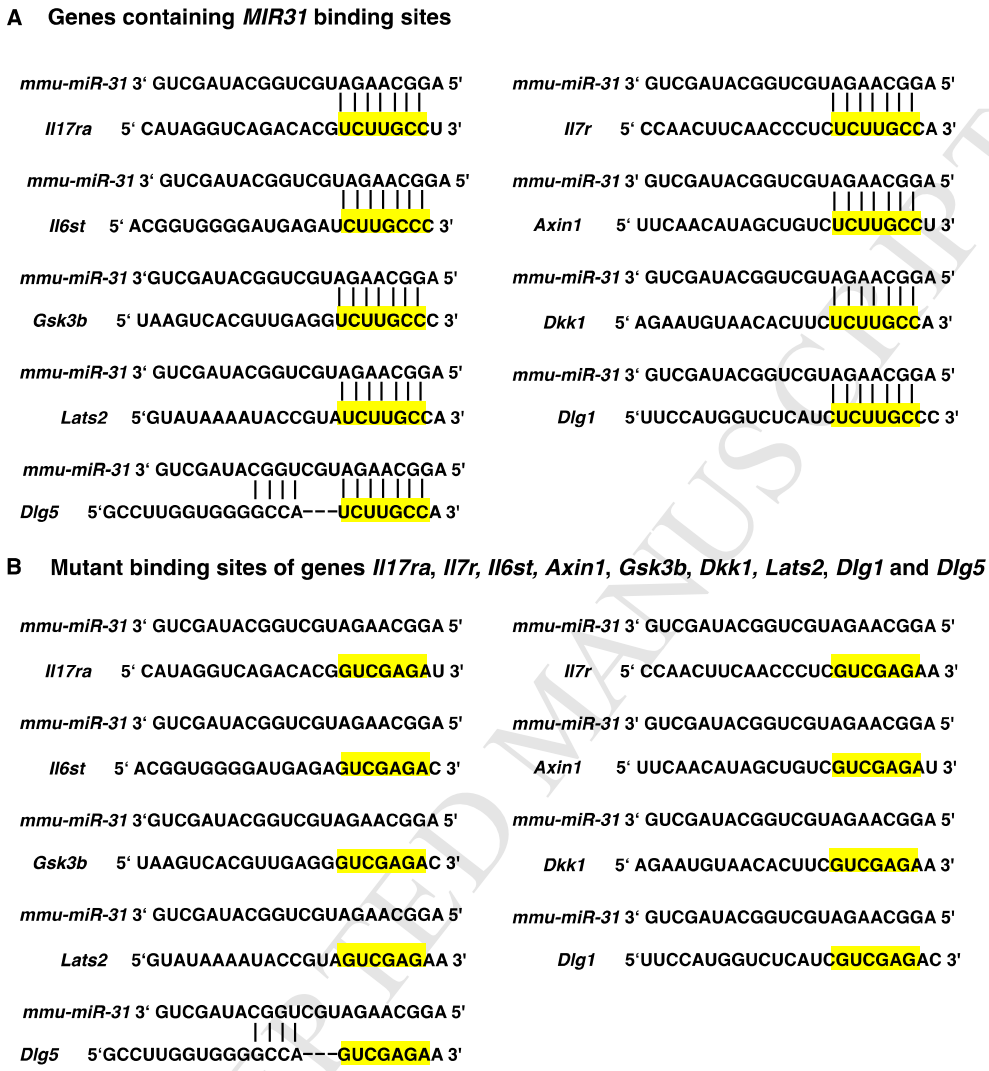
Supplementary Figure 8



Supplementary Figure 8. Enhanced inflammatory reaction in cKO mice following DSS treatment. (*A* and *B*) Immunohistochemistry for IFNγ and IL1β in colon from *Vil-Cre* and cKO mice following 5 days of DSS treatment. n = 3. Scale bar: 50 μm. (*C*) qRT-PCR analysis for *Il1b*, *Il18* and *Nlrp3* in the colon from *Vil-Cre* and cKO mice following 5 days of DSS treatment. n = 3. ***P* < .01; ****P* < .001. (*D*) Western blotting for Nlrp3 and IL1β in colon from *Vil-Cre* (n = 3) and cKO (n = 3) mice following 5 days of DSS treatment. β-Tubulin was used as a loading control. Statistical analysis was performed using independent *t*-test for panels C.

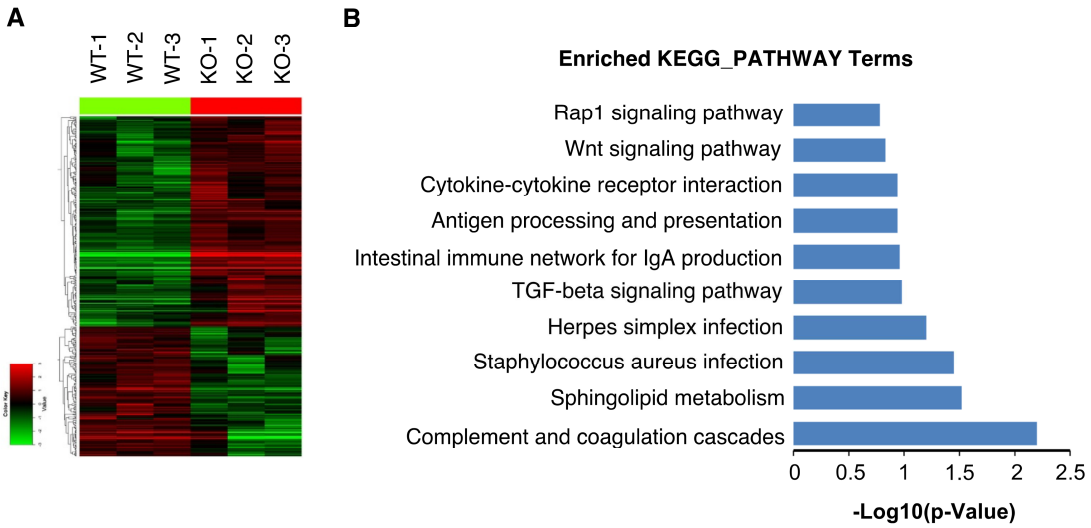
ACCEPTED MANUSCRIPT

Supplementary Figure 9



Supplementary Figure 9. Identification of *MIR31* target genes. (*A*) The 3'UTR in *Il6st*, *Il7r*, *Il17ra*, *Axin1, Dkk1*, *Gsk3b*, *Lats2*, *Dlg1* and *Dlg5* contain *MIR31* binding site. (*B*) Mutant binding sites of genes, *Il6st*, *Il7r*, *Il17ra*, *Axin1, Dkk1*, *Gsk3b*, *Lats2*, *Dlg1* and *Dlg5*.

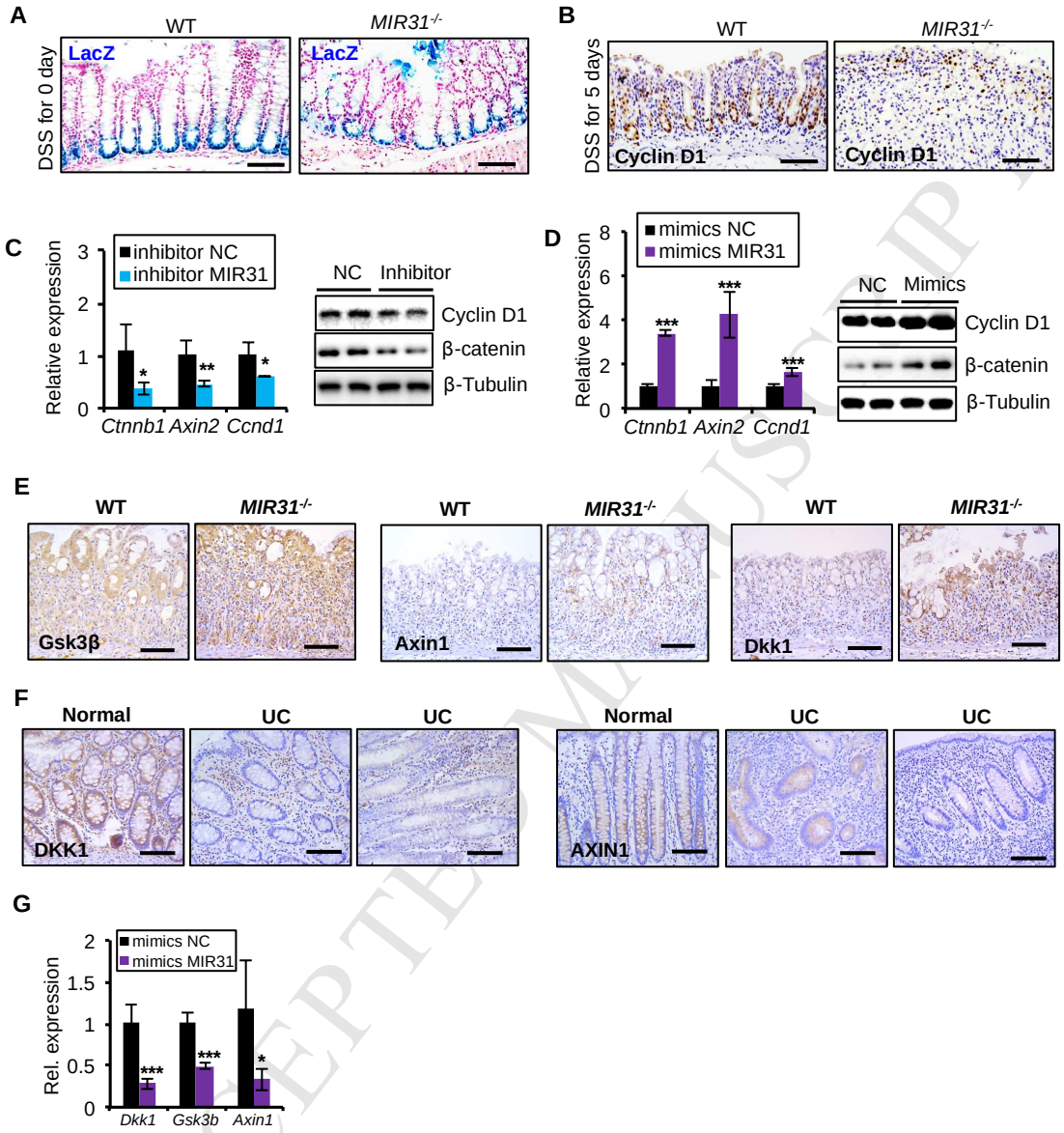
Supplementary Figure 10



Supplementary Figure 10. Microarray analysis on WT and *MIR31*$^{-/-}$ colonic epithelial cells. (*A*) Heatmaps of differentially expressed genes (DEGs) in WT and *MIR31*$^{-/-}$ epithelial cells. Note: the cutoff is $P < .05$. (*B*) GO and KEGG pathway analysis of DEGs in *MIR31*$^{-/-}$ colonic epithelial cells.

ACCEPTED MANUSCRIPT

Supplementary Figure 11



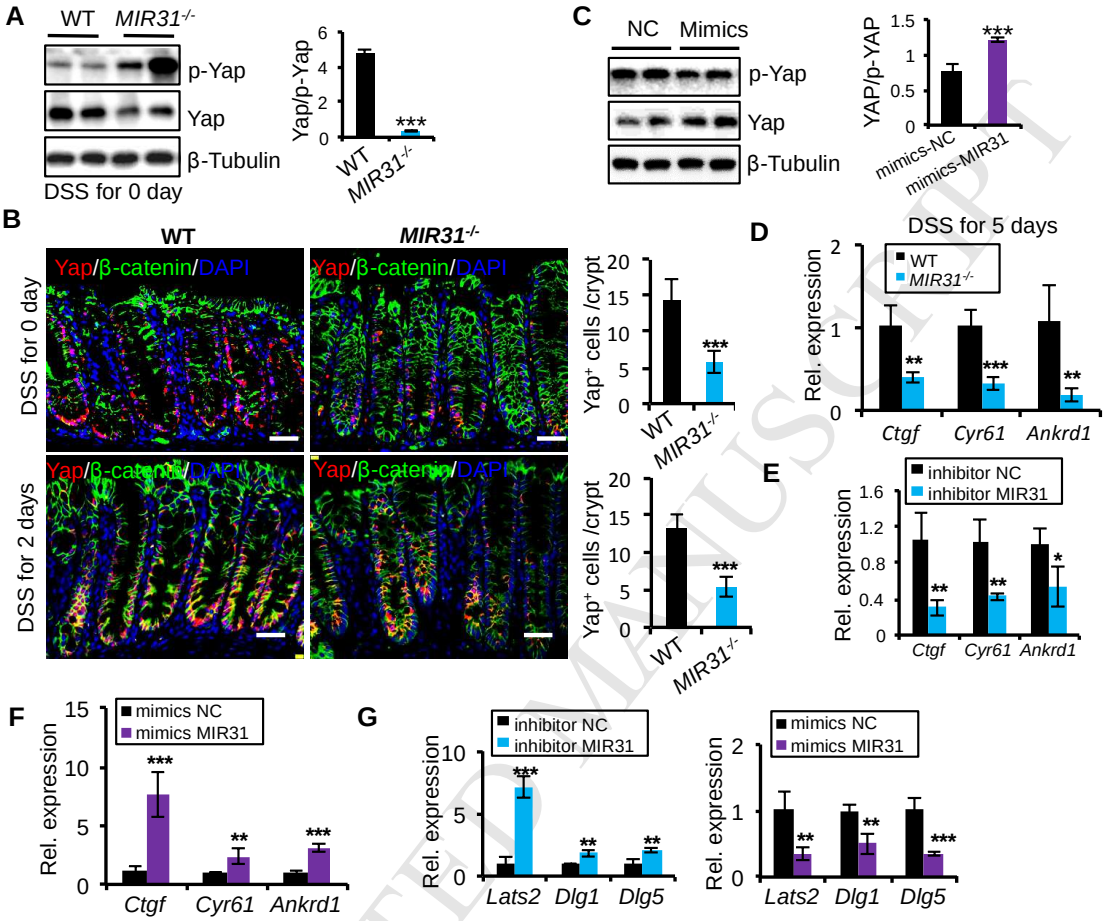
Supplementary Figure 11. MIR31 activates WNT signaling pathway in response to DSS treatment. (*A*) WNT activity was evaluated by *Axin2-LacZ* reporter activity in WT and *MIR31*$^{-/-}$ colon before DSS treatment. Blue, LacZ signals. n = 3 biological replicates. Scale bar: 50 μm. (*B*) Immunohistochemistry for Cyclin D1 in the colon from WT (n = 3) and *MIR31*$^{-/-}$ (n = 3) mice following 5-day DSS treatment. Scale bar: 50 μm. (*C*) qRT-PCR analysis for *Ctnnb1, Ccnd1*, and *Axin2* (left panel), as well as Western blotting for Cyclin D1 and β-catenin (right panel) in LOVO cells upon MIR31 inhibitor. n = 3 technical replicates. **P* < .05; ***P* < .01. β-Tubulin was used as a loading control, which is identical to main Figure 5H. (*D*) qRT-PCR analysis for *Ctnnb1, Ccnd1*, and *Axin2* (left panel),

as well as Western blotting for Cyclin D1 and β-catenin (right panel) in LOVO cells upon MIR31 mimics. n = 3 technical replicates. ***P < .001. β-Tubulin was used as a loading control. (*E*) Immunohistochemistry for Dkk1, Gsk3β and Axin1 in WT and *MIR31*$^{-/-}$ colon following 5-day DSS treatment. Scale bar: 100 μm. (*F*) Immunohistochemistry for DKK1 and AXIN1 in normal human colon (n = 4) and human UC samples (n = 5). Scale bar: 100 μm. (*G*) qRT-PCR analysis for *Dkk1*, *Gsk3b* and *Axin1* in LOVO cells in response to MIR31 mimics. *P < .05; ***P < .001. Statistical analysis was performed using independent *t*-test for panels C, D, and G.

ACCEPTED MANUSCRIPT

ACCEPTED MANUSCRIPT

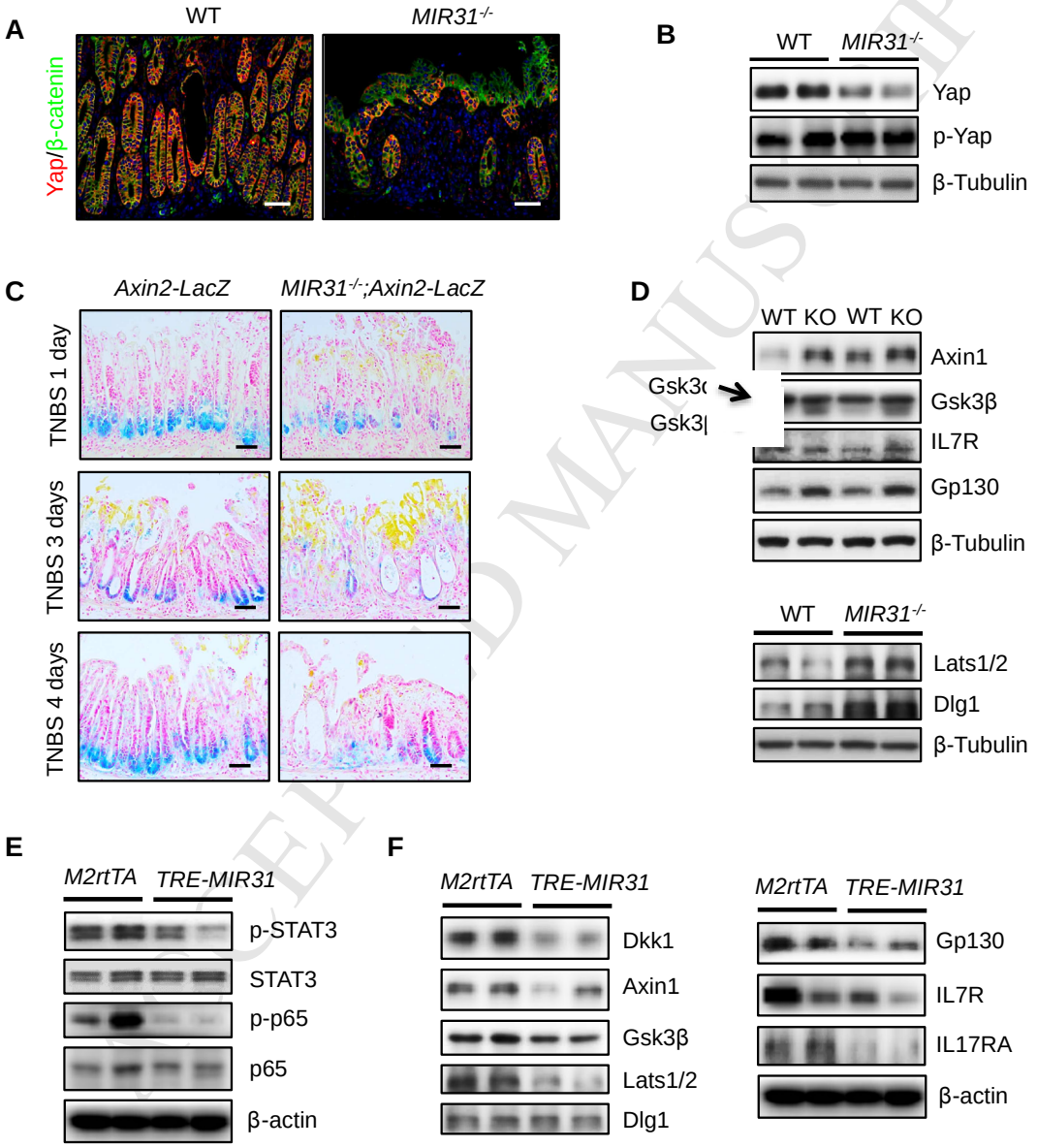
Supplementary Figure 12



Supplementary Figure 12. MIR31 represses the Hippo signaling pathway. (*A*) Western blotting for p-Yap and Yap in the colon from WT (n = 3) and *MIR31*$^{-/-}$ (n = 3) littermates before DSS treatment. β-Tubulin was used as a loading control. Quantification of Yap/p-Yap ratio is shown in right panel. ***P < .001. (*B*) Immunofluorescence for Yap in the colon WT (n = 3) and *MIR31*$^{-/-}$ (n = 3) mice before DSS treatment or following 2 days of DSS treatment. Scale bar: 50 μm. Quantification of Yap^{+} epithelial cells per crypt is shown in right panel. ***P < .001. (*C*) Western blotting for p-Yap and Yap in LOVO cells in response to MIR31 mimics. n = 3 technical replicates. β-Tubulin was used as a loading control, which is identical to Supplementary Figure 11D. Quantification of Yap/p-Yap ratio is shown in Right panel. (*D*) qRT-PCR analysis for *Ctgf*, *Cyr61* and *Ankrd1* in the colon from WT (n = 5) and *MIR31*$^{-/-}$ (n = 5) mice following 5 days of DSS treatment. **P < .01; ***P < .001. (*E*) qRT-PCR analysis for *Ctgf*, *Cyr61* and *Ankrd1* in LOVO cells in response to MIR31 inhibitor. n = 3 technical replicates. *P < .05; **P < .01. (*F*) qRT-PCR analysis for *Ctgf*, *Cyr61* and *Ankrd1* in LOVO cells in response to MIR31 mimics. n = 3 technical replicates. **P < .01; ***P

< .001. (*G*) qRT-PCR analysis for *Lats2*, *Dlg1* and *Dlg5* in LOVO cells in response to MIR31 mimics and inhibitors. n = 3 technical replicates. ***P* < .01; ****P* < .001. Statistical analysis was performed using independent *t*-test for panels A-G.

Supplementary Figure 13

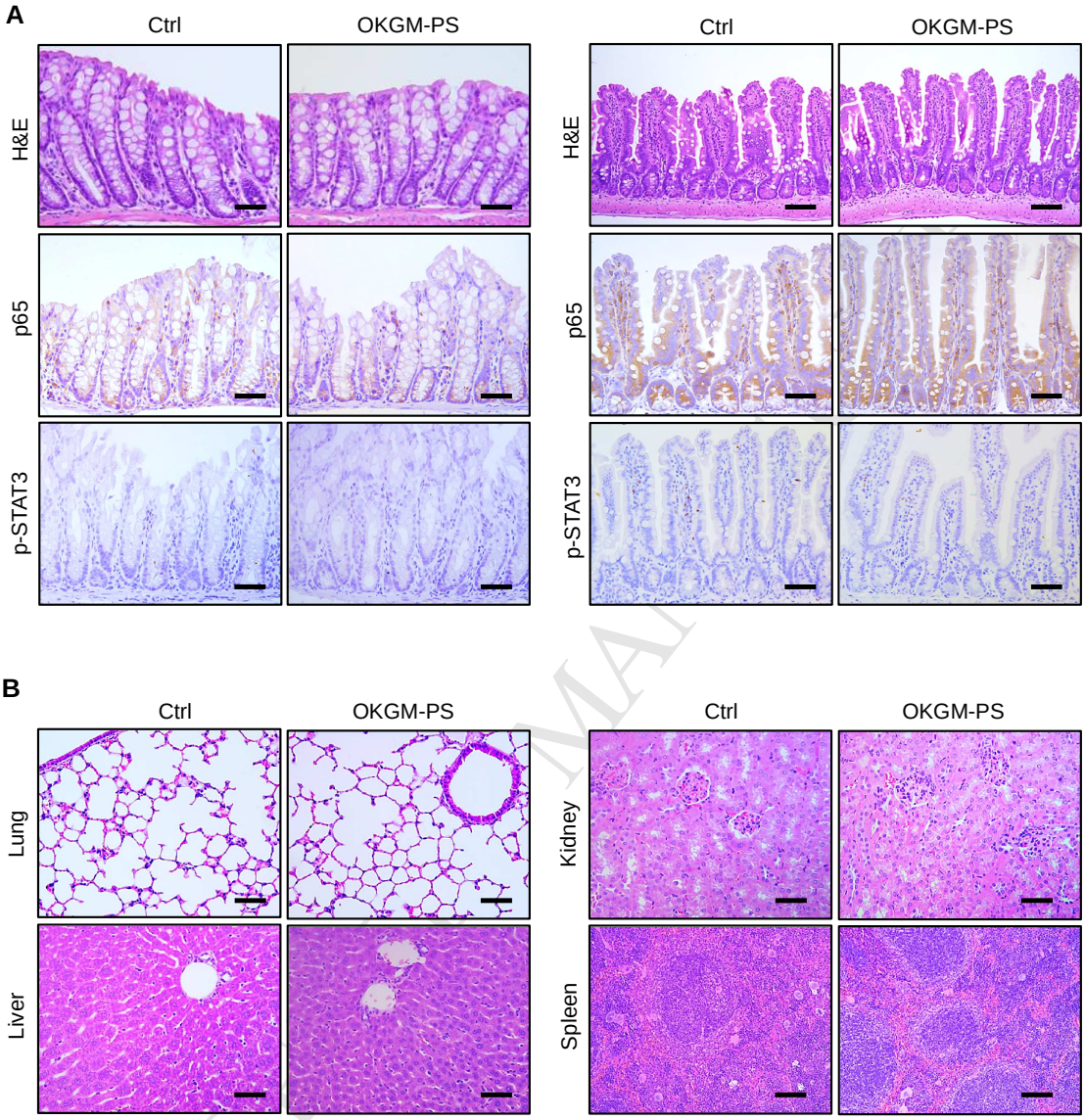


Supplementary Figure 13. MIR31 regulates the WNT and Hippo signaling pathways in TNBS-induced colitis. (*A*) Immunofluorescence for Yap in colon from WT (n = 3) and *MIR31*$^{-/-}$ (n = 3) littermates after 4 days of TNBS treatment. Scale bar: 50 µm. (*B*) Western blotting for p-Yap and Yap in colon from WT (n =

3) and *MIR31*$^{-/-}$ (n = 3) littermates after 4 days of TNBS treatment. β-Tubulin was used as a loading control. (*C*) WNT activity was evaluated by *Axin2-LacZ* reporter activity in WT and *MIR31*$^{-/-}$ colon after TNBS treatment at indicated time points. Blue, LacZ signals. n = 3 biological replicates. Scale bar: 50 μm. (*D*) Western blotting for Axin1, Gsk3β, IL7R, Gp130, Lats1/2 and Dlg1 in colon from WT (n = 3) and *MIR31*$^{-/-}$ (n = 3) littermates after 4 days of TNBS treatment. β-Tubulin was used as a loading control, which is identical to Supplementary Figure 4F. (*E*) Western blotting for p-STAT3, STAT3, p-p65 and p65 in the colon from *M2rtTA* and *TRE-MIR31* mice after 4 days of TNBS treatment. β-actin was used as a loading control. (*F*) Western blotting for MIR31 target gene Dkk1, Axin1, Gsk3β, Lats1/2, Dlg1, Gp130, IL7R and IL17RA in the colon from *M2rtTA* and *TRE-MIR31* mice after 4 days of TNBS treatment. β-actin was used as a loading control, which is identical to panel E.

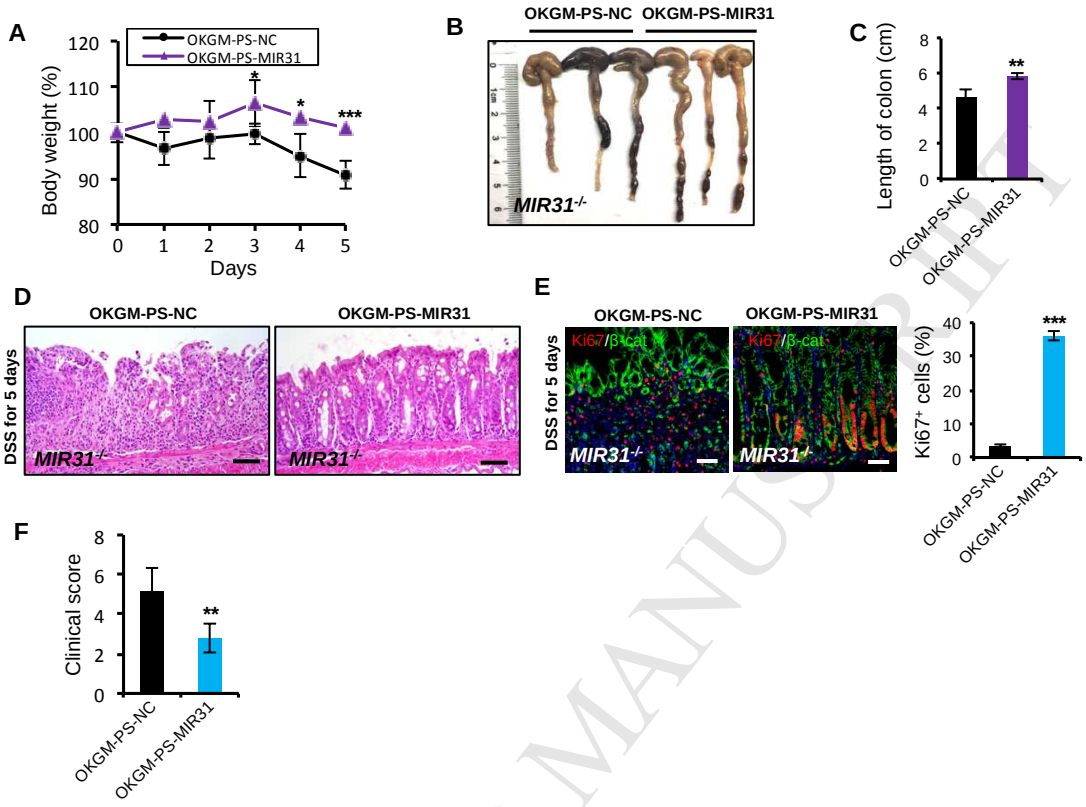
ACCEPTED MANUSCRIPT

Supplementary Figure 14



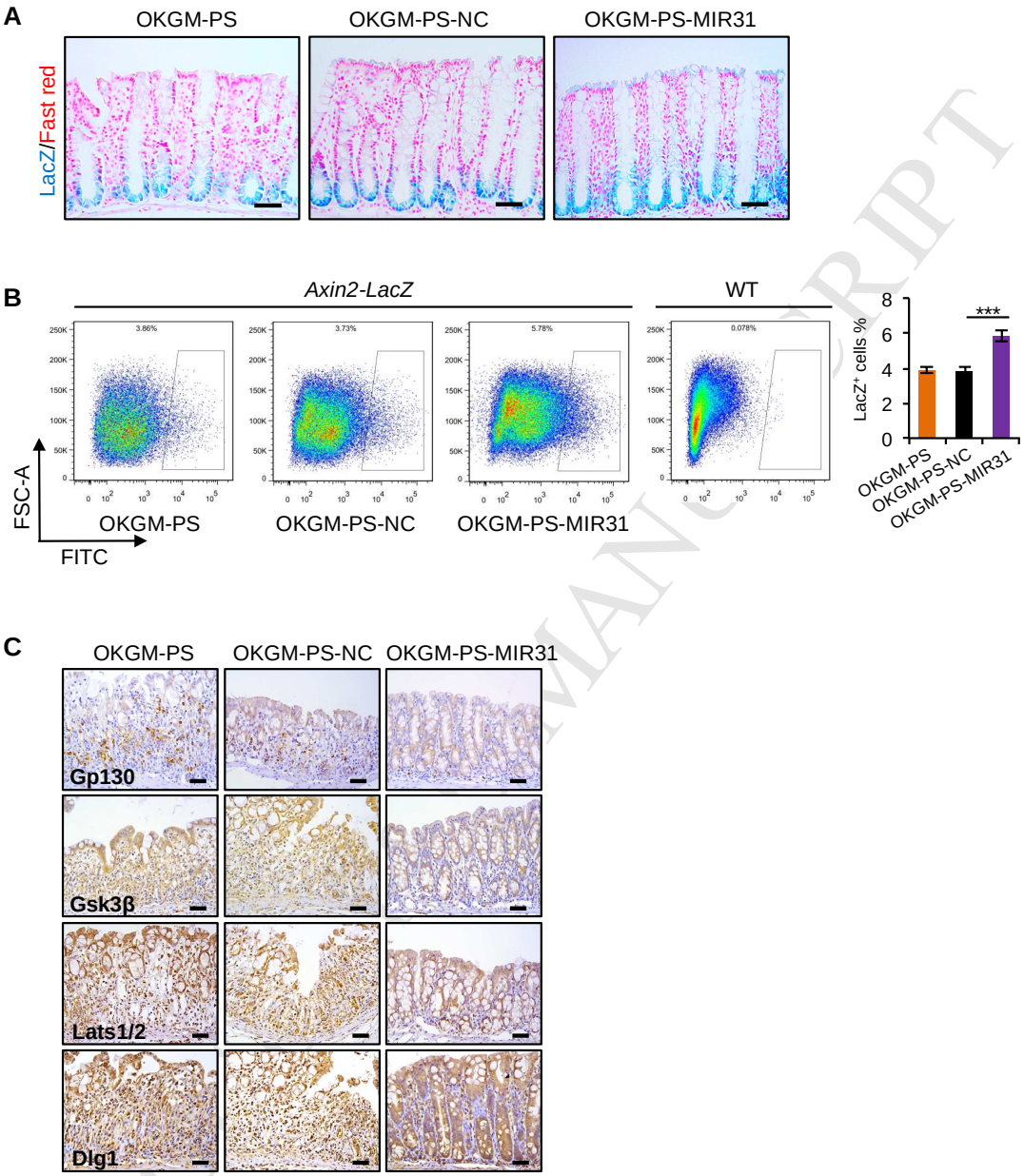
Supplementary Figure 14. OKGM-PS microsphere exhibits no toxicity. (*A*) Histology and immunohistochemistry for p65 and p-STAT3 in colon and intestine from control (n = 5) and OKGM-PS microsphere (n = 5) treated mice. Scale bar: 50 μm. (*B*) Histology for lung, kidney, liver and spleen from control (n = 5) and OKGM-PS microsphere (n = 5) treated mice. Scale bar: 50 μm.

Supplementary Figure 15



Supplementary Figure 15. OKGM-PS-MIR31 microspheres at least partially rescues the DSS-induced colitis in *MIR31*$^{-/-}$ mice. (*A*) Quantification of weight loss in *MIR31*$^{-/-}$ mice following 5 days of DSS treatment, coupling with OKGM-negative control (OKGM-PS-NC) and OKGM-PS-MIR31 treatment. n = 5 biological replicates for each treatment. **P* < .05; ****P* < .001. (*B*) Representative gross images of colons from *MIR31*$^{-/-}$ mice following 5 days of DSS treatment, coupling with treatment of OKGM-PS-NC and OKGM-PS-MIR31. n = 5 biological replicates for each treatment. (*C*) Quantification of colon length under different conditions in Panel B. ***P* < .01. (*D* and *E*) H&E and double immunofluorescence for Ki67 and β-catenin in *MIR31*$^{-/-}$ colons following 5 days of DSS treatment, coupling with treatment of OKGM-PS-NC and OKGM-PS-MIR31. Quantification Ki67^{+} cells per crypt. Scale bar: 50 μm. ****P* < .001. (F) Quantification of clinical scores in *MIR31*$^{-/-}$ colons following 5 days of DSS treatment, coupling with treatment of OKGM-PS-NC and OKGM-PS-MIR31. ****P* < .001. Statistical analysis was performed using independent *t*-test for panels A, C, E, and F.

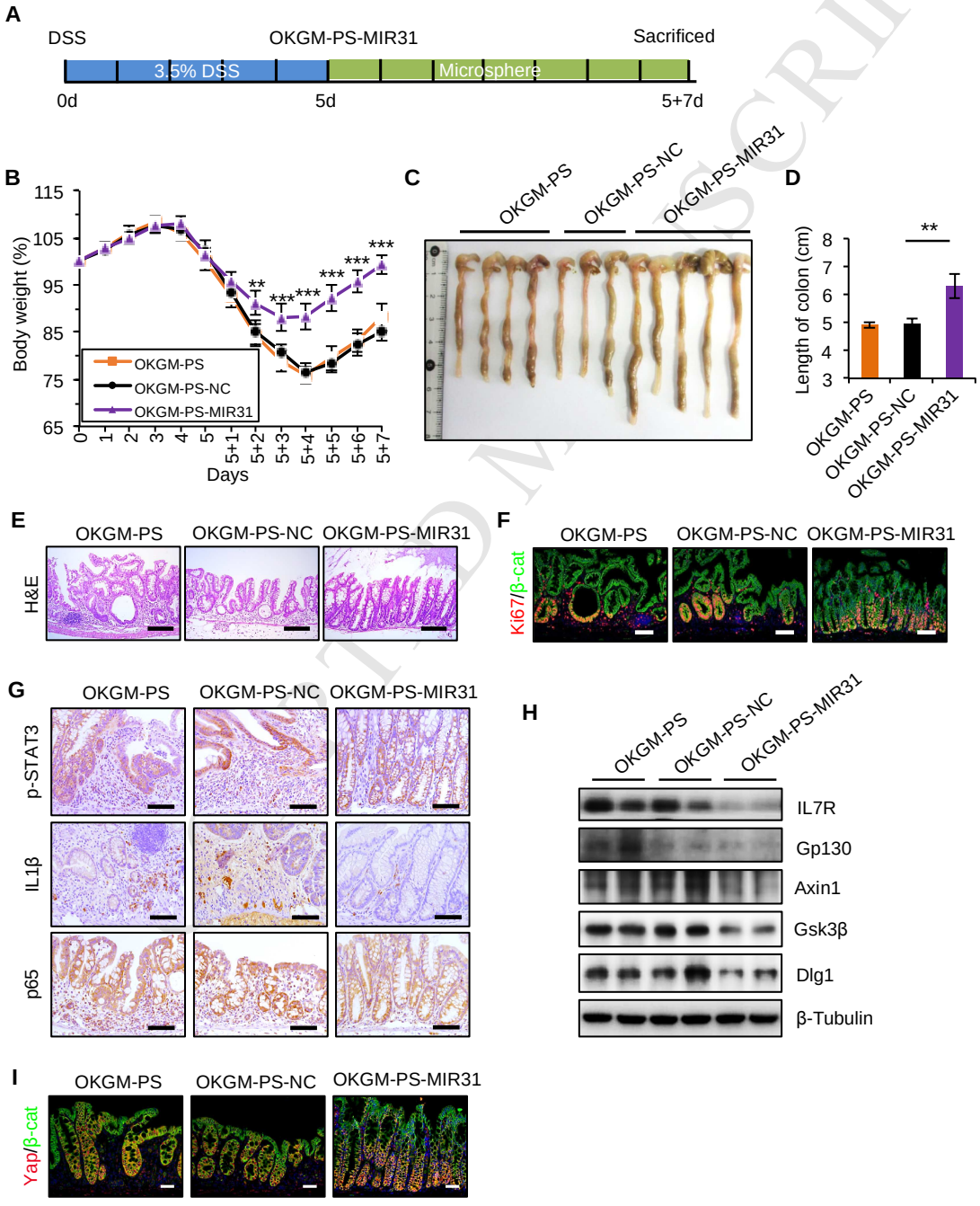
Supplementary Figure 16



Supplementary Figure 16. OKGM-PS-MIR31 microspheres activate WNT signaling pathway and downregulates MIR31 target genes. (*A*) WNT signaling pathway was evaluated by *Axin2-LacZ* reporter in OKGM-PS (n = 3), OKGM-PS-NC (n = 3) and OKGM-PS-MIR31 (n = 3) treated colons. Scale bar: 50 µm. (*B*) Flow cytometry analysis of Axini2-lacZ^{+} cells in colonic epithelium from Axin2-LacZ mice treated with from OKGM-PS (n = 4), OKGM-PS-NC (n = 4) and OKGM-PS-MIR31 (n = 4) microspheres. EpCAM-PE was used to identify epithelial cells. WT mice were used as negative control. Quantification of Axin2-

LacZ$^+$ cells under various treatments. ***P < .001. (C) Immunohistochemistry for Gp130, Gsk3β, Dlg1 and Lats2 in the colon from WT mice following 5 days of DSS treatment, and treated with OKGM-PS (n = 5), OKGM-PS-NC (n = 5) and OKGM-PS-MIR31 (n = 5) microspheres. Scale bar: 50 μm. Statistical analysis was performed using independent t-test for panels B.

Supplementary Figure 17

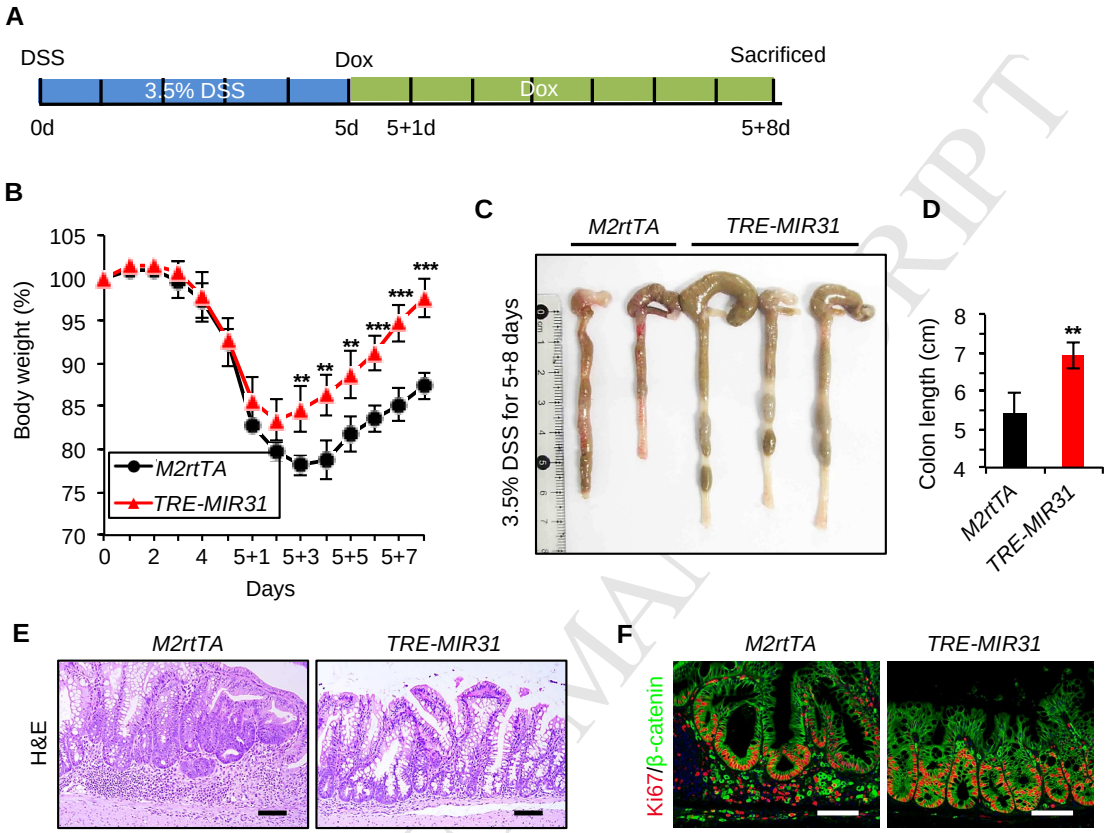


ACCEPTED MANUSCRIPT

Supplementary Figure 17. OKGM-PS-MIR31 microspheres enhance the recovery of active colitis. (*A*) Strategy for OKGM-PS-MIR31 microsphere in treating an established DSS-induced colitis. (*B*) Quantification of weight loss in WT mice for 5 days of DSS treatment, then following 7 days of OKGM-PS (n = 4), OKGM-PS-NC (n = 3) and OKGM-PS-MIR31 (n = 5) treatment. (*C)* Gross images of colons from mice treated for 5 days of DSS treatment, then following 7 days of OKGM-PS, OKGM-PS-NC and OKGM-PS-MIR31 treatment. (*D*) Quantification of colon length under different conditions in panel C. $^{**}P < .01$. (*E*) Histology of colons from mice after 7 days of OKGM-PS, OKGM-PS-NC and OKGM-PS-MIR31 microspheres treatment. Scale bar: 50 μm. n = 3 for each treatment. (*F*) Double immunofluorescence for Ki67 and β-catenin in the colon from mice after 7 days of OKGM-PS, OKGM-PS-NC and OKGM-PS-MIR31 microspheres treatment. Scale bar: 50 μm. n = 3 for each treatment. (*G*) Immunohistochemistry for p-STAT3, IL1β and p65 in colons from mice after 7 days of OKGM-PS, OKGM-PS-NC and OKGM-PS-MIR31 microspheres treatment. Scale bar: 50 μm. n = 3 for each treatment. (*H*) Western blotting for MIR31 targets IL7R, Gp130, Axin1, Gsk3β and Dlg1 in the colon from mice after 7 days of OKGM-PS, OKGM-PS-NC and OKGM-PS-MIR31 microspheres treatment. β-Tubulin was used as a loading control. (I) Double immunofluorescence for Yap and β-catenin in the colon from mice after 7 days of OKGM-PS, OKGM-PS-NC and OKGM-PS-MIR31 microspheres treatment. Scale bar: 50 μm. n = 3 for each treatment. Statistical analysis was performed using independent *t*-test panels B, D.

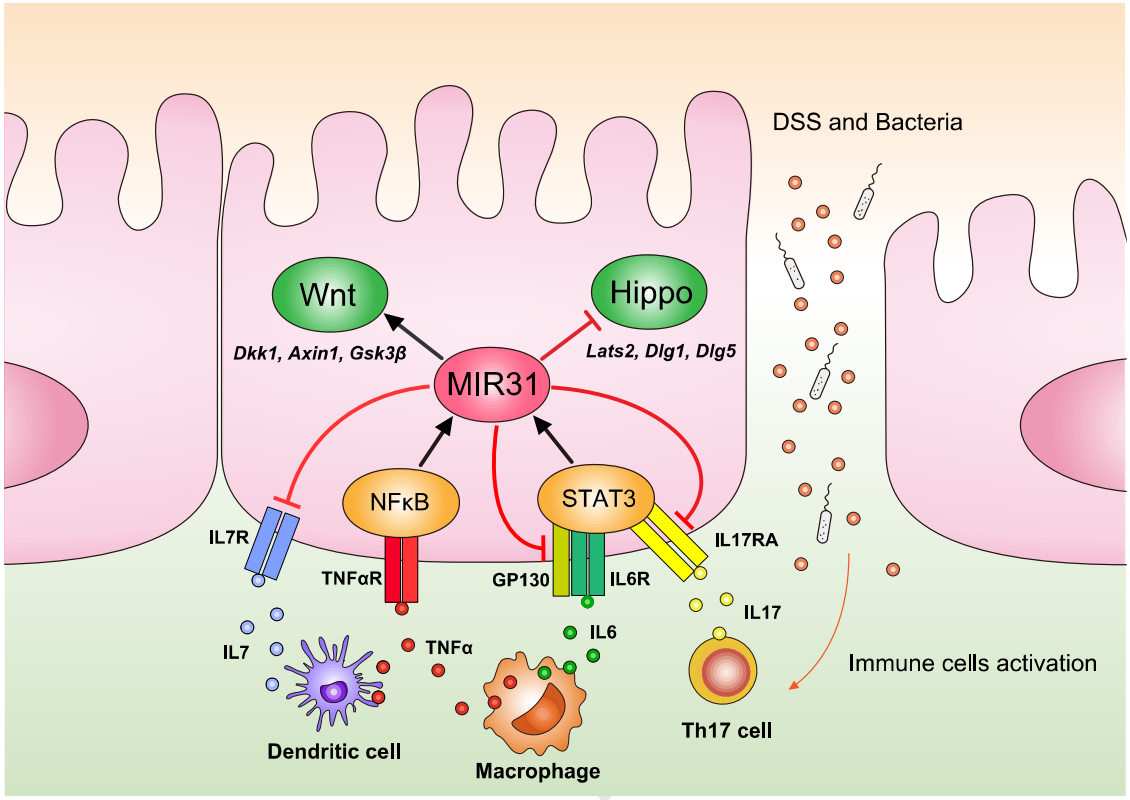
ACCEPTED MANUSCRIPT

Supplementary Figure 18



Supplementary Figure 18. MIR31 *in vivo* overexpression enhances the recovery of an established colitis. (*A*) Strategy for MIR31 induction in treating an established DSS-induced colitis. (*B*) Quantification of weight loss in *M2rtTA* (n = 4) and *TRE-MIR31* (n = 4, *M2rtTA*;*TRE-MIR31*) littermates for 5 days of DSS treatment, then following 7 days of Dox treatment. (*C*) Representative gross images of colons from *M2rtTA* (n = 4) and *TRE-MIR31* (n = 4) littermates for 5 days of DSS treatment, then following 7 days of Dox treatment. (*D*) Quantification of colon length in panel C. ***P* < .01. (*E*) Histology of the colon from *M2rtTA* (n = 3) and *TRE-MIR31* (n = 3) littermates after the treatments. Scale bar: 100 μm. (*F*) Double immunofluorescence for Ki67 and β-catenin in the colon from *M2rtTA* (n = 3) and *TRE-MIR31* (n = 3) littermates after the treatments. Scale bar: 100 μm. Statistical analysis was performed using independent *t*-test panels B, D.

Supplementary Figure 19



Supplementary Figure 19. The working model of MIR31 in colitis. Inflammatory signals-induced MIR31 attenuated the inflammatory response by directly targeting *Il17ra*, *Il7r* and *Il16st* (encoding Gp130) in the colonic epithelium through a negative-feedback loop. Concomitantly, MIR31 promoted epithelial regeneration by directly regulating both the WNT and Hippo signaling pathways.

ACCEPTED

ACCEPTED MANUSCRIPT

Supplementary Table 1. Characteristics of patients with IBD and healthy controls

	HC	CD	UC
Number of patients	34	79	82
Age (years)	38.2 ± 11.8	35.3 ± 10.2	45.8 ± 13.1
Gender			
Male	16	42	51
Female	18	37	31
Active/Remission		41/38	45/37
Disease duration (months)		37.3 ± 17.2	34.4 ± 18.1
Current therapy			
5-aminosalicylates		23	61
Salazosulfapyridine		0	4
Azathioprine		62	4
Glucocorticoids		23	57
Methotrexate		13	2
Biologics		48	8
Nutritional therapy		31	5

ACCEPTED MANUSCRIPT

Supplementary Table 2. Primers for qRT-PCR in this study

Gene	Forward Primer 5'-3'	Reverse Primer 5'-3'
Axin1	TTCTGGGTTGAGGAAGCAGC	GATTAGGGGCTGGATTGGGT
Dkk1	TCCGAGGAGAAATTGAGGAA	CCTGAGGCACAGTCTGATGA
Gsk3β	CCAACAAGGGAGCAAATTAGAGA	GGTCCCGCAATTCATCGAAA
Ctnnb1	TCCTAGCTCGGGATGTTCAC	TTCTGCAGCTTCCTTGTCCT
Ifng	ATGAACGCTACACACTGCATC	CCATCCTTTTGCCAGTTCCTC
Tnfa	CCCTCACACTCAGATCATCTTCT	GCTACGACGTGGGCTACAG
Il6	GCCAGAGTCCTTCAGAGAGA	GGTCTTGGTCCTTAGCCACT
Tgfb	CTCCCGTGGCTTCTAGTGC	GCCTTAGTTTGGACAGGATCTG
Il10	GCTCTTACTGACTGGCATGAG	CGCAGCTCTAGGAGCATGTG
Il12	TGGTTTGCCATCGTTTTGCTG	ACAGGTGAGGTTCACTGTTTCT
Pink1	TTCTTCCGCCAGTCGGTAG	CTGCTTCTCCTCGATCAGCC
Map1lc3a (Lc3a)	GACCGCTGTAAGGAGGTGC	CTTGACCAACTCGCTCATGTTA
Map1lc3b (Lc3b)	TTATAGAGCGATACAAGGGGGAG	CGCCGTCTGATTATCTTGATGAG
Bnip3	TCCTGGGTAGAACTGCACTTC	GCTGGGCATCCAACAGTATTT
Nlrp3	ATTACCCGCCCGAGAAAGG	TCGCAGCAAAGATCCACACAG
Caspase1	ACAAGGCACGGGACCTATG	TCCCAGTCAGTCCTGGAAATG
IL1b	TACCTGTGTCTTTCCCGTGG	TTGTTCATCTCGGAGCCTGT
Il18	GTCTACCCTCTCCTGTAAGAACA	TGGCAAGCAAGAAAGTGTCC
Il23a	ATGCTGGATTGCAGAGCAGTA	ACGGGGCACATTATTTTTAGTCT
Il17a	TTTAACTCCCTTGGCGCAAAA	CTTTCCCTCCGCATTGACAC
Il6st	CTCTGTTGACAAGCAATGAGACG	TCTTCAGTATGTCTAGCCCCTG
Il7r	GCGGACGATCACTCCTTCTG	AGCCCCACATATTTGAAATTCCA
Il17ra	AGTGTTTCCTCTACCCAGCAC	GAAAACCGCCACCGCTTAC
Axin2	GGCTAGCTGAGGTGTCGAAG	GCCAGTTTCTTTGGCTCTTT
Ccnd1	TGGTGAACAAGCTCAAGTGG	GGCGGATTGGAAATGAACT
Ctgf	GGGCCTCTTCTGCGATTTC	ATCCAGGCAAGTGCATTGGTA
Cyr61	CTGCGCTAAACAACTCAACGA	GCAGATCCCTTTCAGAGCGG
Ankrd1	GGAACAACGGAAAAGCGAGAA	GAAACCTCGGCACATCCACA
Lats2	GGACCCCAGGAATGAGCAG	CCCTCGTAGTTTGCACCACC
Dlg1	CGAAGAGTCACGTCGTTTTGA	TCTCCAAAGCGGAAGTTCAGT
Dlg5	CTTTTCCAACGACTCCATTCCT	AGAGAGGTACAGTCCACTTTCTG
Rela	AGATACCACCAAGACCCACC	GGTGACCAGGGAGATTCGAA
Il25	ACAGGGACTTGAATCGGGTC	TGGTAAAGTGGGACGGAGTTG
Il23a	ATGCTGGATTGCAGAGCAGTA	ACGGGGCACATTATTTTTAGTCT
Il12b	TGGTTTGCCATCGTTTTGCTG	ACAGGTGAGGTTCACTGTTTCT
Tslp	ACGGATGGGGCTAACTTACAA	AGTCCTCGATTTGCTCGAACT
Camp	GCTGTGGCGGTCACTATCAC	TGTCTAGGGACTGCTGGTTGA
Defb1	AGGTGTTGGCATTCTCACAAG	GCTTATCTGGTTTACAGGTTCCC

ACCEPTED MANUSCRIPT

ACCEPTED MANUSCRIPT

Supplementary Table 3. Primers Used for identifying MIR31 target genes

Gene	Forward Primer 5'-3'	Reverse Primer 5'-3'
Dkk1	GCGCTCGAGTGGGCTTGAATTTGGTAT	TTAGCGGCCGCGTCCCGACTATCCTGTGA
Gsk3β	TTAGCGGCCGCTCAGTTTCACAGGGTTAT	GCGCTCGAGACAAAGGCATTCAAGTAG
Axin1	GCCTCGAGTCAGTCAGGTGGACAGCC	TAGCGGCCGCACACGGACACTTGGAAGG
Lats2	GCGCTCGAGGTCACGAGGACCGCTTATCT	ATAGCGGCCGCTTACATTTGCCTCCCGAAGA
Dlg1	GCGCTCGAGGAACAGTCTGGGCCTTACAT	ATAGCGGCCGCTTGCTCAAGGTCCACTAAAT
Dlg5	GCGCTCGAGATAGCCAGCCCAGCAGAGGT	ATAGCGGCCGCCCAAGGAGGCAGGAGAAAGG
Il6st	GCGCTCGAGGAGTACAGAAGGGCACAGCA	ATAGCGGCCGCTGAAGCCACTCGTCTTTAGC
Il7r	GCGCTCGAGTTCTCATTTCTTCCTCACAA	ATAGCGGCCGCTCATCCCTATAGCCACTTTA
Il17ra	GCGCTCGAGGAAAGATGTGAGGGTAGTGG	ATAGCGGCCGCGAAGAAATAGAGCTGGGAAA

ACCEPTED MANUSCRIPT

ACCEPTED MANUSCRIPT

Supplementary MATERIALS AND METHODS

Ethics

All mouse experimental procedures and protocols were evaluated and authorized by the Beijing Laboratory Animal Management and were performed strictly in accordance with the guidelines of the Institutional Animal Care and Use Committee of China Agricultural University (approval number: SKLAB-2011-04-03).

In situ Hybridization

The MIR31 *in situ* hybridization assay was performed as described previously with modifications[1]. Digoxigenin (DIG)-labeled LNA probes (Exiqon, Vedbaek, Denmark) were used following the manufacturer's protocol. Both DIG-labeled MIR31 and scrambled LNA probes (Exiqon) were hybridized at 61℃. The U6 probe was used as a positive control. *In situ* signals were detected by staining with anti-digoxigenin-AP antibody (Roche) and developing using BM purple substrate (Roche).

DSS Treatment

Mice were treated with 3.5% w/v dextran sulfate sodium (DSS) with molecular weight 36,000–50,000 (MP Biochemicals) in drinking water for 5 days and DSS was withdrawn for another 3 days. The severity of colitis was scored daily by recording standard parameters, including body weight as well as the presence of diarrhea, and bloody stools. The colonic tissues were removed and fixed in 10% PFA for 24 hours, embedded in paraffin, sectioned, and stained with hematoxylin and eosin (H&E). The histological grade of colonic inflammation was graded from 0 to 4 as previously described[2]. The disease activity index (DAI) was measured as previously reported[2]. Clinical scores were evaluated by an independent investigator who was blinded to the experiment.

TNBS Treatment

TNBS induced-colitis was generated as described previously. [3] To induce acute TNBS colitis, the mice were weighed and anesthetized with isoflurane-mixed gas and 150 μL of 1% (wt/vol) TNBS (Sigma, cat. no. p2297) pre-sensitization solution was applied to a 1.5 x 1.5-cm shaved area of skin on the back of the mouse between the shoulders. On day 8, after weighing and anesthetizing the mice, we slowly inject 125 μL of 2.5% (wt/vol) TNBS solution into the lumen of the colon with a 1 ml syringe and 3.5 F catheter and remove the catheter and position the mouse head down for 5 minutes. The severity of colitis was scored daily by recording standard parameters including body weight, diarrhea, and bloody stools. The mice were sacrificed at the time points of choice for colon samples.

To induce the chronic TNBS colitis, the mouse was pre-sensitized as described above on day 1 and 100 μL of designated concentration TNBS was intrarectally

administered to the mice at designated time points as previously described [3]. During this process, animal weight and signs of distress were monitored daily. The mice were sacrificed after 6 cycles of TNBS treatments.

qRT-PCR Analysis

qRT-PCR analysis was performed to determine the expression levels of MIR31 and coding genes in human and mouse colon tissues. To detect expression of MIR31, reverse transcription was carried out using TaqMan microRNA RT Kit (ABI). Real-time PCR was carried out in triplicate using the TaqMan Universal Master Mix II. The expression levels of MIR31 were normalized to the levels of U6 snRNA. To detect mRNA level, reverse transcription was carried out using oligo (dT) primers. Real-time PCR was performed using LightCycler 480 SYBR Green I master mix. GAPDH were used as the internal control. The primers used are located in Supplementary Table 2.

Isolation of Colonic Epithelial and Mesenchymal Cells

Intestinal epithelium cells (IEC) were isolated as described previously[2, 4]. Briefly, the large intestine was removed and placed in cold-DPBS to remove debris. The colon was opened longitudinally and cut into pieces 1-2 cm in size, which were then Incubated in 1x DPBS containing 5 mM EDTA and 0.2 mM DTT for 30 min at 4℃ on a rotating platform to isolate primary IE Cs. Suspended epithelial cells were collected following gentle vortexing. After isolating the epithelial cells, the remaining tissue was incubated in digestion solution containing 1.5% FBS, 1.0 mg/mL collagenase B (Roche Diagnostics GmbH, Mannheim Germany) and 0.1 mg/mL DNase (Sigma) for 1 hour at 37℃. Single mese nchymal cells were collected with centrifuge.

Intestinal Permeability Assay

WT and *MIR31*$^{-/-}$ littermates were fasted for 4 hours, and administered FITC dextran tracer (40 KDa, 0.6 mg/g body weight) intragastrically in 0.1 mL of PBS; Hemolysis-free serum was then collected after 3 hours (using convenient method). A standard curve for a FITC-dextran was ascertained by serially diluting a known amount of FITC-dextran in mouse serum. The samples were diluted using PBS, and the absorbance at 520 nm was measured using Hitachi F-4500 Fluorescence Spectrophotometer.

Cell Culture and Transfection

LOVO human colorectal cancer cell were cultured under standard culture conditions. TNF (RMTNFAI, ThermoFisher) and IL6 (PMC0061, GibcoTM) were used to stimulate cells and induce an inflammatory response. Colonic epithelial cells were transfected using Lipofectamine 2000 reagent with 100 nM of MIR31-5p mirVana microRNA mimics (mimic-MIR31) or the negative control (mimic-NC) or MIR31-5p mirVana microRNA inhibitor (inhibitor-MIR31) or the scramble RNA (inhibitor-NC) according to the manufacturer's protocol (Invitrogen). The sequence of inhibitor-MIR31 is 5'-AGCUAUGCCAGCAUCUUGCCU-3'. The sequence of ibhibitor-NC is 5'-CAGUACUUUUGUGUAGUACAA-3'. The

Sequence of MIR31 mimics-MIR31:
5'-AGGCAAGAUGCUGGCAUAGCU-3'
3'-CUAUGCCAGCAUCUUGCCUUU-5'
The sequence of negative control for mimics-NC:
5'-UUCUCCGAACGUGUCACGUUU-3'
3'-ACGUGACACGUUCGGAGAAUU-5'.

Histology, Immunofluoresence, and Immunochemistry

For histological analysis, the colon was rinsed with 1x DPBS, fixed in 10% formalin, paraffin-embedded and sectioned at 5 μm. The sections were deparaffinized with xylene (2x15 min) followed by treatment with serial dilutions of ethanol (100%, 100%, 95%, 95%, 80% and 70% for 5 min at each step) and two washes with ddH_2O. The sections were stained with hematoxylin for 10 min at room temperature (RT) and then washed in running water for 5 min. The sections were stained with eosin for 20 seconds, dehydrated with serial dilutions of ethanol (95%, 95%, 100% and 100% for 5 min at each step) and then mounted with coverslips in neutral gum mounting medium.

For immunofluorescence, antigen retrieval was performed by heating slides in 0.01 M citrate buffer (pH 6.0) in a microwave. Sections were rinsed three times with ddH_2O, immersed in 3% H_2O_2 for 20 min, washed once with TBS-T (TBS, 0.1% Tween-20) and twice with PBS and blocked for 1 hour with blocking solution (10% normal goat serum [5425, Cell Signaling Technology] in TBS-T). The sections were incubated with anti-Ki67 (1:150, Leica), anti-CD45 (1:200, Santa Cruz), anti-F4/80 (1:200, Santa Cruz), anti-IL-1β(1:200, Santa Cruz), anti-β-catenin (1:500, Sigma), anti-Gp130 (1:200, Santa Cruz), anti-IL-7R (1:200, Santa Cruz), anti-IL-17RA (1:200, Santa Cruz), anti-Cyclin D1 (1:50, Abcam), anti-Axin1 (1:100, Cell Signaling Technology), anti-Gsk3β (1:2000, Abcam), anti-Dkk1 (1:50, Santa Cruz), anti-Yap (1:400, Cell Signaling Technology), anti-Lats1/2 (1:1000, Cell Signaling Technology), anti-Dlg1 (1:1000, Cell Signaling Technology), anti-BrdU (1:50, Abcam), anti-mucin2 (1:100, Santa Cruz), anti-claudin1 (1:200, Cell Signaling), anti-p65 (1:400, Cell Signaling) and anti-p-STAT3 (1:800, Cell Signaling) overnight at 4℃. After incubation with the antibodies, sections were washed three times with TBS-T and incubated for 1 hour at RT with Alexa Fluor 488 Goat anti-mouse or anti-Rabbit IgG (H+L). The sections were then washed 3 times with TBS-T and stained with DAPI for 8 min, followed by covering sections with agent for quenching resistance.

Dual Luciferase Activity Assays

To generate reporter constructs for luciferase assays, 300-600 bp fragments containing predicted MIR31 target site in the 3'UTRs of *Il6st*, *Il7r*, *Il17ra*, *Axin1*, *Dkk1*, *Gsk3β, Lats2*, *Dlg1* and *Dlg5* were cloned into the psi-CHECK2 vector (Promega) between the XhoI and NotI sites, immediately downstream of the *Renilla* luciferase gene. To generate reporters with mutant 3'UTRs, nucleotides in the MIR31 binding site were mutated using a QuikChange Site-Directed Mutagenesis kit (Stratagene). For the 3'UTR assays, 293T cells were

cotransfected with the vectors, mimics-NC and mimics-MIR31, as well as inhibitor-NC and inhibitor-MIR31 respectively. After 24 hours, latter firefly and renilla luciferase activities were measured using the Dual-Glo luciferase assay according to the manufacturer's instructions (Promega) and then calculated using the following formula (WT-mimic/WT-mimic NC) /(MUT-mimic/MUT-mimic NC). The primers used for amplifying 3'-UTRs of MIR31 target genes were shown in Supplementary Table 3.

Western Blotting

Tissues or cell lysates were subjected to western blotting according to standard procedures. Frozen tissue biopsies were homogenized using IP buffer (Beyotime Biotechnology, Shanghai, China), followed by treatment with TissueLyserLT. After the protein concentration was measured using a BCA protein assay kit (Beyotime), 30 μg of total protein was separated by 8-12% SDS-PAGE under denaturing conditions and transferred to PVDF membranes (GE Healthcare). The PVDF membranes were blocked with 5% nonfat dry milk and incubated for 1 hour at RT. The following antibodies were applied: phospho-STAT3 (Tyr705), STAT3, anti-GAPDH (Sigma), anti-β-Tubulin (Sigma), anti-cyclin D1 (Santa Cruz), anti-β-catenin (Sigma), anti-Dkk1 (Santa Cruz), anti-Gsk3β (Abcam), anti-Axin1 (Cell Signaling), anti-p-p65 (Cell Signaling), anti-Gp130 (Santa Cruz), anti-IL7R (Santa Cruz), anti-IL17RA(Santa Cruz), anti-Lats1/2 (Cell Signaling), anti-Dlg1(Cell Signaling), anti-IL-1β(Cell Signaling), anti-IFNγ (Santa Cruz), anti-YAP (Cell Signaling), anti-p-YAP (Cell Signaling), anti-14-3-3 (Abcam), anti-CD45 (Santa Cruz), anti-Nlrp3 (Cell Signaling) and anti-caspase1(Santa Cruz). Protein bands were quantified using Image Lab software (Bio-Rad).

Luciferase Assay for MIR31 Promoter Activity

The sequence of primary MIR31 is located at chromosome 4, NC_000070.6 (88910557**..**88910662, complement) in the mouse genome. The 2 kb region upstream of transcript start site (TSS) was identified as the MIR31 promoter in this study, which is located at chromosome 4, NC_000070.6 (88910663**..**88912663) and was cloned into the pGL3-Basic reporter constructs. Binding sites 1 and 2 of p65 are located at 88912038-88912048 and 88912409-88912419, respectively. The binding site of STAT3 is located at 88911572-88911582. Nucleotides at MIR31 binding site were mutated using QuikChange Site-Directed Mutagenesis kit (Stratagene). The wildtype and mutant plasmide were transcripted to cells with TK plasmide respectively. At 24 hours after transfection, firefly and renilla luciferase activities were measured using the Dual-Glo luciferase assay according to the manufacturer's instructions (Promega).

Chromatin Immunoprecipitation (ChIP) Assay

Using the simple ChIP enzymatic chromatin immunoprecipitation kit (Cell Signaling Technology, #9002), ChIP assay was performed according to the manufacturer's protocol with minor modifications. Harvested cells were first cross-linked with 1% (v/v) formaldehyde for 10 min at RT. After isolating nuclei by the lysis of cytoplasmic fraction, the cells was incubated with

micrococcalnuclease (400 gel units) for 20 min at 37℃ to further digest chromatin into fragments of 150–900 bp. The sonicated nuclear fractions were divided for input control and incubated at anti-p65, anti-p-STAT3, H3 as a positive control, and IgG as a negative control at 4℃ for overnight. The recruited genomic DNA obtained from the ChIP assay was quantified by qPCR with primers specific to p-Stat3 and p65 binding elements of the *MIR31* promoter regions. Primers were as follows: p-STAT3-binding site forward: 5'-TCCAGGCAAGAAAGTGAGGG -3'; p-STAT3- binding site reverse: 5'-TGAGTAACAGTGCAACAGAGC-3'; p65-binding site forward: 5'-AGATACCACCAAGACCCACC -3'; p65-binding site reverse: 5'-GGTGACCAGGGAGATTCGAA-3'.

Generation of MIR31-Based Peptosomes (PSs)

A total of 3 mg of α-Lactalbumin was partially hydrolyzed by 2 μL Bacillus licheniformis protease (BLP) in 3 mL of Tris-HCl buffer (75 mM, pH7.4) at 50℃ for 30 min. PSs were formed by self-assembly at 4℃ overnight. N-(2-Aminoethy) maleimide (Mal) was conjugated with the –COOH groups on the surface of PSs after EDC activation for 2 hours (the micelle : Mal : EDC weight ratio was 4 : 1 : 1). Excess EDC, Mal was removed using a centrifugal filter device (3 kDa, Amicon® Ultra-4, Millipore Co., Germany) at 4000 rpm for 20 min. MIR31 mimic was then added into the PSs at Micelle :: MIR31 mimics weight ratio of 70 : 1, and vortexed gently for 10 seconds and stored in 4°C.

Characterization of PS-MIR31 Nanoparticles

The size distribution and zeta ζ-potential of α-La PSs in ddH_2O at pH 7.4 were analyzed by dynamic light scattering (Zetasizer Nano ZS90, UK) at RT. Prior to the measurement, the samples were diluted properly to reduce multiple scattering effects. The measurements were performed in triplicate.

Preparation of OKGM-PS-MIR31 Microspheres

Oxidized konjac glucomannan (OKGM) microspheres were prepared by an inverse emulsion method described in previous work[5]. α-La PSs were prepared via self-assembly of partial hydrolyzed protein according to previous work[6]. PS-MIR31 particles were then encapsulated inside the OKGM microspheres via an inverse-emulsion cross-linking method. Subsequently, 25 mg of DO80 (Degree of oxidation of 80%) OKGM polymer, 6 mg of $FeSO4 \cdot 7H_2O$ and 3 mg of PS-MIR31 were dissolved in 500 μL of deionized water, and 0.75 g of Span80 was dissolved in 20 mL of paraffin oil. The water phase was gradually added into the oil phase under mild stirring to form a water-in-oil emulsion. Air was then bubbled through the emulsion at 35 ℃ under mildly stirring for 4 hours to oxidize Fe^{2+} into Fe^{3+}, leading to cross-linking of OKGM in the aqueous droplets. Finally, the microparticles were washed three times with hexane to remove paraffin oil and another three times with methanol to remove hexane. After the washing step, the system was centrifuged (3000 g, 2 min), the liquid was decanted, and the particles were resuspended. After the last washing step, the OKGM-PS-MIR31 gel particles were stored in 2 mL of pH 3 HCl aqueous solution.

Application of OKGM-PS-MIR31 Microspheres in Mice

In preventive mode, 150 μL of OKGM-PS-MIR31 microsphere (21 μg/mL) was administered by enema once per day for 7 consecutive days. Drinking water with 3.5% DSS was provided to the mice for 5 days starting two days after the microsphere treatment. Samples were collected immediately after DSS treatment. In the therapeutic model, 3.5% DSS drinking water was administered to the mice for 5 days. Immediately thereafter, the mice were treated with 150 μL of OKGM-PS-MIR31 microspheres (21 μg/mL) once per day for 7 consecutive days. Samples were collected after microsphere treatment.

Flow Cytometry of LacZ$^+$ Cells

Axin2-LacZ mice were treated with OKGM-PS, OKGM-PS-NS and OKGM-PS-MIR31 microspheres two times daily for 4 consecutive days. Dissected colons were incubated with 7.5mM EDTA and 1mM DTT in HBSS for 30 min at 37℃, and single cell suspensions of colonic epithelium were produced following 2.5U Dispase (BD Biosciences) treatment and passing cells through 40 μm cell strainer. The flow cytometry of LacZ$^+$ cells was performed as described previously with modifications[7, 8]. Cells were loaded for 1 min with hypotonic fluorescein digalactoside (FDG, F-1930, Invitrogen) according to the manufacturer's protocol, and then suspended in staining medium (phosphate-buffered saline, 4% (v/v) fetal calf serum, 10 mM HEPES, pH 7.2) to stop this reaction. Then, the cells were incubated with CD326-PE (EpCAM-PE) (12-5791-81, eBioscience). Fixable Viability Dye eFluor™ 450 (65-0863-14, Invitrogen) was used to exclude dead cells. β-galactosidase hydrolyses FDG to fluorescein, with excitation at 491 nm and emission at 514 nm. Flow cytometry analysis was performed on a BD FACS Diva 8.0.1 (BD Pharmingen) and LacZ$^+$ cells were analyzed using the Flow-Jo 7.6.1 program.

References:

1. **Tian Y**, **Ma X**, **Lv C**, et al. Stress responsive miR-31 is a major modulator of mouse intestinal stem cells during regeneration and tumorigenesis. Elife 2017;6.
2. **He C**, **Shi Y**, Wu R, et al. miR-301a promotes intestinal mucosal inflammation through induction of IL-17A and TNF-alpha in IBD. Gut 2016;65:1938-1950.
3. Wirtz S, Popp V, Kindermann M, et al. Chemically induced mouse models of acute and chronic intestinal inflammation. Nat Protoc 2017;12:1295-1309.
4. Aaltonen T, Adelman J, Akimoto T, et al. Search for the associated production of the standard-model Higgs Boson in the all-hadronic channel. Phys Rev Lett 2009;103:221801.
5. Chen X, Wang S, Lu M, et al. Formation and characterization of light-responsive TEMPO-oxidized konjac glucomannan microspheres. Biomacromolecules 2014;15:2166-71.

ACCEPTED MANUSCRIPT

6. Li Y, Li W, Bao W, et al. Bioinspired peptosomes with programmed stimuli-responses for sequential drug release and high-performance anticancer therapy. Nanoscale 2017;9:9317-9324.
7. **Berg T**, **Rountree CB**, **Lee L**, et al. Fibroblast growth factor 10 is critical for liver growth during embryogenesis and controls hepatoblast survival via beta-catenin activation. Hepatology 2007;46:1187-97.
8. Asahina K, Tsai SY, Li P, et al. Mesenchymal origin of hepatic stellate cells, submesothelial cells, and perivascular mesenchymal cells during mouse liver development. Hepatology 2009;49:998-1011.

Author names in bold designate shared co-first authorship

ACCEPTED MANUSCRIPT